

AO-A161 149

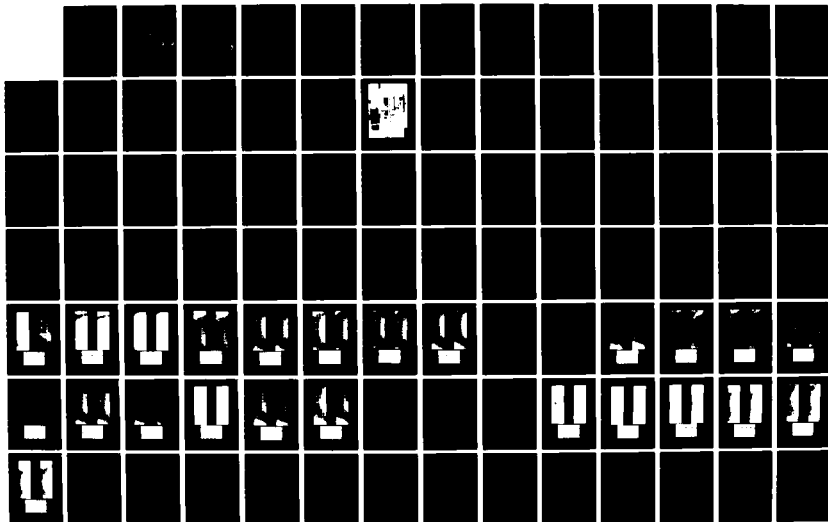
EFFECT OF SMALL PRESSURE DISTURBANCES ON THE BREAKDOWN
OF ROUND LAMINAR AND TURBULENT JETS(U) NAVAL
POSTGRADUATE SCHOOL MONTEREY CA 2 Z GIKAS SEP 85

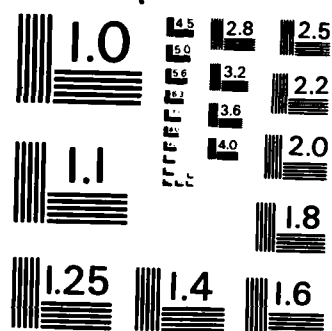
1/2

UNCLASSIFIED

F/G 20/4

NL





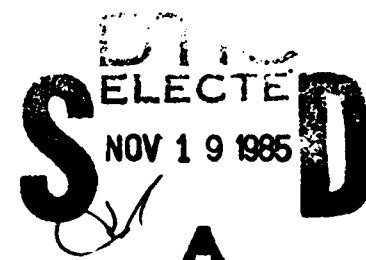
MICROCOPY RESOLUTION TEST CHART
NATIONAL BUREAU OF STANDARDS-1963-A

AD-A161 149

NAVAL POSTGRADUATE SCHOOL
Monterey, California



THESIS



EFFECT OF SMALL PRESSURE DISTURBANCES
ON THE BREAKDOWN
OF ROUND LAMINAR AND TURBULENT JETS

by

Zacharias Z. Gikas

September 1985

Thesis Advisor:

J.A. Miller

DTIC FILE COPY

Approved for public release; distribution unlimited

UNCLASSIFIED

SECURITY CLASSIFICATION OF THIS PAGE (When Data Entered)

REPORT DOCUMENTATION PAGE		READ INSTRUCTIONS BEFORE COMPLETING FORM
1. REPORT NUMBER	2. GOVT ACCESSION NO. AD-A161 149	3. RECIPIENT'S CATALOG NUMBER
4. TITLE (and Subtitle) Effect of Small Pressure Disturbances on the Breakdown of Round Laminar and Turbulent Jets		5. TYPE OF REPORT & PERIOD COVERED Master's Thesis; September 1985
7. AUTHOR(s) Zacharias Z. Gikas		6. PERFORMING ORG. REPORT NUMBER
9. PERFORMING ORGANIZATION NAME AND ADDRESS Naval Postgraduate School Monterey, California 93943		8. CONTRACT OR GRANT NUMBER(s)
11. CONTROLLING OFFICE NAME AND ADDRESS Naval Postgraduate School Monterey, California 93943		10. PROGRAM ELEMENT PROJECT, TASK AREA & WORK UNIT NUMBERS
14. MONITORING AGENCY NAME & ADDRESS (if different from Controlling Office)		12. REPORT DATE September 1985
		13. NUMBER OF PAGES 99
		15. SECURITY CLASS. (of this report) Unclassified
		15a. DECLASSIFICATION DOWNGRADING SCHEDULE
16. DISTRIBUTION STATEMENT (of this Report) Approved for public release; distribution unlimited		
17. DISTRIBUTION STATEMENT (of the abstract entered in Block 20, if different from Report)		
18. SUPPLEMENTARY NOTES		
19. KEY WORDS (Continue on reverse side if necessary and identify by block number) Laminar , Turbulent , Transitional Flow Small Disturbances Theory		
20. ABSTRACT (Continue on reverse side if necessary and identify by block number) The objective of the present work was to experimentally investigate the effect of small sinusoidal perturbations on the breakdown of circular water jets issuing from long tubes aiming to examine how the mean velocity profile for a fully		

DTIC
ELECTE

NOV 19 1985

A

DD FORM 1473

EDITION OF 1 NOV 65 IS OBSOLETE
S N 0102-LF-014-6601

UNCLASSIFIED

1 SECURITY CLASSIFICATION OF THIS PAGE (When Data Entered)

#20 - ABSTRACT - (CONTINUED)

developed laminar , transitional and turbulent flow as well as the frequency affects the mechanism of breakdown of the jet flow.

Observations using a high frequency stroboscope were recorded using a high speed photographic technique , for the most distinctive phenomena observed, for three selected Reynolds numbers corresponding to laminar , transitional and turbulent flow . Markedly different behavior of flow breakdown and droplet formation was observed for each of these flows as frequency waveform or phase angle was altered.

Approved for public release; distribution is unlimited.

Effect of Small Pressure Disturbances on the
Breakdown of Round Laminar and Turbulent Jets

by

Zacharias Z. Gikas
Captain, Hellenic Air Force
B.S., Hellenic Air Force Academy, 1974
B.S., University of Patras Greece, 1981

Submitted in partial fulfillment of the
requirements for the degree of

MASTER OF SCIENCE IN AERONAUTICAL ENGINEERING

from the

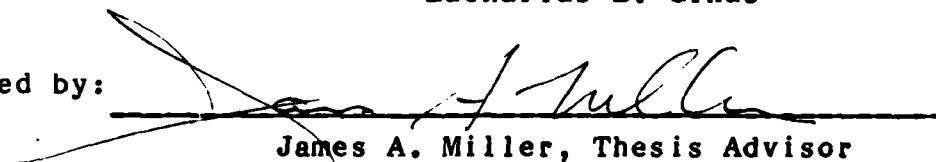
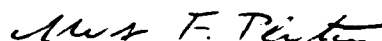
NAVAL POSTGRADUATE SCHOOL
September 1985

Author:



Zacharias Z. Gikas

Approved by:


James A. Miller, Thesis Advisor

Max F. Platzer, Chairman,
Department of Aeronautics



John N. Dyer,
Dean of Science and Engineering

Decision For	
NTIS Office	<input checked="" type="checkbox"/>
DTIC TAB	<input type="checkbox"/>
Unannounced	<input type="checkbox"/>
Justification	



A1

ABSTRACT

The objective of the present work was to experimentally investigate the effect of small sinusoidal perturbations on the breakdown of circular water jets issuing from long tubes aiming to examine how the mean velocity profile for a fully developed laminar , transitional and turbulent flow as well as the frequency affects the mechanism of breakdown of the jet flow.

Observations using a high frequency stroboscope were recorded using a high speed photographic technique , for the most distinctive phenomena observed, for three selected Reynolds numbers corresponding to laminar , transitional and turbulent flow . Markedly different behavior of flow breakdown and droplet formation was observed for each of these flows as frequency waveform or phase angle was altered.

TABLE OF CONTENTS

I.	INTRODUCTION	11
II.	EXPERIMENTAL APPARATUS AND PROCEDURE	14
	A. DESCRIPTION OF EXPERIMENTAL APPARATUS	14
	B. EXPERIMENTAL PROCEDURE	19
III.	THEORETICAL ANALYSIS	21
	A. BREAKDOWN OF LAMINAR PIPE FLOW	21
	B. NONSTEADY FLOW IN A CIRCULAR TUBE	27
	C. SOLUTION FOR A UNIFORM PULSATING FLOW	30
	D. VELOCITY DISTRIBUTION AND ASYMPTOTIC EXPRESSIONS	36
	1. Slow Oscillation ($\delta R \ll 1$)	36
	2. Rapid Oscillation ($\delta R \rightarrow \infty$)	38
	E. SECTIONAL MEAN VELOCITY	43
	F. SURFACE FRICTION AND BALANCE OF FORCE	45
IV.	RESULTS AND CONCLUSIONS	49
	A. PRELIMINARY RESULTS	49
	1. Laminar Flow at Reynolds Number 1760	53
	2. Transitional Flow at Reynolds Number 2200	62
	3. Turbulent Flow at Reynolds Number 2640	74

B. CONCLUSIONS	75
APPENDIX. CALCULATIONS AND DATA REDUCTION	83
A. CALCULATION OF CRITICAL REYNOLDS NUMBER	83
B. CALCULATION OF INDICATED PRESSURE IN LAMINAR FLOW	84
C. DYNAMIC RESPONSE OF INDICATED PRESSURE	87
D. CALIBRATION DIAGRAMS	91
LIST OF REFERENCES	95
INITIAL DISTRIBUTION LIST	98

LIST OF TABLES

I.	SUMMARY OF BREAKDOWN DISTANCE	50
II.	SUMMARY OF EXPERIMENTAL CONDITIONS	51

LIST OF FIGURES

1.	Schematic Diagram of Experimental Apparatus . . .	15
2.	Aluminum Block and Loudspeaker Mounting Adapter Details	16
3.	Photo of Overall Experiment Setup	18
4.	Cylindrical Coordinates in a Round Pipe	28
5.	Oscillation Amplitude of the Local Velocity . . .	37
6.	Velocity Profile for $or = 1$	40
7.	Velocity Profile for $or = 3$	41
8.	Velocity profile for $or = 10$	42
9.	Coefficients of Amplitude and Phase Lag of Mean Velocity	45
10.	Coefficients of Amplitude and Phase Lag of the Shearing Stress	47
11.	Periodic Force Component (A - Pressure Gradient, B - Acceleration , C - Shearing Force)	48
12.	Breakdown Length Versus Frequency	52
13.	Photos Illustrating Jet Breakdown and Oscilloscope Trace of Pressure at $Re=1760$ and $f=50$ Hz	54
14.	Photos Illustrating Jet Breakdown and Oscilloscope Trace of Pressure at $Re=1760$ and $f=100$ Hz	55
15.	Photos Illustrating Jet Breakdown and Oscilloscope Trace of Pressure at $Re=1760$ and $f=150$ Hz	56
16.	Photos Illustrating Jet Breakdown and Oscilloscope Trace of Pressure at $Re=1760$ and $f=200$ Hz	57
17.	Photos Illustrating Jet Breakdown and Oscilloscope Trace of Pressure at $Re=1760$ and $f=250$ Hz	58
18.	Photos Illustrating Jet Breakdown and Oscilloscope Trace of Pressure at $Re=1760$ and $f=266$ Hz	59

19.	Photos Illustrating Jet Breakdown and Oscilloscope Trace of Pressure at $Re=1760$ and $f=300$ Hz	60
20.	Photos Illustrating Jet Breakdown and Oscilloscope Trace of Pressure at $Re=1760$ and $f=380$ Hz	61
21.	Photos Illustrating Jet Breakdown and Oscilloscope Trace of Pressure at $Re=2200$ and $f=50$ Hz	64
22.	Photos Illustrating Jet Breakdown and Oscilloscope Trace of Pressure at $Re=2200$ and $f=100$ Hz	65
23.	Photos Illustrating Jet Breakdown and Oscilloscope Trace of Pressure at $Re=2200$ and $f=150$ Hz	66
24.	Photos Illustrating Jet Breakdown and Oscilloscope Trace of Pressure at $Re=2200$ and $f=200$ Hz	67
25.	Photos Illustrating Jet Breakdown and Oscilloscope Trace of Pressure at $Re=2200$ and $f=233$ Hz	68
26.	Photos Illustrating Jet Breakdown and Oscilloscope Trace of Pressure at $Re=2200$ and $f=250$ Hz	69
27.	Photos Illustrating Jet Breakdown and Oscilloscope Trace of Pressure at $Re=2200$ and $f=266$ Hz	70
28.	Photos Illustrating Jet Breakdown and Oscilloscope Trace of Pressure at $Re=2200$ and $f=300$ Hz	71
29.	Photos Illustrating Jet Breakdown and Oscilloscope Trace of Pressure at $Re=2200$ and $f=380$ Hz	72
30.	Photos Illustrating Jet Breakdown and Oscilloscope Trace of Pressure at $Re=2200$ and $f=787$ Hz	73
31.	Photos Illustrating Jet Breakdown and Oscilloscope Trace of Pressure at $Re=2640$ and $f=50$ Hz	77
32.	Photos Illustrating Jet Breakdown and Oscilloscope Trace of Pressure at $Re=2640$ and $f=100$ Hz	78
33.	Photos Illustrating Jet Breakdown and Oscilloscope Trace of Pressure at $Re=2640$ and $f=200$ Hz	79
34.	Photos Illustrating Jet Breakdown and Oscilloscope Trace of Pressure at $Re=2640$ and $f=250$ Hz	80
35.	Photos Illustrating Jet Breakdown and Oscilloscope Trace of Pressure at $Re=2640$ and $f=300$ Hz	81

36.	Photos Illustrating Jet Breakdown and Oscilloscope Trace of Pressure at $Re=2640$ and $f=600$ Hz	82
B-1.	Sketch of the Apparatus	85
C-1.	Schematic Diagram of Pressure Transducer Connection	88
D-1.	Pressure Calibration Diagram	92
D-2.	Flow Rate vs Pressure Indicated (in.Hg) Diagram .	93
D-3.	Flow rate vs Pressure Indicated (V.DC) Diagram . .	94

1. INTRODUCTION

An important physical phenomenon which has many practical consequences in technology, ranging from fuel injection sprays to ink jet printers, is the breakdown of a circular jet of fluid issuing into a quiescent environment .

This problem has been extensively studied previously by Rayleigh and others, [Refs. 1, 2 and 3], for steady uniform jets issuing from an orifice , but only recently have the effects of jet velocity profiles or other initial conditions on the flow been investigated, [Refs. 4, 5 and 6].

Theoretical investigators have typically assumed jet breakdown to be physically similar to transition from laminar to turbulent flow and have examined the phenomena using classical stability theory.

Rayleigh , [Ref. 1], studied the inviscid stability of Poiseuille flow and concluded that the flow was stable to infinitesimal disturbances. This work attracted the interest of many investigators and sixty years later Tatsumi [Ref. 2] published his work related to the study of the velocity distribution in the axisymmetric laminar inlet flow through a circular tube, under the assumption of ' almost similarity ' of velocity profiles . He obtained fairly good agreement of theoretical with experimental velocity distribution curves

in a rather limited region near the entrance where the approximation was valid .

Batchelor and Gill, [Ref. 3], have analyzed the stability of steady axisymmetric jets considering the typical small disturbance as a Fourier component with sinusoidal dependence on both axes in cylindrical coordinates .

Crow and Champagne, [Ref. 4] , have employed a loudspeaker to generate a wave train on a turbulent jet and found that the phase velocity of the waves could be described by applying linear theory of temporally growing instability to a 'top hat' velocity profile.

Salwen , Chester and Grosch, [Ref. 5], have studied the stability of Poiseuille flow in a pipe of circular cross section with axisymmetric disturbances . They formulated the problem by expanding the perturbation velocity and pressure in a complete set of orthonormal functions which satisfied the boundary conditions .

In a recent work by Anderson and Bejan, [Ref. 6], the authors presented a linear stability analysis of the large scale structure of a round jet surrounded by an annular shear layer . Their study was limited to the developing region near the jet nozzle at very large Reynolds number ($Re \rightarrow \infty$). They examined the radial dependence of the amplitude of growing disturbances in order to illustrate the extent to which the disturbance penetrates into the jet and its surroundings

and found that the region influenced by a disturbance was directly proportional to the wavelength of the disturbance. They also pointed out that amplified disturbances exhibit a phase lag across the shear layer , which may account for the spade-like structures evident in flow visualizations of turbulent jets.

In the present work we seek to investigate experimentally the effects of small sinusoidal perturbations on the breakdown of circular jets issuing from long tubes , which permit some control of their mean velocity profiles , for both fully developed laminar and turbulent flows.

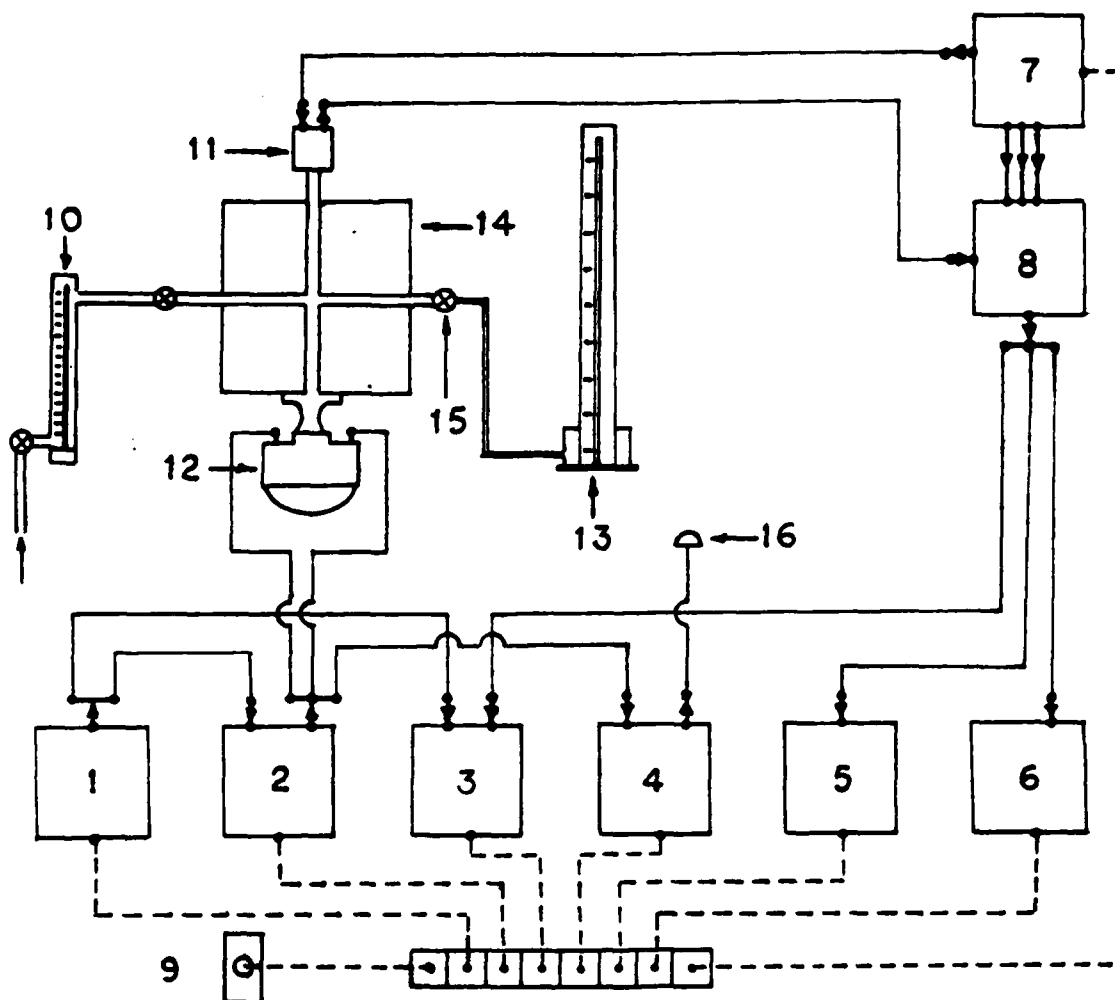
11. EXPERIMENTAL APPARATUS AND PROCEDURE

A. DESCRIPTION OF EXPERIMENTAL APPARATUS

The experiment was carried out in a vertical falling jet produced at the outlet of a 70.0 inch long length of 0.1875 inch inside diameter stainless steel tube. The inlet of the tube was fed from a phenum chamber machined into an aluminum block, which also contained a 75 Watt loudspeaker driver unit mounted properly to this block, used to introduce the pressure perturbations. A schematic diagram of the experimental apparatus is illustrated in Fig. 1. Details of the aluminum block and adapter are shown in Fig. 2.

Pressure fluctuations as well as mean pressure within the phenum chamber was monitored by the Statham differential pressure transducer shown in Fig. 1 and a mercury manometer. Mean water flow was controlled with a needle valve and measured with a 0.6 gpm rotameter as shown in Fig. 1. In order to minimize effects of geometry at the exit end of the steel tube, it was very carefully machined to ensure sharp edges and an absence of burrs.

The loudspeaker driver was excited with a Wavetec audio oscillator capable of producing sine waves, as well as triangular, unit functions and ramp functions from 1 Hz to 10 MHz, amplified by a Hewlett Packard power amplifier.



- 1 Wavetec H.F VCG Generator , Model 142
- 2 Hewlett Packard Power Amplifier , Model 467A
- 3 Tektronix Dual Beam Oscilloscope , Type 551
- 4 High Frequency Stroboscope , Model 839
- 5 Cimcon Digital Multimeter DMM 51
- 6 Hewlett Packard RMS Voltmeter , Model 3400A
- 7 Intronic Power Supply +15 VDC
- 8 Calibration Bridge
- 9 110 VAC Outlet
- 10 Rotameter 0.6 gpm
- 11 Statham Pressure Transducer PM131 TC
- 12 University Sound Driver Unit ID-75
- 13 Mercury Manometer
- 14 Aluminum Block
- 15 Needle Valve
- 16 L.E.D Strobolight

Figure 1. Schematic Diagram of Experimental Apparatus

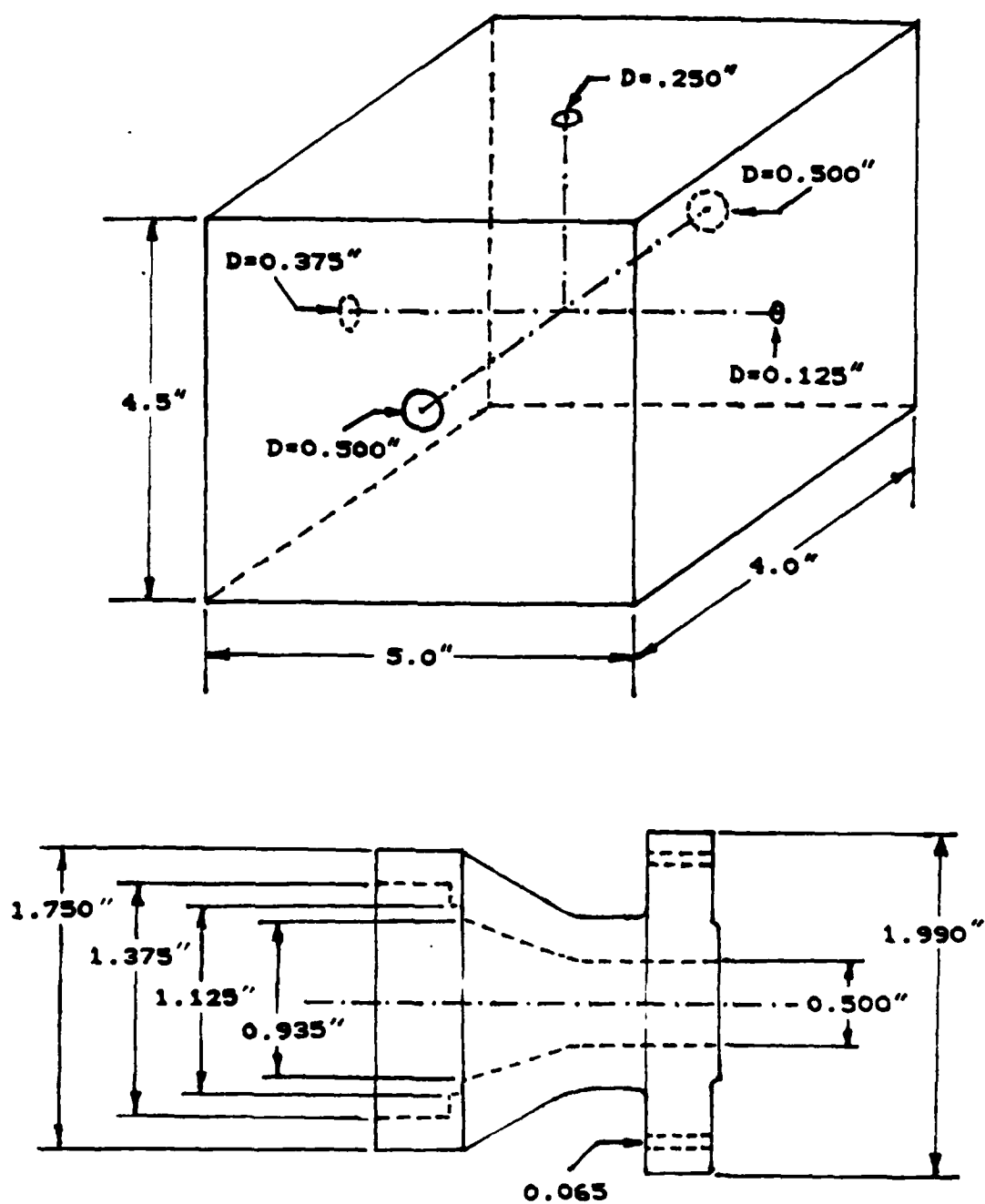


Figure 2. Aluminum Block and Loudspeaker Mounting Adapter Details

Excitation voltage as well as the output of the plenum chamber pressure transducer were monitored on a two channel Tektronix oscilloscope.

Visual observations of the jet breakdown process was made with the aid of a high frequency LED stroboscope, developed at the Max-Planck Institute for Fluids Research¹ which produces a constant mean light output from 100 Hz to 1 MHz. This device not only may be set for any phase angle but also contains circuitry which produces automatic phase angle sweep at an adjustable rate which permits periodic phenomena to be visualized as they develop. Unfortunately the light output was not sufficient for photographic recording.

Photographic recording of the observed phenomena was made with the illumination from a General Radio Microflash unit, which although brighter than the LED stroboscope, lacked the sophisticated triggering circuitry to permit control of the phase angle. A 4x5 inch view camera fitted with a 210 mm objective was used to photograph on Kodak Tri-X film which was force developed to achieve an effective film speed of ISO 3200.

An overall view of the experimental apparatus concerning and the photographic equipment used is shown in Fig. 3.

¹The author extends his gratitude to Dr. G.E.A Meier who made the instrument available for this work.

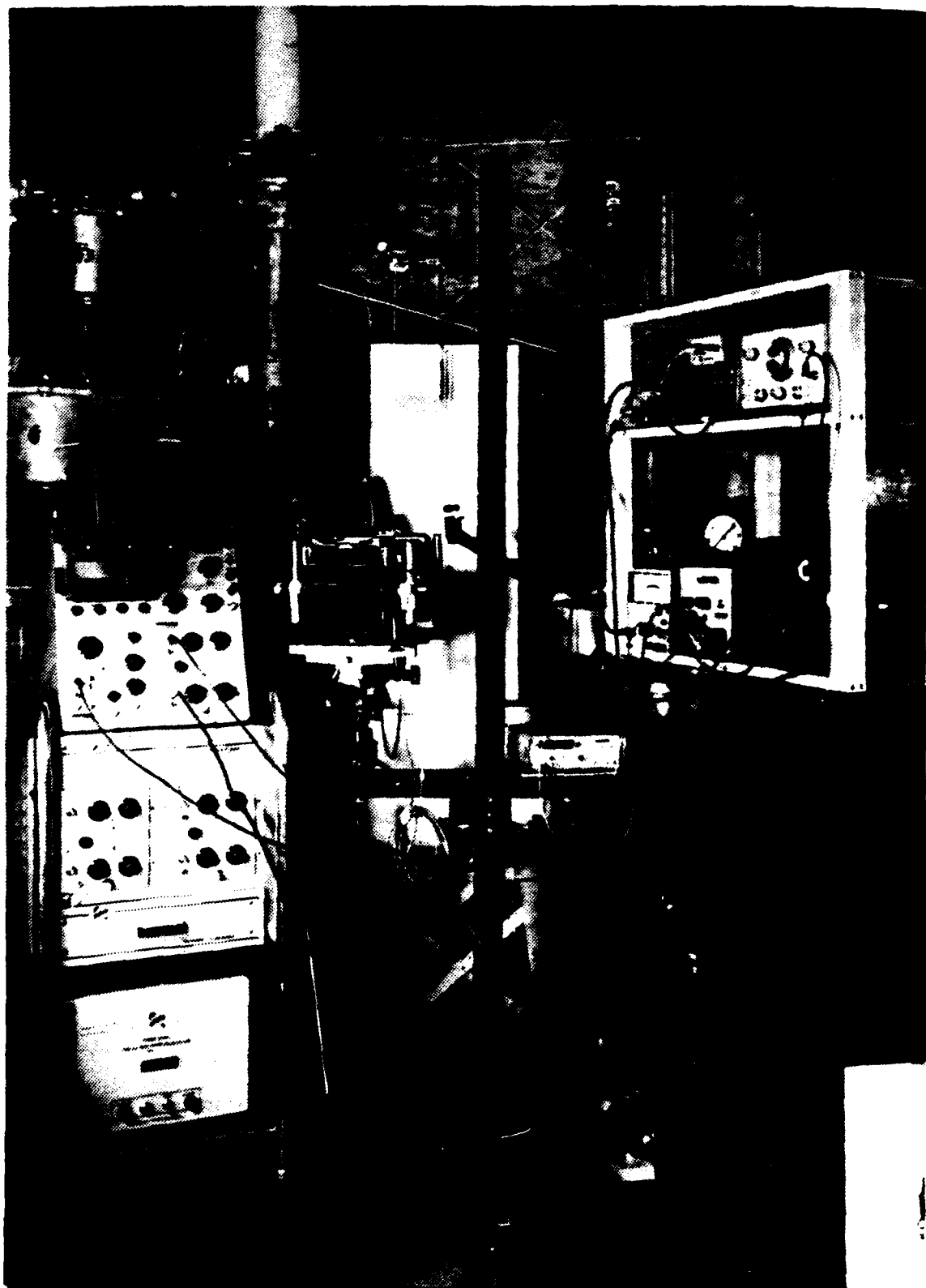


Figure 3. Photo of Overall Experiment Setup

B. EXPERIMENTAL PROCEDURE

The first part of the experiment was devoted to calibration and determination of the steady flow behavior of the jet without the introduction of external perturbations. As the flow rate was increased a laminar flow column was observed to develop which converged and began to breakdown into a turbulent flow at 100 to 125 diameters downstream of the tube exit corresponding to Reynolds numbers of 880 to 2200 .

Increasing the Reynolds number above 2200 resulted in a turbulent jet which was sudden and easily identified with the naked eye . Breakdown of the turbulent jet was observed with the high frequency stroboscope and was observed to range from 55 diameters downstream at Reynolds number of 2288 to 25 diameters as the Reynolds number was increased to 4400

Based on these preliminary results , a subcritical Reynolds number of 1760 was adopted for laminar flows and 2640 for turbulent flows and the effects of small perturbations on the flow at these two Reynolds numbers was investigated over the frequency range of 0 to 2000 Hz using the high frequency stroboscope to observe the flow.

Based on these observations , photographic records were made at selected frequencies at which significant characteristic phenomena occurred . Because of the difficulty in accurately describing the pressure fluctuations actually

produced in the plenum chamber, oscilloscope traces of these pressure variations as well as the driving signal were also recorded. These results are presented and discussed in Chapter IV. A discussion of the effects of plenum pressure variation on the flow at the exit of a long tube is presented in Chapter III. An analysis of the dynamic response of the pressure transducer and its calibration curves may be found in Appendices C and D.

III. THEORETICAL ANALYSIS

A. BREAKDOWN OF LAMINAR PIPE FLOW

One of the most important problems in fluid mechanics, one which has attracted the interest of investigators for many years, is that of the transition from laminar to turbulent flow.

The theoretical analysis of the stability of laminar flow is based upon the assumption that turbulence is produced by the growth of what are initially small perturbations or disturbances of the basic, laminar velocity profile.

The theoretical analyses have generally been limited to infinitesimal disturbances for which the differential equations of the disturbance can be linearized.

The basic problem of the small-disturbance theory is to determine whether a small disturbance is amplified or damped. If any small disturbance is amplified, it is assumed that a transition to turbulent flow will ultimately occur. However, the small disturbance theory cannot reveal any of the details of the actual transition because it applies only while the disturbance is small. The question of how 'small' the disturbance must be in order to apply the linearized equations has not been adequately answered.

An axisymmetric flow is always stable to a disturbance which has only a tangential component of velocity, [Ref. 7].

Therefore the theoretical analyses have generally been limited to axisymmetrical disturbances . Such analyses have been carried out by many investigators, [Refs. 2,3 and 7] , although some doubt still remains concerning the details of the mathematics.

Steady flow in a tube has been found to be stable to small, axisymmetrical disturbances by a number of investigators,[Refs. 5,7 and 8], and may be considered as an accepted conclusion.

Several investigators have attempted to derive a critical Reynolds number , for a flow subjected to external disturbances , after which transition to turbulence occurs. Leite, [Ref. 9], studied the behavior of small, axisymmetrical disturbances in steady flow in a tube . He found that they were always damped for Reynolds number up to 13000 , as long as their amplitude was not too large. Darling,[Ref.10], working with pulsating flows in tubes , found that the transition Reynolds number dropped from 2510 in steady flow to 1500 in pulsating flow. Sarpkaya,[Ref. 11], determined experimentally the critical Reynolds number for pulsating Poiseuille flow as a function of a frequency parameter and velocity ratio . Gilbrech and Combs, [Ref. 12], using water as working fluid, found a critical Reynolds number which was higher than 2220 , under some conditions, for steady flow .

They also pointed out that earlier investigators had found no upper limit to the upper critical Reynolds numbers.

These experimental results confirm the conclusion that steady, fully developed flow in tube is stable to small disturbances, and the critical Reynolds number is a function of the frequency of external disturbances and the physical properties of the fluid. In spite of this confirmation, transition to turbulent flow is invariably observed to occur at sufficiently high Reynolds number and it is necessary to consider this fact.

The most obvious explanation is that transition is caused by finite disturbances which are not damped, even though smaller disturbances are. This possibility is strongly supported by the observation made by Gilbrech and Combs [Ref. 13], that the critical Reynolds number **decreases** as the magnitude of the disturbance **increases**.

The theoretical analysis of finite disturbances has been limited by mathematical difficulties, however, Stuart [Ref. 14], has shown that a flow may be unstable to finite disturbances, while it is stable to infinitesimal ones. In addition, Spielberg, [Ref. 15], has pointed out that stability to two dimensional disturbances does not necessarily imply stability to three dimensional disturbances. This latter result creates a problem in comparing accurately the theoretical and experimental results.

In the present work, it was assumed that an axisymmetrical disturbance was propagated without confirming the non-existence of three dimensional disturbances .

Another explanation of the origin of turbulence in pipe flow may be that the transition occurs in the entrance region of the pipe, in which the velocity distribution is of the boundary-layer type . A theoretical analysis by Tatsumi, [Ref. 2], indicates that the flow in the entrance region is unstable to small disturbances. He found a point of maximum instability near the entrance to the tube, where the maximum Reynolds number for stability was 19400 . However , the critical Reynolds number increases rapidly in both directions, so that one cannot conclude that this local instability will lead to transition. This is because amplification required to produce transition remains undetermined.

Sparrow and Lin, [Ref. 16], pointed out, in their effort to determine the detailed nature of the flow development in the entrance region, that even for a laminar flow, the velocity problem for the entrance region does not yield an exact solution, regardless of the shape of the duct cross section. Their explanation for the difficulties in the analysis was that the essential nonlinearity of the inertia terms which appear in the **equation of motion**, preclude linear analysis.

From a more sophisticated point of view , the problem becomes especially complicated if we attempt to reveal the

nature of motion in the non-linear range of **boundary layer instability** and the **onset of turbulence**.

Klebanoff and others , [Ref. 17] , who attacked the problem in the general form , pointed out that despite the success of the linearized theories in revealing the nature of the initial stages of boundary-layer instability , there remains a **deep void** in the understanding of the subsequent non-linear behavior and the actual **breakdown** of the laminar boundary-layer.

Miller and Fejer, [Ref. 18] , who studied the transition in **Blasius-type boundary-layer** produced by a free stream having an oscillatory component of velocity , found that the transition Reynolds number depends only on the **amplitude** of the oscillations , and that the **dimensionless transition length** is a function only of the **frequency**.

Obremski and Fejer , [Ref. 19] , continued the previous work and pointed out that below a critical value of the parameter $[(\text{Re})_{\text{NS}} = L\Delta U/2\pi v]$, transition occurs at a relatively constant Reynolds number , which appeared **independent** of the amplitude and frequency of the oscillation , at least over the range investigated.

Finally Landahl , [Ref. 25], used **kinematic wave theory** to determine under what conditions **breakdown** of a steady or unsteady laminar flow into high frequency oscillations

should occur . Isolating the three different ingredients of the mechanism of breakdown , he pointed out:

- a. The primary instability process itself is only incidental to breakdown and transition , since one can easily produce a breakdown condition by a sufficiently intense local disturbance of the shear flow , for example through free stream disturbances.
- b. If the breakdown is to be self maintained as it travels downstream however , hydrodynamic instability is required. In a sense , the breakdown mechanism is the one most essential in transition of a boundary-layer to turbulence rather than the classical hydrodynamic instability one, since the former represents a strongly irreversible process.
- c. An unstable small - amplitude wave packet of the **Tolmien-Schlichting type** may amplify for a while , as it moves downstream , but once it has passed through some streamwise position in the boundary-layer it will leave the shear flow practically as undisturbed as before the passage of the packet , except for a small deformation of the mean flow of second order in disturbance amplitude . At breakdown on the contrary there is an **irreversible redistribution** of the basic shear flow vorticity due to a **nonlinear rectification mechanism** .

In view of the difficulties encountered in applying the small disturbance theory to steady axisymmetrical flow , it is likely that considerable time and effort will be required to obtain an exact solution for unsteady flow problems , especially if we consider a three dimensional flow .

The use of a ' quasi-steady ' analysis would reduce the problem to one which could be handled more easily. Using this technique one would analyze an instantaneous velocity profile as though it were a steady-flow problem.

By considering the stability of the velocity profiles at various times, one might then draw some conclusions about the stability of the unsteady flow an approach used by Shen, [Ref. 21], as well as Greenspan and Benney, [Ref. 22].

In the present work, although Reynolds Numbers as high as 19400 were not reached, we recognize that the flow in the entrance region has, in all probability, affected the downstream flow and may well have introduced turbulence subsequently damped along the tube, for low Reynolds numbers, creating a laminar or laminar-like flow at the tube exit.

B. NONSTEADY FLOW IN A CIRCULAR TUBE

In order to study how the pressure disturbances, introduced at the entrance of a long tube used to form the jet, affect the flow at the exit of the tube, which constitutes the initial conditions of the flow of interest, we may examine the nonsteady flow in a long tube of circular cross section. We adopt, as shown in Fig. 4, cylindrical coordinates whose x-axis is identified with the center line of the pipe.

The equation of continuity is:

$$\nabla(\rho \vec{V}) + \frac{\partial \rho}{\partial t} = 0 \quad (\text{Eq. 1})$$

In cylindrical coordinates Eq. 1 becomes:

$$\frac{1}{\rho} \frac{\partial}{\partial \rho} (r \rho v_r) + \frac{1}{\rho} \frac{\partial}{\partial \theta} (\rho v_\theta) + \frac{\partial}{\partial x} (\rho v_x) + \frac{\partial \rho}{\partial t} = 0 \quad (\text{Eq. 2})$$

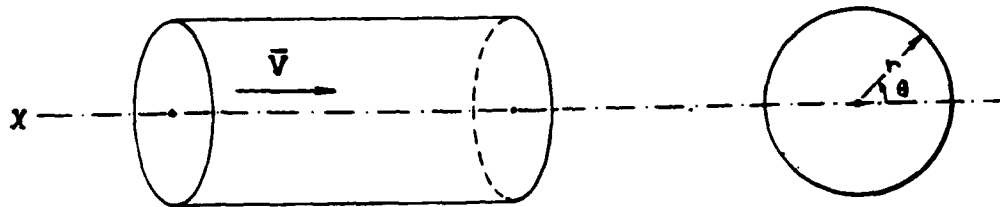


Figure 4. Cylindrical Coordinates in a Round Pipe.

Assuming incompressibility, ($\rho = \text{constant}$), and a non-twisting flow ($v_\theta = 0$), Eq. 2 may be written as:

$$\frac{1}{\rho} \frac{\partial}{\partial \rho} (r \rho v_r) + \frac{\partial}{\partial x} (\rho v_x) = 0$$

$$\text{or: } \frac{\partial v_x}{\partial x} + \frac{\partial v_r}{\partial r} + \frac{v_r}{r} = 0 \quad (\text{Eq. 3})$$

Neglecting external forces, (i.e gravity), the Navier-Stokes equations in two components can be written:

$$\frac{\partial v_x}{\partial t} + v_x \frac{\partial v_x}{\partial x} + v_r \frac{\partial v_x}{\partial r} = -\frac{1}{\rho} \frac{\partial P}{\partial x} + \frac{\mu}{\rho} \left[\frac{\partial^2 v_x}{\partial x^2} + \frac{\partial^2 v_x}{\partial r^2} + \frac{1}{\rho} \frac{v_x}{r} \right] \quad (\text{Eq. 4})$$

$$\frac{\partial v_r}{\partial t} + v_x \frac{\partial v_r}{\partial x} + v_r \frac{\partial v_r}{\partial r} = - \frac{1}{\rho} \frac{\partial P}{\partial x} + \frac{\mu}{\rho} \left[\frac{\partial^2 v_r}{\partial x^2} + \frac{\partial^2 v_r}{\partial r^2} + \frac{1}{\rho} \frac{\partial v_r}{\partial r} - \frac{v_r}{r^2} \right] \quad (\text{Eq. 5})$$

If we assume quasi-steady flow, the equation of continuity Eq. 3 becomes:

$$\frac{\partial v_x}{\partial t} = 0 \quad \text{or:} \quad v_x = v(r, t) \quad (\text{Eq. 6})$$

This indicates that the velocity in the direction parallel to the center line is a constant at each moment.

Substituting $v_r = 0$ into Eq. 5 we get:

$$\frac{\partial P}{\partial r} = 0 \quad \text{or:} \quad P = P(x, t) \quad (\text{Eq. 7})$$

Inserting these results in the equation of motion (Eq. 4) :

$$\frac{\partial v_x}{\partial t} = - \frac{1}{\rho} \frac{\partial P}{\partial x} + \nu \left[\frac{\partial^2 v_x}{\partial r^2} + \frac{1}{r} \frac{\partial v_x}{\partial r} \right] \quad (\text{Eq. 8})$$

where: $\nu = \frac{\mu}{\rho}$

is the kinematic viscosity of the fluid.

C. SOLUTION FOR A UNIFORM PULSATING FLOW

Assuming that the pressure pulses introduced by the drive unit, (a loudspeaker driver), are propagated instantly along the flow direction, (justified by the fact that the mean flow velocity is very small compared with the speed of sound in the fluid), with the aid of Eqs. 6, 7 and 8 we can show that the pressure gradient, $(\partial P / \partial x)$, becomes a function only of time, t .

Using Fourier series we can express the pressure gradient as follows :

$$-\frac{1}{\rho} \frac{\partial P}{\partial x} = \alpha_0 + \sum_{n=1}^{\infty} \alpha_n \cos(nt) + \sum_{n=1}^{\infty} b_n \sin(nt) \quad (\text{Eq. 9})$$

or, for the sake of simplicity of calculation, in a complex form:

$$-\frac{1}{\rho} \frac{\partial P}{\partial x} = \alpha_0 + \sum_{n=1}^{\infty} \gamma_n e^{int}, \quad \gamma_n = \alpha_n - ib_n \quad (\text{Eq. 10})$$

where : α_n , b_n are constants representing the amplitudes of elemental vibrations.

The corresponding solution for the axial velocity may be assumed to be of the form :

$$v_x = v_{x_0} + \sum_{n=1}^{\infty} v_{n_1} \cos(nt) + \sum_{n=1}^{\infty} v_{n_2} \sin(nt) \quad (\text{Eq. 11})$$

or, in complex form:

$$v_x = v_{x_0} + \sum_{n=1}^{\infty} v_n e^{int}, \quad v_n = v_{n_1} - i v_{n_2} \quad (\text{Eq. 12})$$

where coefficients v_{n_1} and v_{n_2} are assumed to be functions of the radial coordinate, r , only.

Substituting Eqs. 10 and 12 into Eq. 8 and comparing the terms of the same order, we obtain the following Differential Equations for the coefficients as independent variables.

$$\frac{d^2 v_{x_0}}{dr^2} + \frac{1}{r} \frac{dv_{x_0}}{dr} + \frac{v_{x_0}}{r} = 0 \quad (\text{Eq. 13})$$

and:

$$\frac{d^2 v_n}{dr^2} + \frac{1}{r} \frac{dv_n}{dr} + \frac{-in}{r} v_n + \frac{\gamma_n}{r} = 0 \quad (\text{Eq. 14})$$

After integration we get:

$$v_{x_0} = -\frac{\alpha_0}{r} \frac{r^2}{4} + A_0 \ln(r) + B_0 \quad (\text{Eq. 15})$$

where: $A_0, B_0 = \text{constant}$

and:

$$v_n = \frac{\gamma_n}{in} + D_n J_0(\delta r i^{3/2}) + E_n K_0(\delta r i^{1/2}) \quad (\text{Eq. 16})$$

where: $\delta = \sqrt{(n/\nu)}$

and J_0 and K_0 are the Bessel functions of the first and second kind of zero order respectively.

The solution for the x-wise component of velocity is given by the real part of the following expression:

$$v_x = -\frac{\alpha_0}{\nu} \frac{r^2}{4} + A_0 \ln r + B_0 + \sum_{n=1}^{\infty} \left[\frac{\gamma_n}{i n} + D_n J_0(\delta r i^{3/2}) + E_n K_0(\delta r i^{1/2}) \right] e^{i n t} \quad (\text{Eq. 17})$$

On the axis of the pipe, ($r = 0$), $\ln(r) = -\infty$ and $K_0(\delta r i^{1/2}) = \infty$, since v_x is finite, we conclude that:

$$A_0 = E_n = 0 \quad (\text{Eq. 18})$$

The Boundary Condition at the wall is given by:

$$v_x = 0 \quad \text{at} \quad r = R \quad (\text{Eq. 19})$$

where: R is the radius of the pipe.

Inserting this boundary condition, Eq. 19, into Eq. 17 we get:

$$B_0 = \frac{\alpha_0 R^2}{4\nu} - \sum_{n=1}^{\infty} \left[\frac{\gamma_n}{i n} + D_n J_0(\delta R i^{3/2}) \right] \quad (\text{Eq. 20})$$

Inserting, Eqs. 18 and 20 into Eq. 17, we finally get the velocity component v_x :

$$v_x = \frac{\alpha_0}{4\nu} [R^2 - r^2] \sum_{n=1}^{\infty} \frac{i\gamma_n}{n} \left[1 - \frac{J_0(\delta r i^{3/2})}{J_0(\delta R i^{3/2})} \right] e^{int} \quad (\text{Eq. 21})$$

The total mean mass flow , \dot{m} , which is transmitted in the x-direction is given by the integral over time and radius of the axial velocity component:

$$\dot{m} = \frac{1}{2\pi} \int_0^{2\pi} dt \int_0^R 2\pi v_x r dr = \frac{\pi R^4 \alpha_0}{8\nu} \quad (\text{Eq. 22})$$

Inserting the time mean pressure gradient:

$$\left[-\frac{\overline{\partial P}}{\partial x} \right] = \rho \alpha_0 \quad (\text{Eq. 23})$$

we get:

$$\dot{m} = \frac{\pi R^4}{8\mu} \left[-\frac{\overline{\partial P}}{\partial x} \right] \quad (\text{Eq. 24})$$

It is seen that the total mean mass flow , in pulsating motion , is identical to that of a steady Poisseuille flow with the same pressure gradient, as the mean pressure gradient in the pulsating flow.

A mean velocity , U , may be defined by:

$$U = \frac{\dot{m}}{\pi R^2} \quad (\text{Eq. 25})$$

Combining Eqs. 24 and 25 we get:

$$U = \frac{R^2}{8\mu} \left[-\frac{\partial P}{\partial x} \right] \quad (\text{Eq. 26})$$

We may express the x-wise velocity as the sum of a perturbation velocity, v'_x , and the mean stream velocity of the fluid, v_{xs} :

$$v_x = v_{xs} + v'_x \quad (\text{Eq. 27})$$

Introducing the Hagen-Poiseuille relation for v_{xs} we get:

$$\frac{v_{xs}}{U} = 2 \left[1 - \frac{r^2}{R^2} \right] \quad (\text{Eq. 28})$$

Dividing Eq. 27 by the total mean velocity, U , we get the non-dimensional expression:

$$\frac{v_x}{U} = \frac{v_{xs}}{U} + \frac{v'_x}{U} \quad (\text{Eq. 29})$$

Combining Eqs. 21 and 29 we get for the perturbation velocity, v'_x :

$$\begin{aligned} \frac{v'_x}{U} = & \sum_{n=1}^{\infty} \frac{\alpha_n}{\alpha_0} \left[\frac{8B}{(\delta R)^2} \cos(n\tau) + \frac{8(1-A)}{(\delta R)^2} \sin(n\tau) \right] + \\ & + \sum_{n=1}^{\infty} \frac{b_n}{\alpha_0} \left[\frac{8B}{(\delta R)^2} \sin(n\tau) - \frac{8(1-A)}{(\delta R)^2} \sin(n\tau) \right] \end{aligned} \quad (\text{Eq. 30})$$

where:

$$\left. \begin{aligned} A &= \frac{\text{ber}(\delta R)\text{ber}(\delta r) + \text{bei}(\delta R)\text{bei}(\delta r)}{\text{ber}^2(\delta R) + \text{bei}^2(\delta R)} \\ B &= \frac{\text{bei}(\delta R)\text{ber}(\delta r) - \text{ber}(\delta R)\text{bei}(\delta r)}{\text{ber}^2(\delta R) + \text{bei}^2(\delta R)} \end{aligned} \right\} \quad (\text{Eq. 31})$$

where: ber and bei are the Kelvin functions .

With the aid of Eqs. 10 and 26 we can obtain the corresponding pressure gradient relation:

$$-\frac{4R}{\rho U^2} \frac{\partial P}{\partial x} = \frac{64}{\text{Re}} \left[1 + \sum_{n=1}^{\infty} \frac{\alpha_n}{\alpha_0} \cos(nt) + \sum_{n=1}^{\infty} \frac{b_n}{\alpha_0} \sin(nt) \right] \quad (\text{Eq. 32})$$

where:

$$\text{Re} = 2RU / \nu$$

Introducing the friction factor for laminar flow :

$$f = 64 / \text{Re}$$

into Eq. 32, we get :

$$-\frac{\partial P}{\partial x} = \frac{\rho U^2}{4R} f \left[1 + \sum_{n=1}^{\infty} \frac{\alpha_n}{\alpha_0} \cos(nt) + \sum_{n=1}^{\infty} \frac{b_n}{\alpha_0} \sin(nt) \right] \quad (\text{Eq. 33})$$

where: α_n/α_0 and b_n/α_0 are dimensionless ratios of amplitude of periodic variation of pressure gradient normalized with the mean amplitude .

D. VELOCITY DISTRIBUTION AND ASYMPTOTIC EXPRESSIONS

The velocity profiles for laminar , pulsating flow constitute the initial conditions for any theoretical analysis of stability. Although no exact theoretical analysis of stability is presented in this work, solution for the velocity profiles will serve to identify the dimensionless parameters which are significant and will permit some qualitative deduction concerning the stability of pulsating flow.

From Eq. 16 we found that the periodic part of the velocity profile is characterized by the parameter $\delta R = \sqrt{n/\nu} R$.

The distribution of α_n / α_0 , the dimensionless velocity amplitude, obtained by Gilbrech and Combs , [Ref. 16] , is plotted in Figure 5.

Uchida, [Ref.23], obtained solutions for limiting values of the parameter δR by means of asymptotic expansions of the Bessel function:

1. Slow Oscillation ($\delta R \ll 1$)

When a highly viscous fluid oscillates slowly in a narrow pipe , δR becomes small and we can approximate:

$$\text{ber}(\delta R) \rightarrow 1 \quad \text{and} \quad \text{bei}(\delta R) \rightarrow 0$$

Using this approximation, we get from Eqs. 28 and 29

$$\frac{v_x}{U} = 2 \left[1 - \frac{r^2}{R^2} \right] \left[1 + \sum_{n=1}^{\infty} \frac{\alpha_n}{\alpha_0} \cos(nt) + \sum_{n=1}^{\infty} \frac{b_n}{\alpha_0} \sin(nt) \right]$$

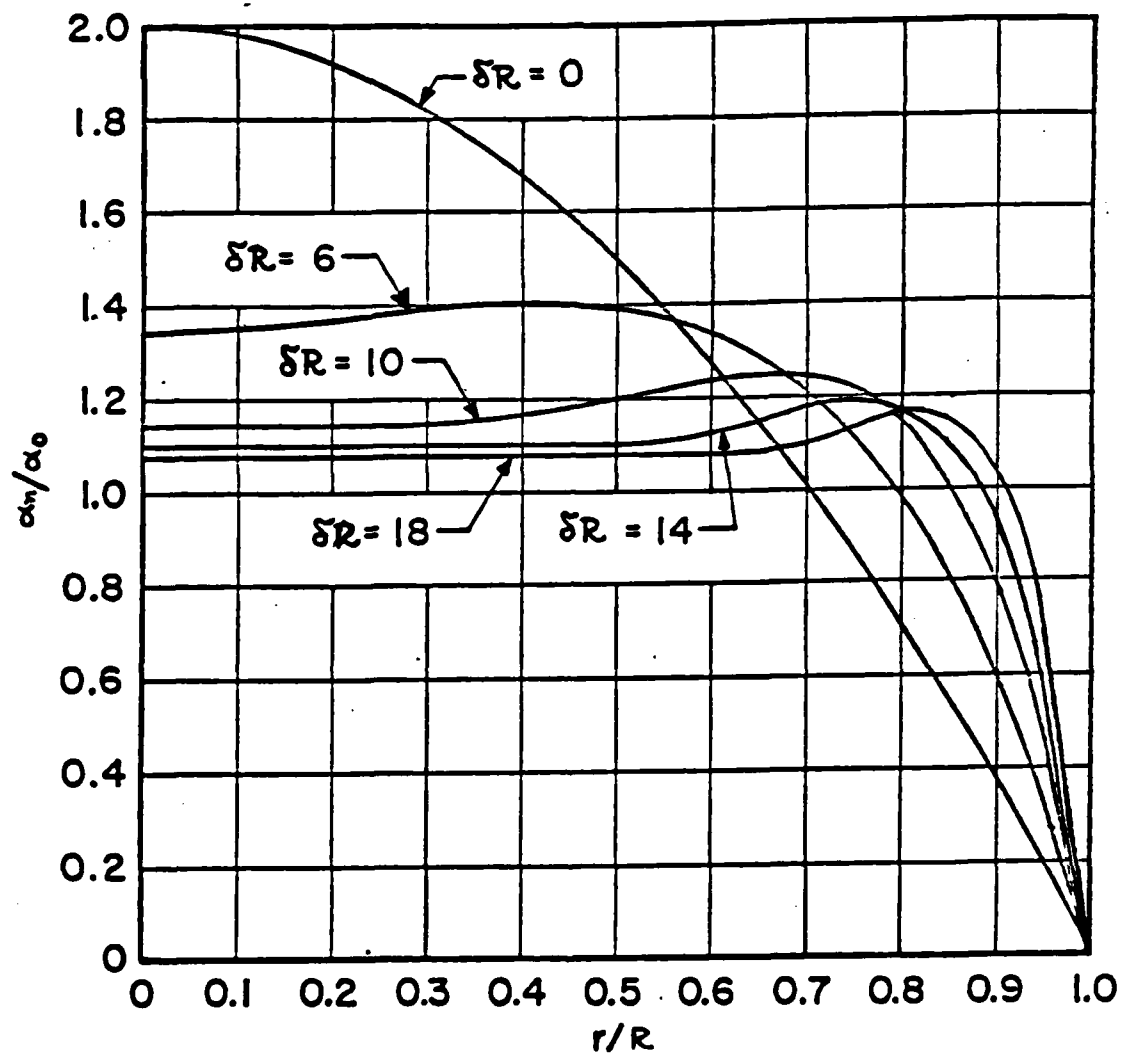


Figure 5. Oscillation Amplitude of the Local Velocity

$$\text{or: } \frac{v_x}{U} = 2 \left[1 - \frac{r^2}{R^2} \right] \frac{1}{\alpha_0} \left[-\frac{1}{\rho} \frac{\partial P}{\partial x} \right]$$

$$\text{or: } v_x = \frac{1}{4\nu} (R^2 - r^2) \left[-\frac{1}{\rho} \frac{\partial P}{\partial x} \right] \quad (\text{Eq. 34})$$

From this we conclude that the velocity distribution is a parabola, as in the case of steady Hagen - Poisseuille flow, while the magnitude of velocity varies periodically in phase with that of the pressure gradient.

2. Rapid Oscillation ($\delta R \rightarrow \infty$)

When a fluid of low viscosity oscillates rapidly in a large pipe, then parameter δR becomes large.

Assuming $\delta R > 10$, asymptotic expansion of Bessel functions may be introduced:

$$\left. \begin{aligned} \text{ber}(\delta R) &= \frac{e^{\delta R/2}}{2 \pi \delta R} \left\{ \cos \left[\frac{\delta R}{2} - \frac{\pi}{8} \right] + o \left[\frac{1}{\delta R} \right] \right\} \\ \text{bei}(\delta R) &= \frac{e^{\delta R/2}}{2 \pi \delta R} \left\{ \sin \left[\frac{\delta R}{2} - \frac{\pi}{8} \right] + o \left[\frac{1}{\delta R} \right] \right\} \end{aligned} \right\} \quad (\text{Eq. 35})$$

To examine the motion of the fluid near the center of the pipe, we put:

$$\delta R \rightarrow \infty \quad \text{and} \quad \delta r \rightarrow 0$$

As before we get:

$$\frac{v_x}{U} = 2 \left[1 - \frac{r^2}{R^2} \right] + \sum_{n=1}^{\infty} \frac{\alpha_n}{\alpha_0} \frac{8}{(\delta R)^2} \sin(nt) - \sum_{n=1}^{\infty} \frac{b_n}{\alpha_0} \frac{8}{(\delta R)^2} \cos(nt)$$

$$\text{or: } \frac{v_x}{U} = 2 \left[1 - \frac{r^2}{R^2} \right] + \sum_{n=1}^{\infty} \frac{\alpha_n}{\alpha_0} \frac{8}{(\delta R)^2} \cos \left[nt - \frac{\pi}{2} \right] +$$

$$+ \sum_{n=1}^{\infty} \frac{b_n}{\alpha_0} \frac{8}{(\delta R)^2} \sin \left[nt - \frac{\pi}{2} \right]$$

$$\text{or: } v_x = \frac{\alpha_0}{4\nu} (R^2 - r^2) + \sum_{n=1}^{\infty} \frac{\alpha_n}{n} \cos \left[nt - \frac{\pi}{2} \right] + \sum_{n=1}^{\infty} \frac{b_n}{n} \sin \left[nt - \frac{\pi}{2} \right]$$

(Eq. 36)

From this result we may conclude that in the case of rapid oscillation, fluid flows at the center of pipe with the phase lag of 90° behind the wave of pressure gradient and its amplitude diminishes with increasing frequency.

To examine motion of the fluid near the wall of the pipe, we put:

$$\delta R \rightarrow \infty \quad \text{and} \quad \delta R \rightarrow \infty$$

Using the same procedure we get:

$$\frac{v_x}{U} = 2 \left[1 - \frac{r^2}{R^2} \right] + \sum_{n=1}^{\infty} \frac{\alpha_n}{\alpha_0} \frac{8}{(\delta R)^2} \left\{ \sin(nt) - \sqrt{\frac{R}{r}} e^{-\frac{\delta(R-r)}{\sqrt{2}}} \sin \left[nt - \frac{\delta}{\sqrt{2}}(R-r) \right] \right\}$$

$$+ \sum_{n=1}^{\infty} \frac{b_n}{\alpha_0} \frac{8}{(\delta R)^2} \left\{ -\cos(nt) + \sqrt{\frac{R}{r}} e^{-\frac{\delta(R-r)}{\sqrt{2}}} \cos \left[nt - \frac{\delta}{\sqrt{2}}(R-r) \right] \right\} \quad (\text{Eq. 37})$$

Because of the obvious complexity of the expression, it is difficult to draw any simple conclusions other than to note that a local maximum in velocity develops in the neighborhood of the wall as it is shown in Fig. 5. We can also get a better confirmation from Figs. 6, 7 and 8, obtained from [Ref. 23], for values of $\delta R = 1, 3$ and 10 respectively.

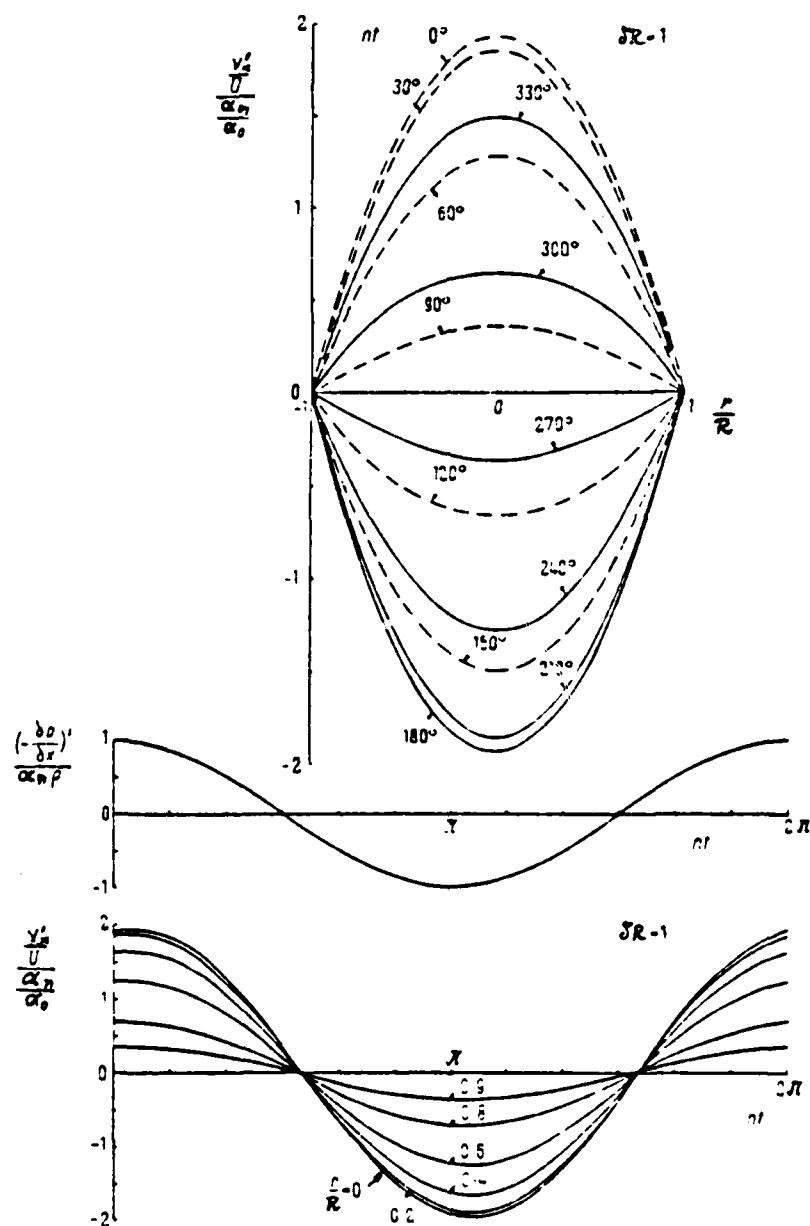


Figure 6. Velocity Profile for $\delta R = 1$

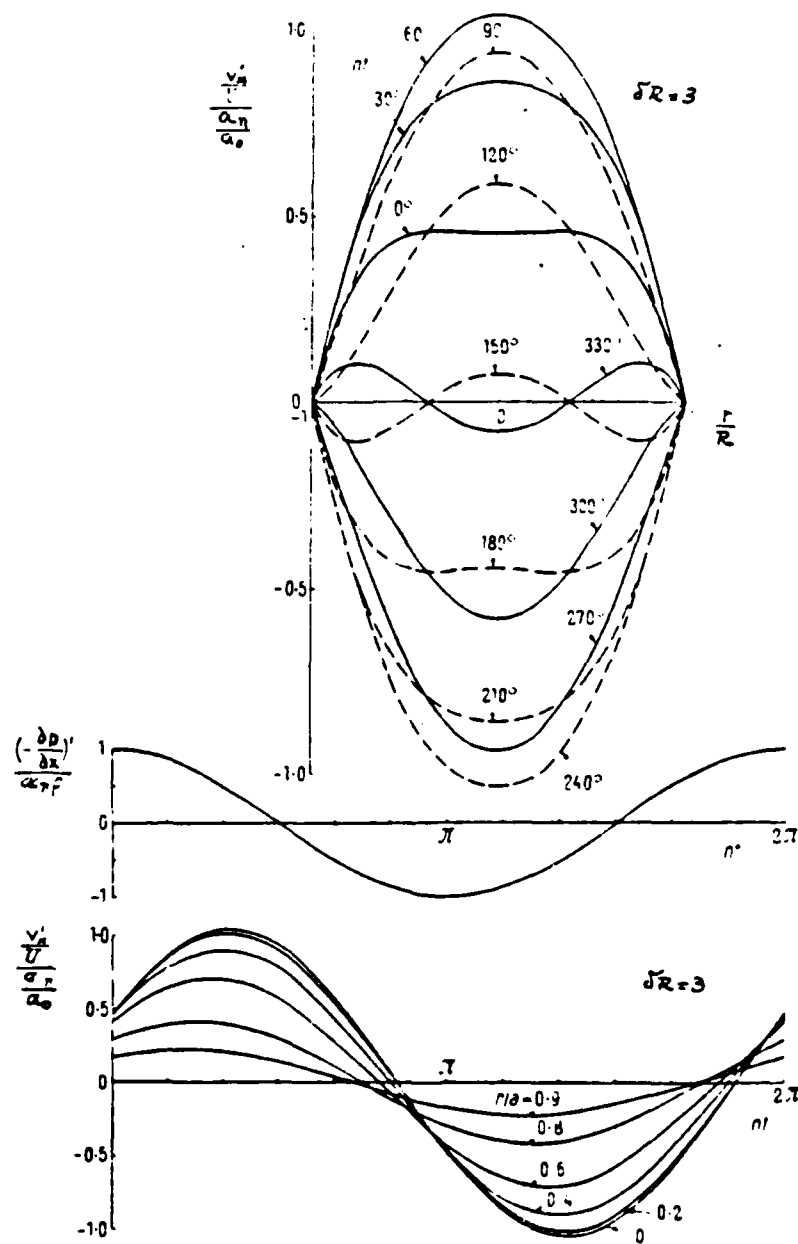


Figure 7. Velocity Profile for $\delta R = 3$

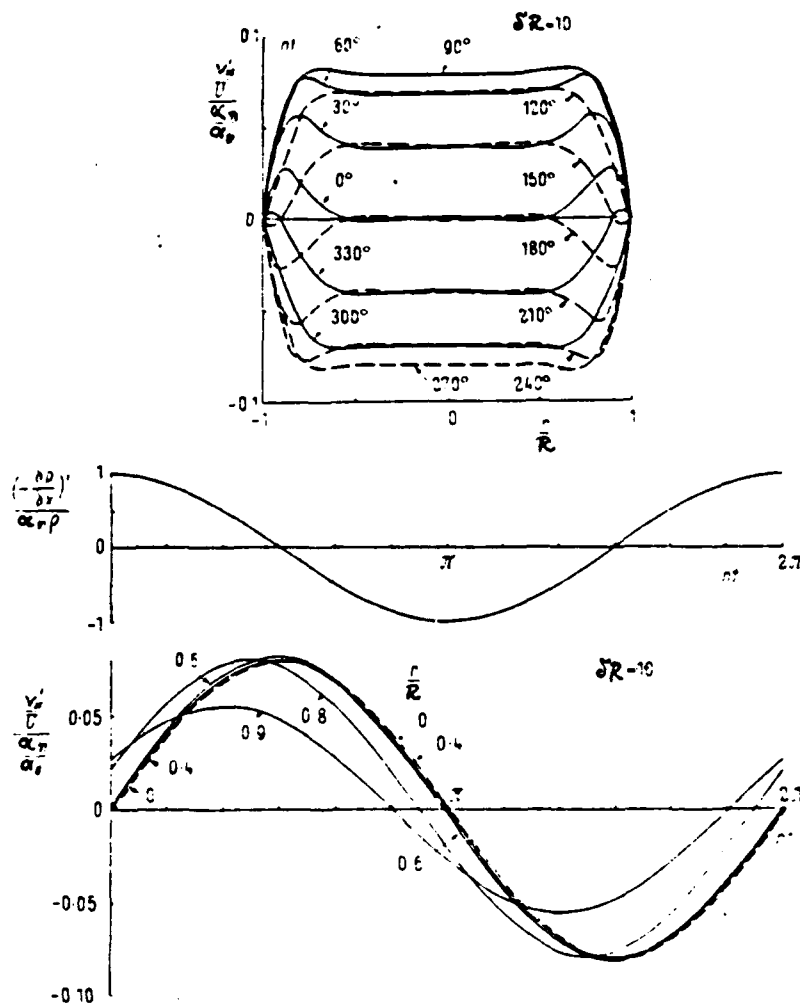


Figure 8. Velocity profile for $\delta R = 10$

E. SECTIONAL MEAN VELOCITY

Since the instantaneous mass flow and accordingly sectional mean velocity, are periodic functions, we seek to link the mean velocity with the applied pressure gradient.

Sectional mean velocity, denoted by v_{xm} , is given by:

$$v_{xm} = \frac{1}{\pi R^2} \int_0^R 2\pi v_x r dr \quad (\text{Eq. 38})$$

Introducing Eq. 34 and integrating we get:

$$\begin{aligned} \frac{v_{xm}}{U} = 1 + \sum_{n=1}^{\infty} \frac{\alpha_n}{\alpha_0} \frac{8}{(\delta R)^2} & \left[\frac{2D}{\delta R} \cos(nt) + \left[1 - \frac{2C}{\delta R} \right] \sin(nt) \right] + \\ & + \sum_{n=1}^{\infty} \frac{\alpha_n}{\alpha_0} \frac{8}{(\delta R)^2} \left[\frac{2D}{\delta R} \sin(nt) - \left[1 - \frac{2C}{\delta R} \right] \cos(nt) \right] \end{aligned} \quad (\text{Eq. 39})$$

where:

$$\text{ber}'(\delta R) = \frac{d[\text{ber}(\delta R)]}{d(\delta R)}, \quad \text{bei}'(\delta R) = \frac{d[\text{bei}(\delta R)]}{d(\delta R)} \quad (\text{Eq. 40})$$

and:

$$\left. \begin{aligned} C &= \frac{\text{ber}(\delta R)\text{bei}'(\delta R) - \text{bei}(\delta R)\text{ber}'(\delta R)}{\text{ber}^2(\delta R) + \text{bei}^2(\delta R)} \\ D &= \frac{\text{ber}(\delta R)\text{ber}'(\delta R) + \text{bei}(\delta R)\text{bei}'(\delta R)}{\text{ber}^2(\delta R) + \text{bei}^2(\delta R)} \end{aligned} \right\} \quad (\text{Eq. 41})$$

An example of simple periodic pulsation is given by:

$$-\frac{1}{\rho} \frac{\partial P}{\partial x} = \alpha_0 + \alpha_n \cos(nt) = \frac{1}{\rho} \left[-\frac{\partial P}{\partial x} \right] + \frac{1}{\rho} \left[-\frac{\partial P}{\partial x} \right]' \quad (\text{Eq. 42})$$

where:

$$\frac{1}{\rho} \left[-\frac{\partial P}{\partial x} \right] = \alpha_0 \quad (\text{average term})$$

$$\frac{1}{\rho} \left[-\frac{\partial P}{\partial x} \right]' = \alpha_n \cos nt \quad (\text{perturbation term})$$

Inserting the above relation into Eq. 39 we get:

$$\frac{v_{xm}}{U} = 1 + \frac{\alpha_n}{\alpha_0} \frac{8}{(\delta R)_2} \left[\frac{2D}{\delta R} \cos(nt) + \left[1 - \frac{2C}{\delta R} \right] \sin(nt) \right]$$

$$\text{or: } \frac{v_{xm}}{U} = 1 + \frac{\alpha_n}{\alpha_0} \frac{8}{(\delta R)^2} \left[1 - \frac{2C}{\delta R} \right]^2 + \left[\frac{2D}{\delta R} \right]^2 \cos(nt - \phi_v)$$

$$\text{or: } \frac{v_{xm}}{U} = 1 + \frac{\alpha_n}{\alpha_0} A_v \cos(nt - \phi_v) \quad (\text{Eq. 43})$$

where:

$$A_v = \frac{8}{(\delta R)^2} \sqrt{\left[1 - \frac{2C}{\delta R} \right]^2 + \left[\frac{2D}{\delta R} \right]^2}$$

is the coefficient of amplitude, and:

$$\phi_v = \tan^{-1} \left[\frac{1 - 2C/\delta R}{2D/\delta R} \right] = \tan^{-1} \left[\frac{\delta R - 2C}{2D} \right]$$

represents the coefficient of phase lag in the wave of pressure gradient.

In Fig. 9, obtained from [Ref. 23], are plotted the coefficients of amplitude and phase lag of mean velocity as a function of the parameter ωR .

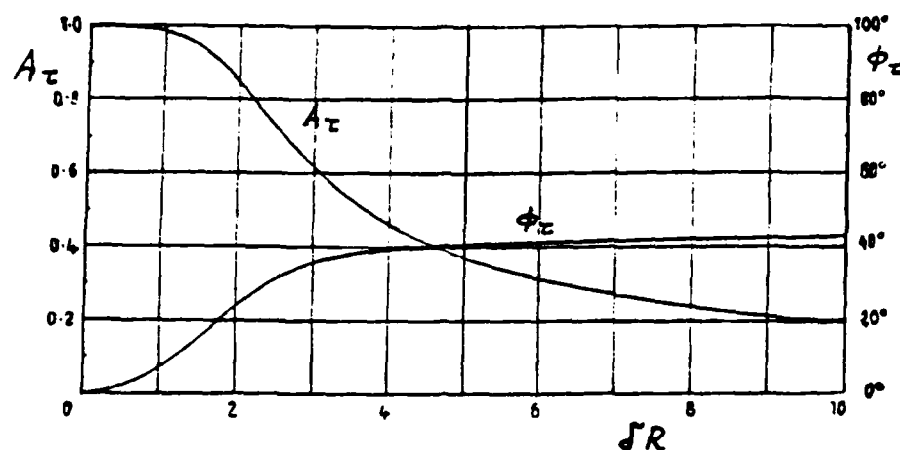


Figure 9. Coefficients of Amplitude and Phase Lag of Mean Velocity.

F. SURFACE FRICTION AND BALANCE OF FORCE

The instantaneous frictional force acting on the pipe wall is given by:

$$\tau = -\mu \left[\frac{dv_x}{dr} \right]_{r=R} \quad (\text{Eq. 44})$$

Dividing Eq. 44 by $(\rho U^2/2)$, and combining with the previously obtained Eqs. 32, 39 and 40 we can get:

$$\begin{aligned} \frac{2\tau}{\rho U^2} = & \frac{16}{\text{Re}} \left[1 + \sum_{n=1}^{\infty} \frac{\alpha_n}{\alpha_0} \left[\frac{2C}{\delta R} \cos(nt) + \frac{2D}{\delta R} \sin(nt) \right] + \right. \\ & \left. + \sum_{n=1}^{\infty} \frac{b_n}{\alpha_0} \left[\frac{2C}{\delta R} \sin(nt) - \frac{2D}{\delta R} \cos(nt) \right] \right] \quad (\text{Eq. 45}) \end{aligned}$$

Considering the simple periodic pulsation described by Eq. 42 we get:

$$\begin{aligned} \frac{2\tau}{\rho U^2} &= \frac{16}{\text{Re}} \left[1 + \frac{\alpha_n}{\alpha_0} \left[\frac{2C}{\delta R} \cos(nt) + \frac{2D}{\delta R} \sin(nt) \right] \right] \\ \text{or: } \frac{2\tau}{\rho U^2} &= \frac{16}{\text{Re}} \left[1 + \frac{\alpha_n}{\alpha_0} A_{\tau} \cos(nt - \phi_{\tau}) \right] \\ \text{or: } \tau &= \frac{4\rho v U}{\text{Re}} \left[1 + \frac{\alpha_n}{\alpha_0} A_{\tau} \cos(nt - \phi_{\tau}) \right] \quad (\text{Eq. 46}) \end{aligned}$$

where:

$$A_{\tau} = \sqrt{\left[\frac{2C}{\delta R} \right]^2 + \left[\frac{2D}{\delta R} \right]^2}$$

represents the coefficient of amplitude of shearing stress at the wall, and:

$$\phi_{\tau} = \tan^{-1} \left[\frac{D}{C} \right]$$

represents the coefficient of phase lag of shearing stress with respect to the wave of pressure gradient.

In the Fig. 10 below , obtained from [Ref. 23], it is shown how the coefficient of amplitude and phase lag of shear stress varies with δR .

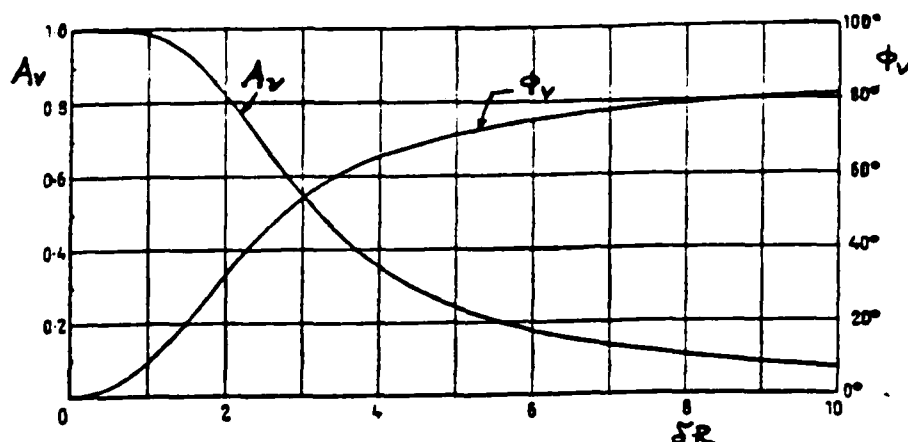


Figure 10. Coefficients of Amplitude and Phase Lag of the Shearing Stress

If we compare Figs. 9 and 10 we observe no substantial differences in amplitude or phase lags. Moreover, the phase of the sectional mean velocity is greatly delayed with respect to the pulsating wave of pressure gradient, while that of shearing stress is less delayed from it.

Using Eq. 8 and integrating over the section of the pipe, from $r=0$ to $r=R$, we can obtain a relationship between the force and acceleration of amass of fluid enclosed in the circular cylinder of unit length:

$$-\pi R^2 \frac{\partial P}{\partial x} = \pi R^2 \rho \frac{dv_{xm}}{dt} + 2 \pi R \tau$$

$$\text{or: } \frac{1 - \partial P / \partial x}{2 \rho U^2 / 4R} = \frac{dv_{xm} / dt}{U^2 / 2R} + \frac{4\tau}{\rho U^2} \quad (\text{Eq. 47})$$

For the present example of a simple periodic pulsation we find the mean frictional force , involved in the shear stress , is just balanced by the term of mean pressure gradient and there results no steady acceleration. The various terms appearing in Eq. 47 are shown in Fig. 11 below , obtained from [Ref. 23].

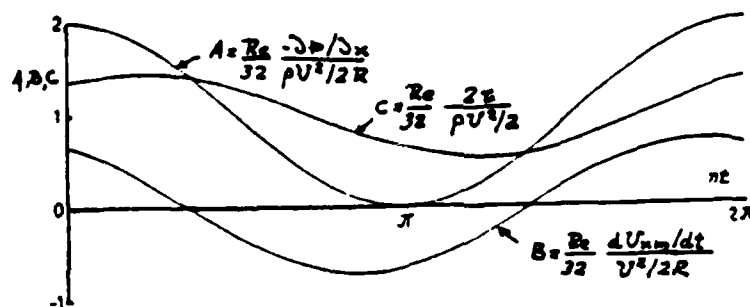


Figure 11. Periodic Force Component (A - Pressure Gradient, B - Acceleration , C - Shearing Force)

IV. RESULTS AND CONCLUSIONS

A. PRELIMINARY RESULTS

After a preliminary survey of the phenomenon of jet breakdown at a single laminar and single turbulent Reynolds number, as mentioned above, it was found that the field was so rich in information that a third, transitional Reynolds number of 2200 was added to the survey. Observations reported are of the most distinctive phenomena at each of the three Reynolds numbers and were observed to occur most frequently at frequencies which were multiples of 33 and 50 Hz. Results include two photographs at each data point of two separate phases along with an oscillogram showing both the excitation waveform and the pressure perturbation it produced, shown in Figs. 13 through 36. Table I is a summary of the observed breakdown length as a function of the frequency and Table II is a summary of oscilloscope and flow parameters, corresponding to each figure.

As Hoyt and Taylor, [Ref. 24], pointed out, jets are unstable to two kinds of disturbances, **axial** and **helical**. Theory suggests that the axial instability (corresponding to the initial waves on the jet surface) die out after a few nozzle diameters downstream and the helical instabilities, amplified by aerodynamic resistance, lead to the final jet

breakup. The initial slight helical motion is amplified until the entire jet may be described as having a corkscrew-like motion. This is well confirmed by the photos obtained in the present work of the jet formation before and after the breakdown and is in good agreement with the observations obtained by Crow and Champagne, [Ref. 4].

TABLE I

SUMMARY OF BREAKDOWN DISTANCE

f (Hz)	#d (Re=1760)	#d (Re=2200)	#d (Re=2640)
0	118.0	125.0	30.0
33	112.6	120.6	31.5
50	110.0	112.0	34.0
66	106.3	103.7	32.2
100	102.0	98.5	29.5
133	98.6	99.2	33.7
150	95.5	100.0	35.0
166	92.7	101.7	37.8
200	88.0	102.5	41.0
233	85.2	101.2	45.2
250	83.5	99.0	49.0
266	81.5	101.5	47.6
300	91.2	88.0	45.0
333	96.1	97.5	44.1
350	101.8	110.3	43.3
366	110.0	121.0	42.0
400	112.0	125.0	42.5

Re = Reynolds Number

f = Introduced Frequency

#d = Number of Diameters

TABLE II

SUMMARY OF EXPERIMENTAL CONDITIONS

Fig.#	Re	f (Hz)	V _p (mV/cm)	V _g (mV/cm)	t/cm (msec/cm)
13	1760	50	5	10	5
14	1760	100	5	10	5
15	1760	150	5	10	2
16	1760	200	5	10	2
17	1760	250	5	10	2
18	1760	270	5	10	2
19	1760	300	5	10	2
20	1760	380	5	10	2
21	2200	50	5	10	5
22	2200	100	5	10	5
23	2200	150	5	10	2
24	2200	200	5	10	2
25	2200	233	5	10	2
26	2200	250	5	10	2
27	2200	266	5	10	2
28	2200	300	5	10	2
29	2200	380	10	10	1
30	2200	787	20	20	0.5
31	2640	50	5	10	5
32	2640	100	5	10	2
33	2640	200	5	10	2
34	2640	250	10	10	2
35	2640	300	10	10	1
36	2640	600	10	10	0.5

Re : Reynolds number

f : Introduced Frequency

V_p : Signal Amplitude from Pressure Transducer

V_g : Signal Amplitude from Frequency Generator

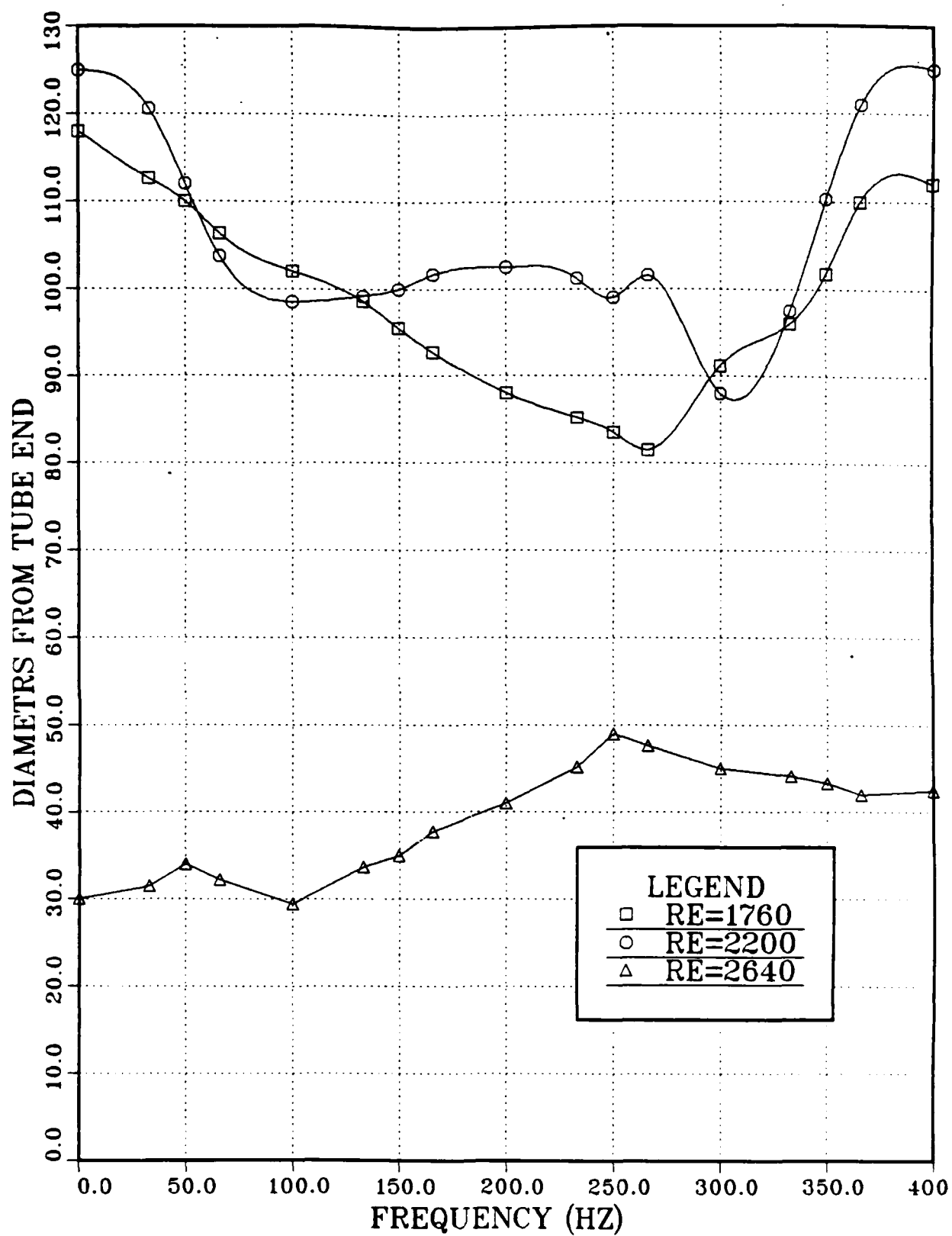


Figure 12. Breakdown Length Versus Frequency

1. Laminar Flow at Reynolds Number 1760

At this Reynolds number the unexcited flow started to breakdown at approximately 118 diameters from the tube exit. Increasing the frequency to 266 Hz produced a gradually movement of the breakdown point upstream to approximately 81.5 diameters from the exit. Above this frequency a reversed trend appeared and the breakdown point started to move downstream as the flow became laminar similar to the unexcited flow, the only difference being in the droplets formed after the breakdown. This phenomenon may be characterized as a **relaminarization** of the flow and was almost complete at 380 Hz. Further increasing of the frequency up to 1000 Hz produced no significant effect in the jet flow.

Results for Reynolds number 1760 are shown in Figs. 13 through 20. As can be observed from the photos, breakdown point is not fixed and oscillates somewhat upstream and downstream, creating a breakdown region. The amplitude of this oscillation was **reduced** as the perturbation frequency was **increased**, starting from about 14 diameters and approaching 4 diameters as the frequency changed from 200 to 266 Hz. At 266 Hz an especially interesting phenomenon was observed concerning the breakdown point and the droplet formation. The breakdown of the jet occurred at the minimum observed distance from the tube exit at 81.5 diameters.

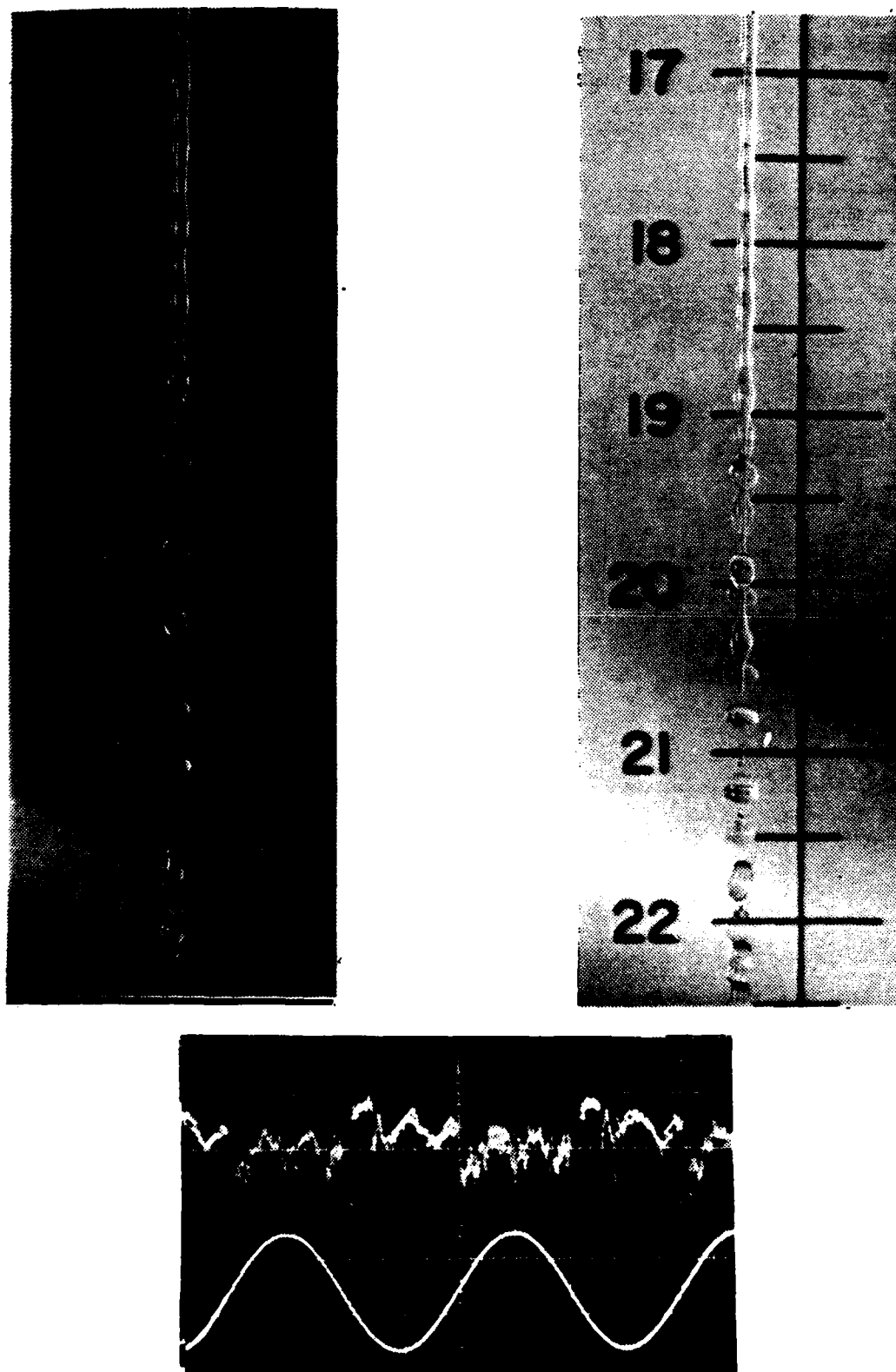


Figure 13. Photos Illustrating Jet Breakdown and Oscilloscope Trace of Pressure at $Re=1760$ and $f=50$ Hz

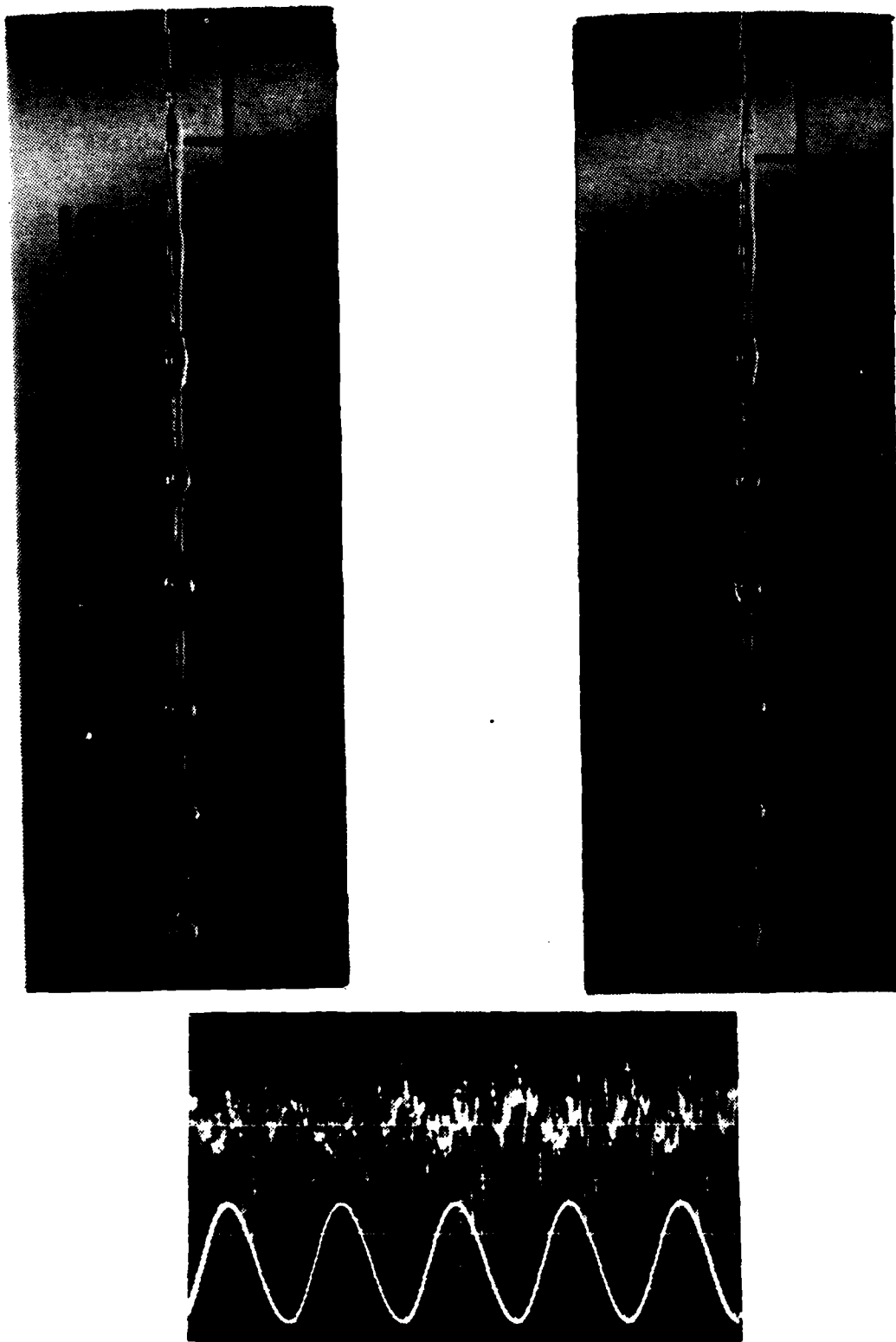


Figure 14. Photos Illustrating Jet Breakdown and Oscilloscope Trace of Pressure at $Re=1750$ and $f=100$ Hz

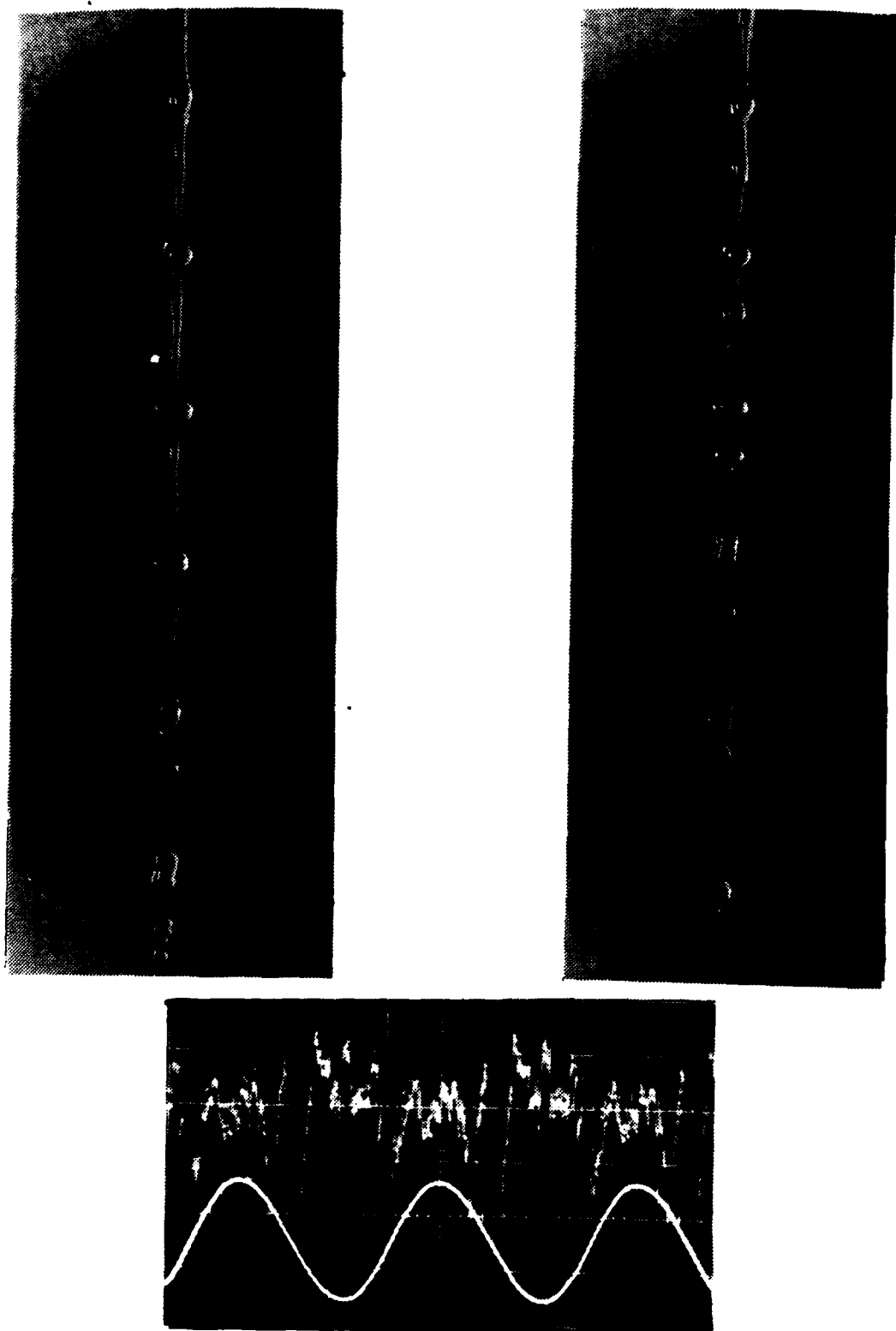


Figure 15. Photos Illustrating Jet Breakdown and Oscilloscope Trace of Pressure at $Re=1760$ and $f=150$ Hz

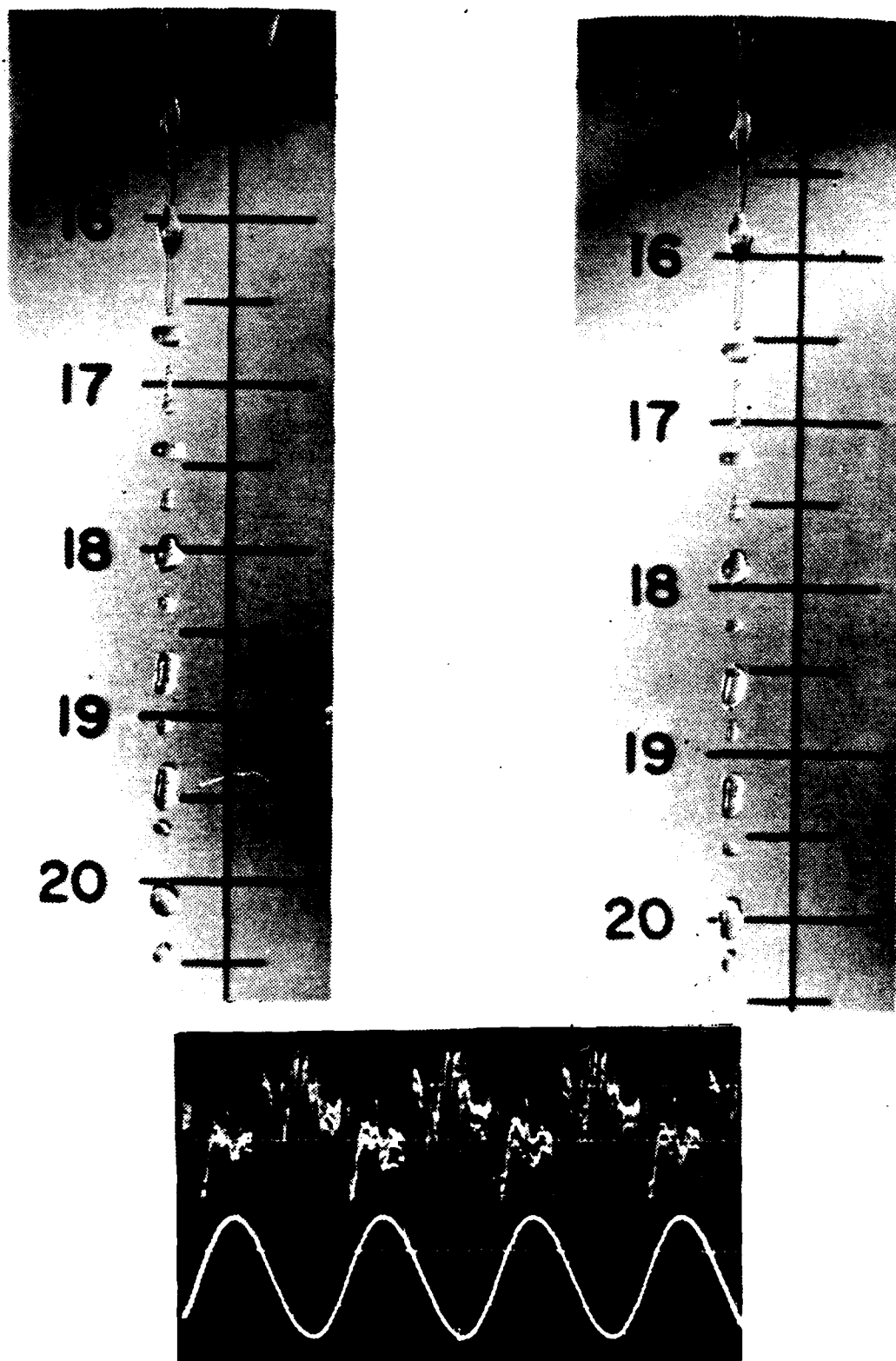


Figure 16. Photos Illustrating Jet Breakdown and Oscilloscope Trace of Pressure at $Re=1760$ and $f=200$ Hz

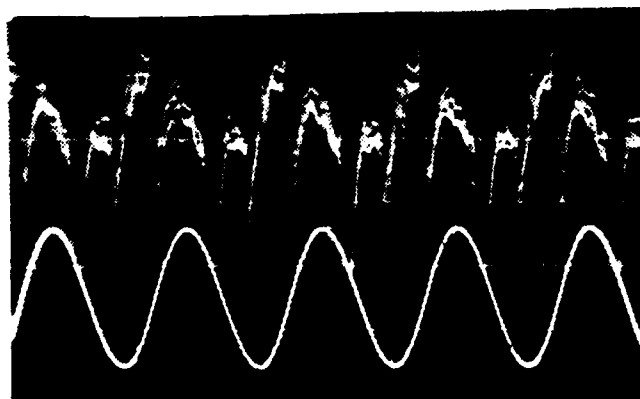
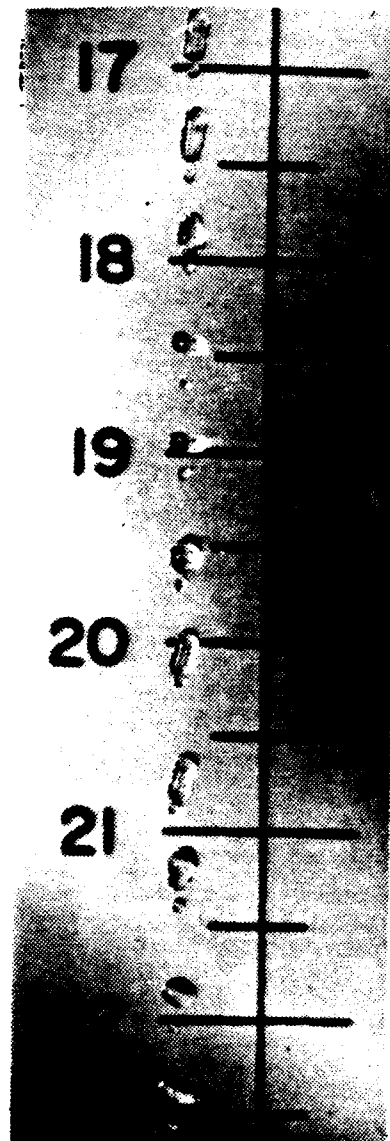
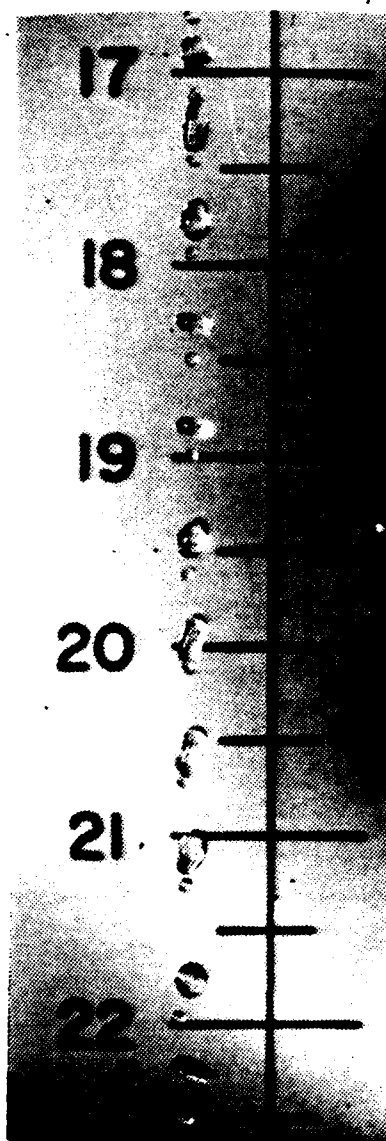


Figure 17. Photos Illustrating Jet Breakdown and Oscilloscope Trace of Pressure at $Re=1760$ and $f=250$ Hz

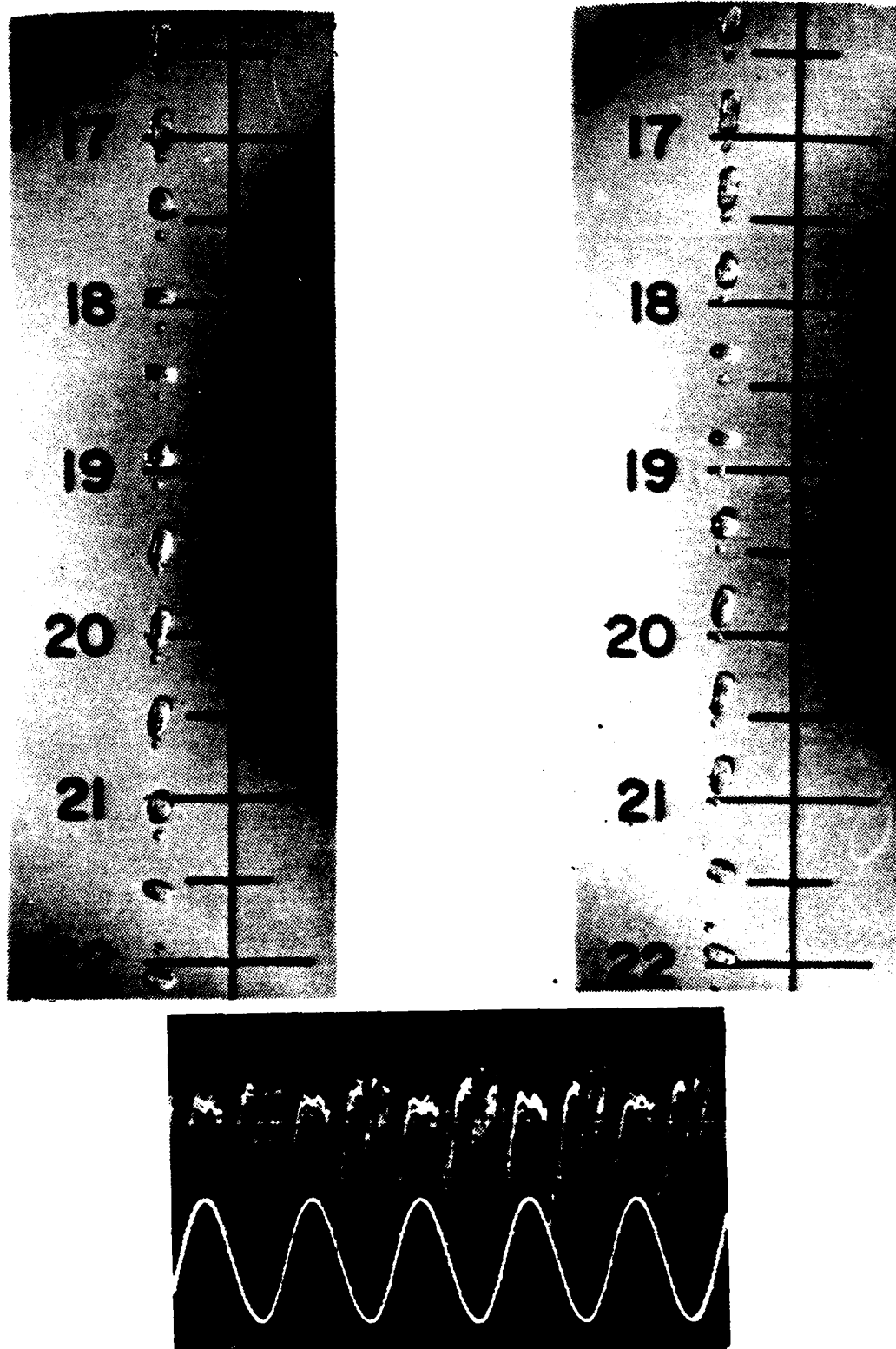


Figure 18. Photos Illustrating Jet Breakdown and Oscilloscope Trace of Pressure at $Re=1760$ and $f=266$ Hz

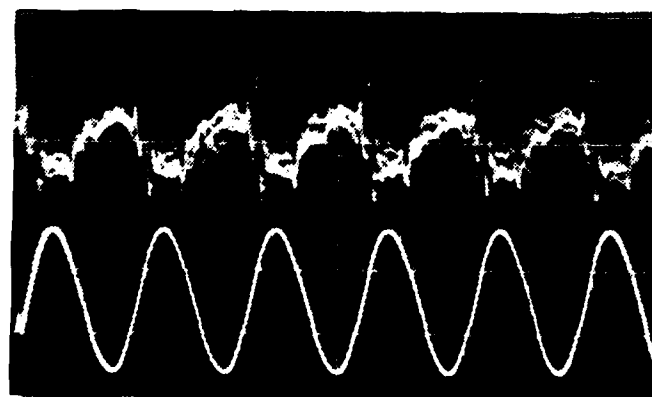
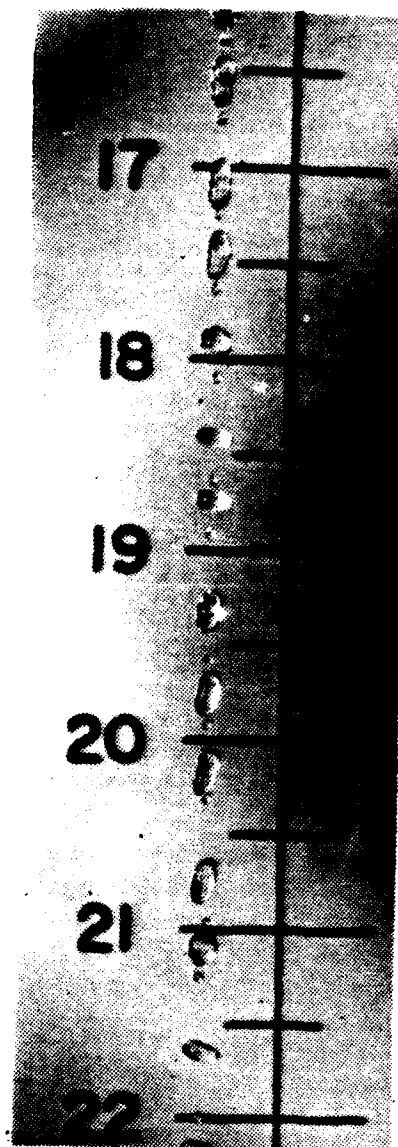
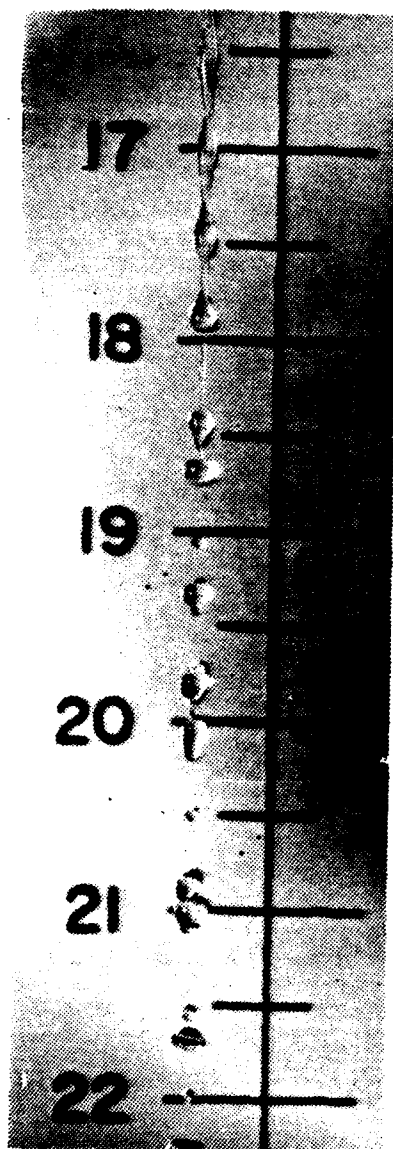


Figure 19. Photos Illustrating Jet Breakdown and Oscilloscope Trace of Pressure at $Re=1760$ and $f=300$ Hz

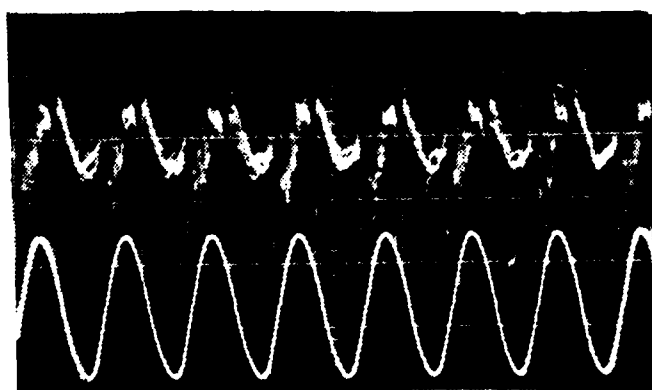
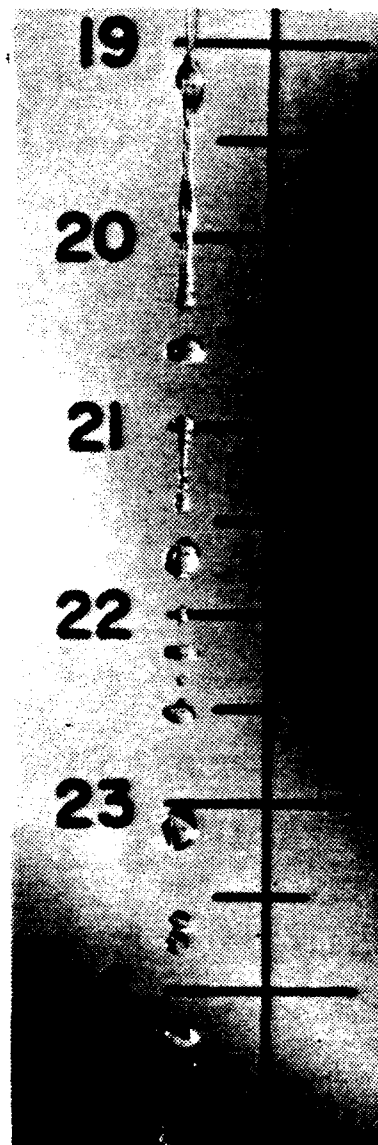
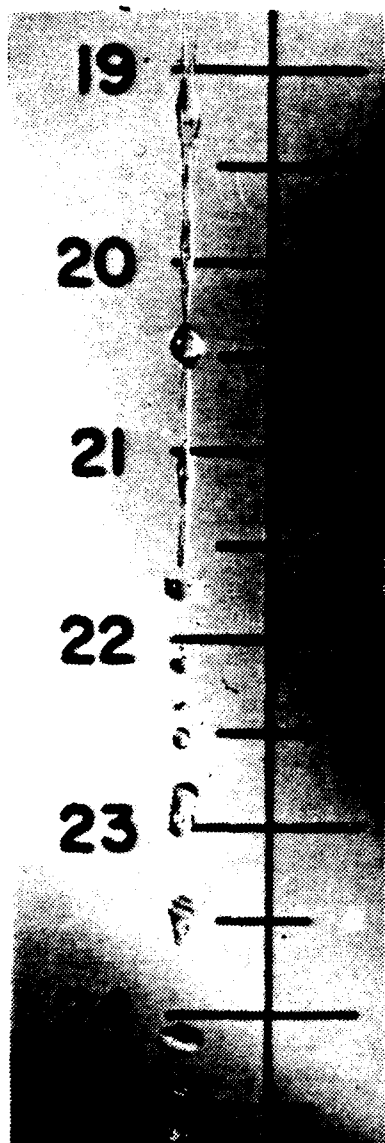


Figure 20. Photos Illustrating Jet Breakdown and Oscilloscope Trace of Pressure at $Re=1760$ and $f=380$ Hz

The oscillation of the breakdown point was minimized to about 4 diameters and the droplets formed, as was observed with the aid of the stroboscope, were exactly the same and appeared stationary in space. This is shown in the jet photos of Fig. 18.

A plot of the breakdown distance as a function of frequency is provided in Fig. 13 where we see that, in the frequency range from zero to 266 Hz, an almost linear variation of the breakdown point with frequency occurs. The minimum at 266 Hz may be characterized as a critical frequency for this specific Reynolds number. Above this frequency one also observes an almost linear variation of the average breakdown point to 380 Hz. This region may be characterized as relaminarization region. The slope of the breakdown curve is greater than at lower frequencies although increasing the frequency above 380 Hz results a zero slope curve, as discussed above.

2. Transitional Flow at Reynolds Number 2200

At this Reynolds number the unexcited flow started to breakdown at approximately 125 diameters from the tube exit. Increasing the frequency to 100 Hz, the breakdown point moved upstream up to about 98 diameters from the tube exit. The oscillation of the breakdown point was reduced at this case, from 12 to 6 diameters.

Increasing the frequency to 266 Hz resulted in only slight variation of the breakdown point . The only unusual observation in this range of frequency was the drastic reduction of the amplitude of breakdown point oscillation as the frequency was increased .

An interesting pressure effect was observed at 266 Hz, as can be seen at Fig. 27 , where a maximum amplitude of pressure signal was recorded.

An interesting change was observed when the frequency reached 300 Hz . The breakdown point was displaced suddenly about 25 diameters upstream and nearly stabilized at 88 diameters . The droplets viewed with the aid of the stroboscope appeared immobile and any oscillation of the breakdown point was difficult to observe . Based on a series of high speed photos it was concluded that the breakdown point was oscillating with an amplitude of about 2 diameters . Also observed at this frequency that the waveforms obtained from the signal generator and the pressure transducer were almost in phase and moreover, the latter waveform appeared nearly sinusoidal as shown in Fig. 28.

Further frequency increases resulted in a flow relaminarization as was observed and discussed in the previous case. A completely laminar flow was observed at a frequency of 380 Hz and no additional significant effects were observed up to 2000 Hz .

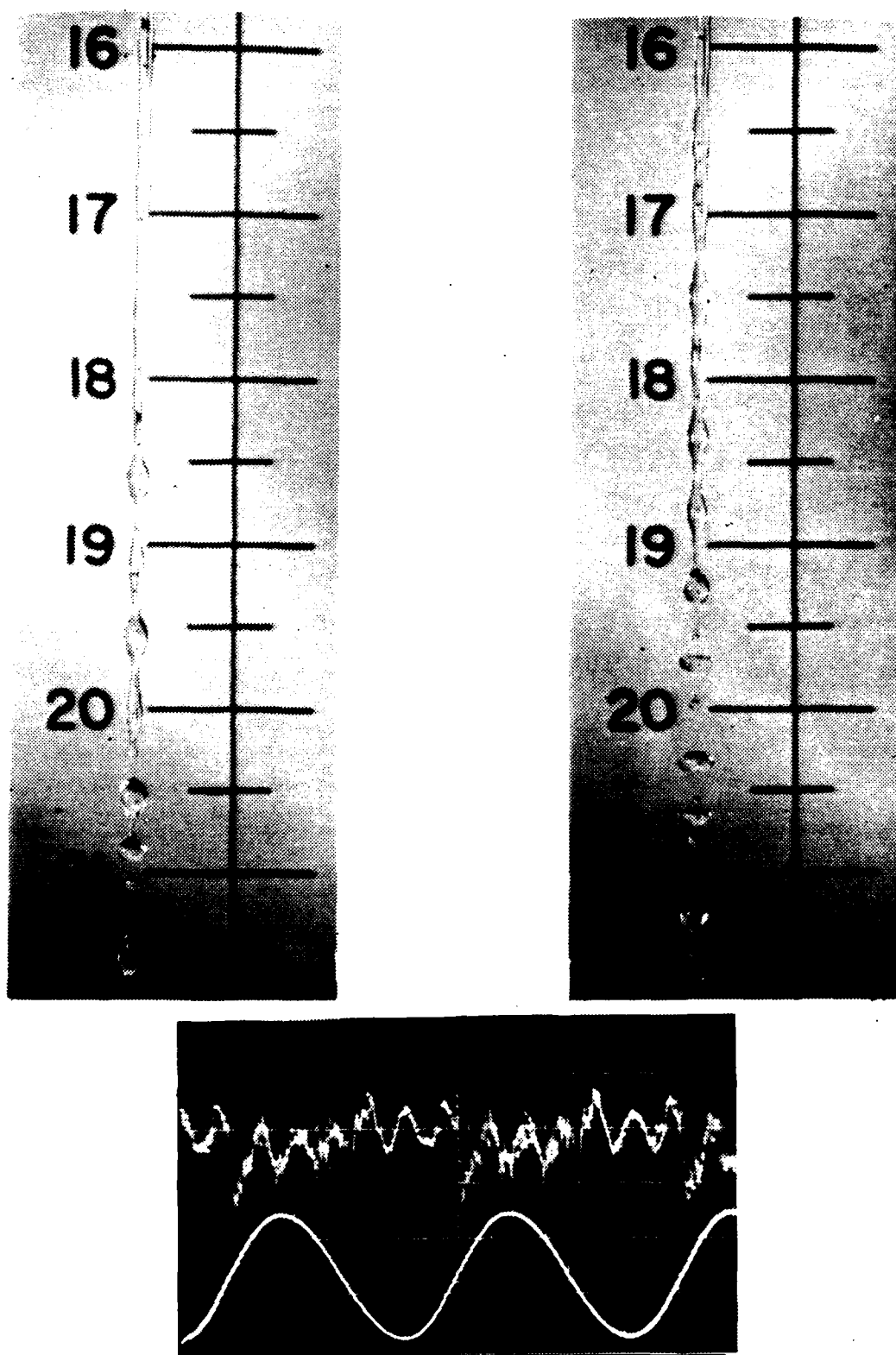


Figure 21. Photos Illustrating Jet Breakdown and Oscilloscope Trace of Pressure at $Re=2200$ and $f=50$ Hz

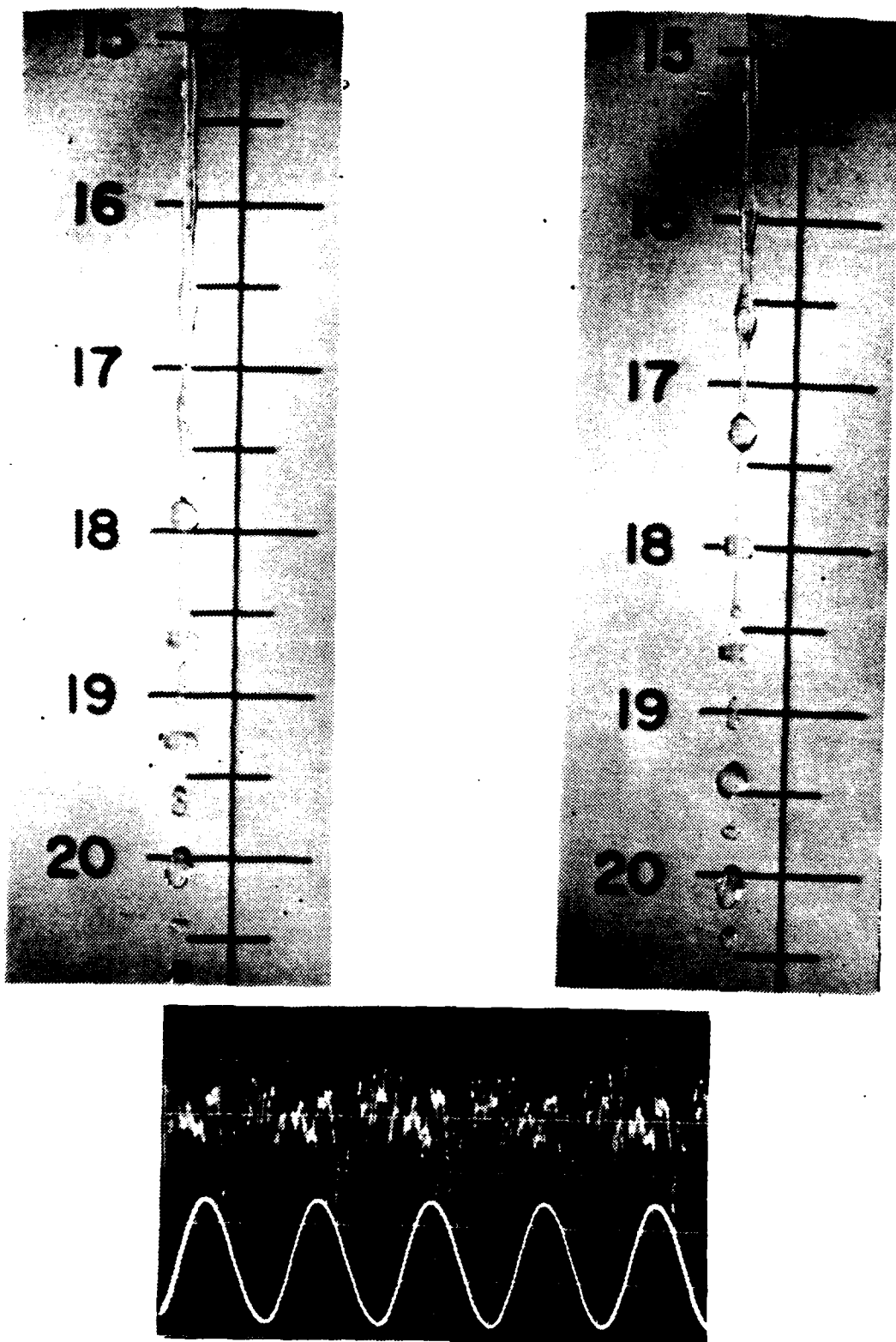


Figure 22. Photos Illustrating Jet Breakdown and Oscilloscope Trace of Pressure at $Re=2200$ and $f=100$ Hz

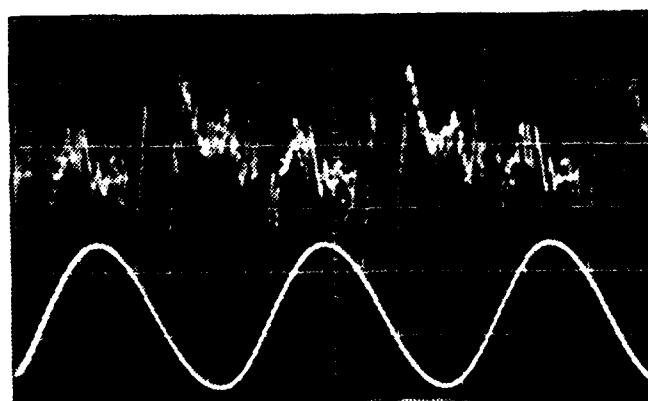
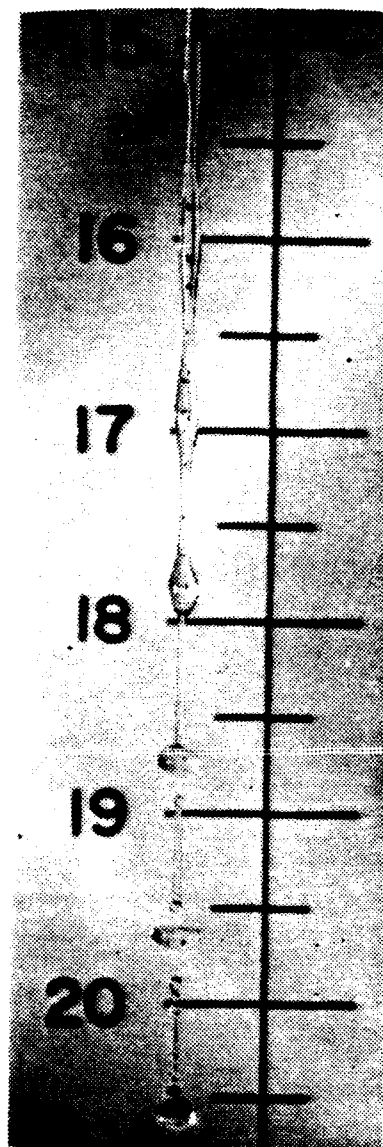
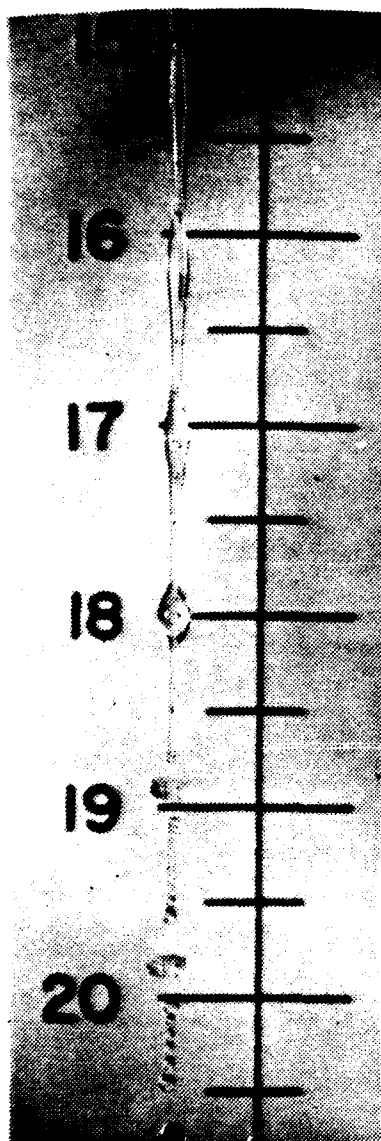


Figure 23. Photos Illustrating Jet Breakdown and Oscilloscope Trace of Pressure at $Re=2200$ and $f=150$ Hz

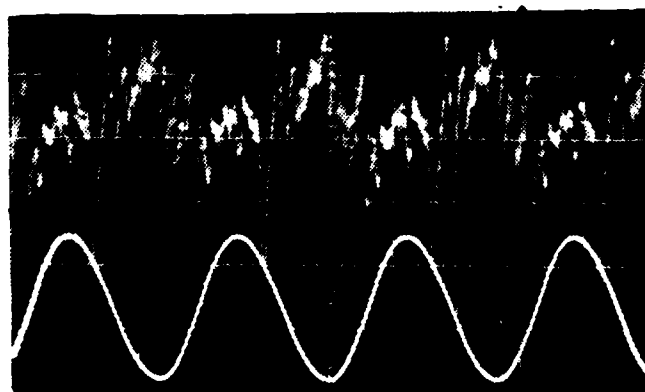
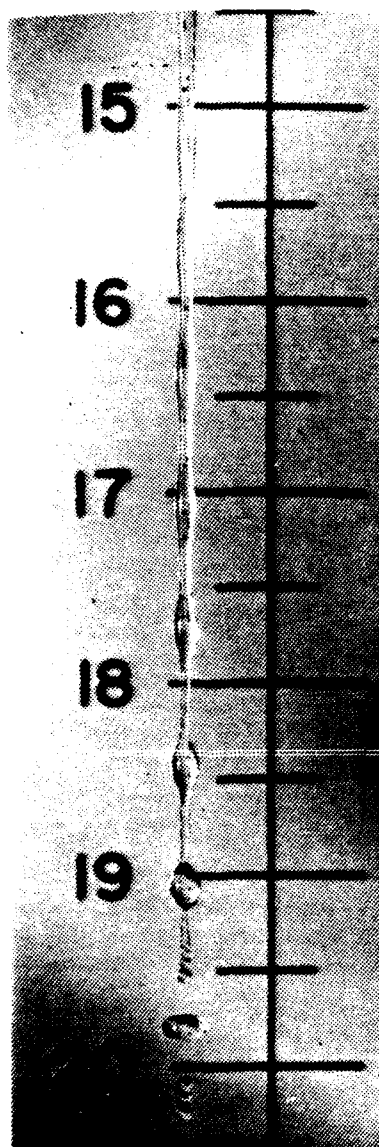


Figure 24. Photos Illustrating Jet Breakdown and Oscilloscope Trace of Pressure at $Re=2200$ and $f=200$ Hz

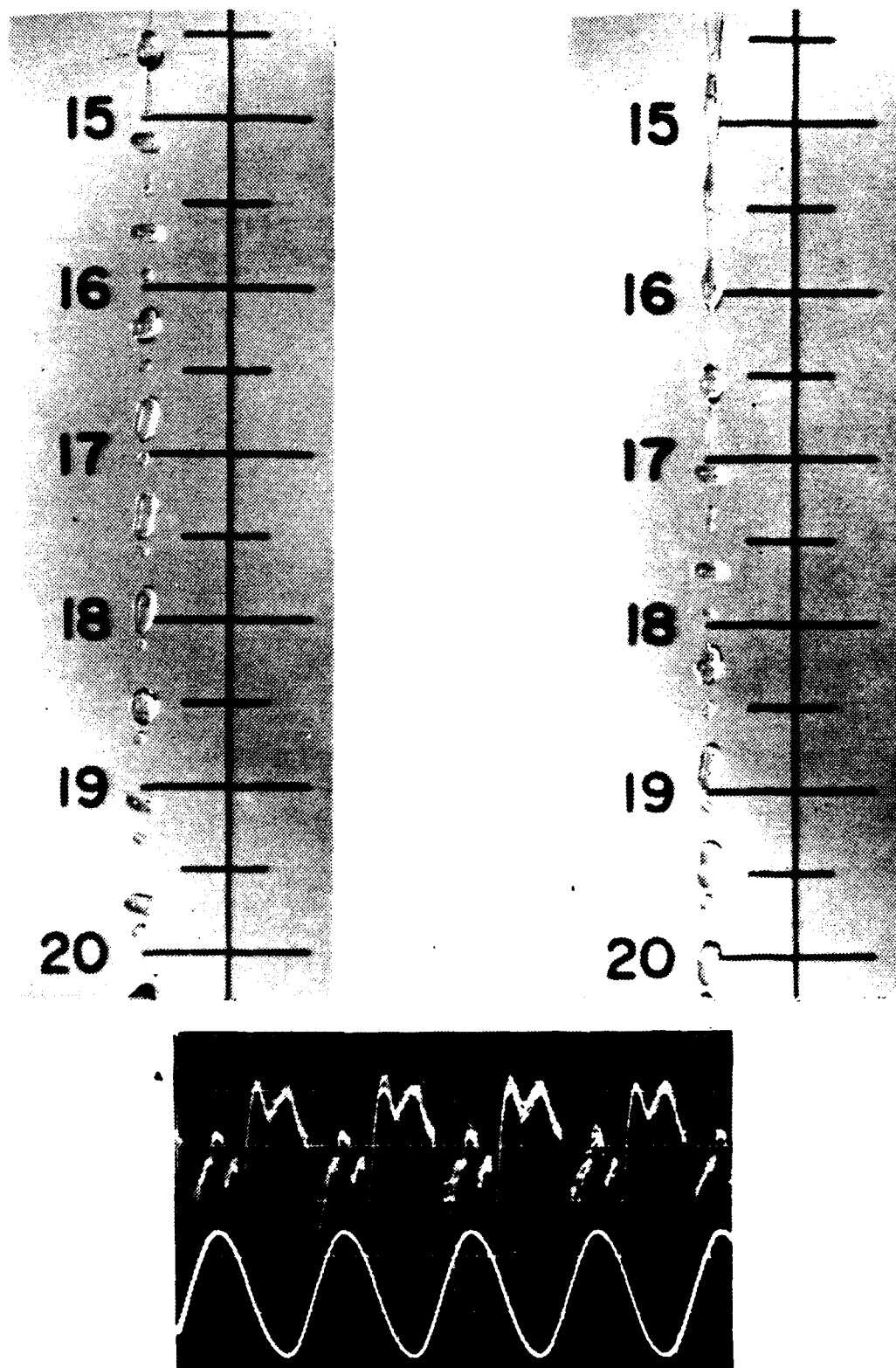


Figure 25. Photos Illustrating Jet Breakdown and Oscilloscope Trace of Pressure at $Re=2200$ and $f=233$ Hz

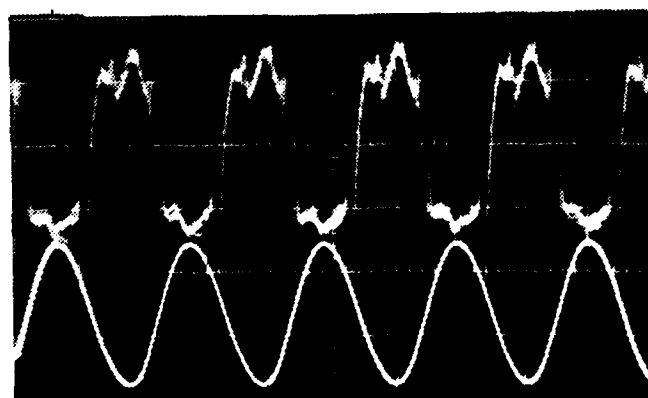
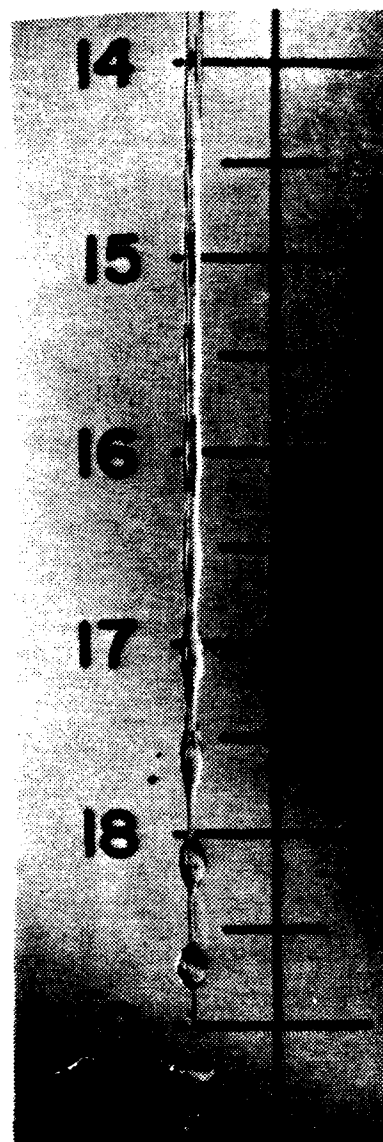
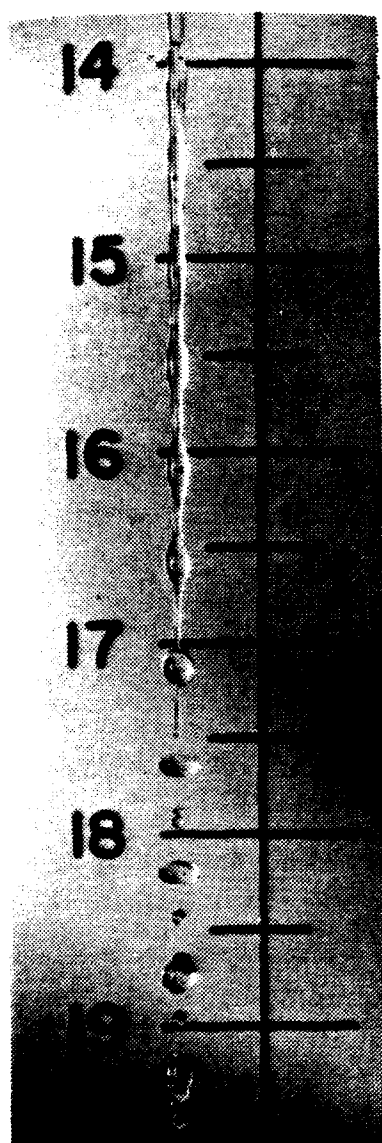


Figure 26. Photos Illustrating Jet Breakdown and Oscilloscope Trace of Pressure at $Re=2200$ and $f=250$ Hz

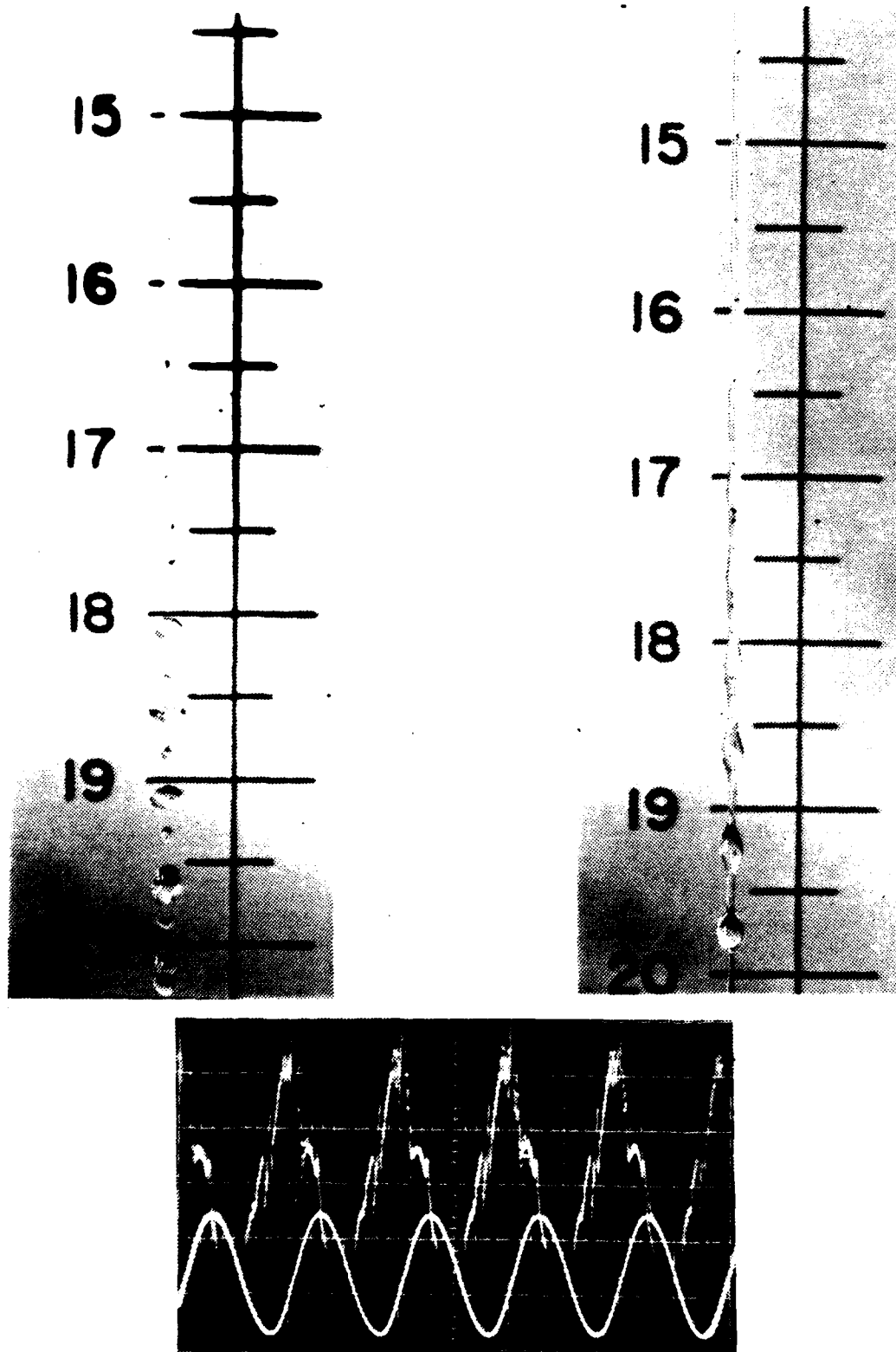


Figure 27. Photos Illustrating Jet Breakdown and Oscilloscope Trace of Pressure at $Re=2200$ and $f=266$ Hz

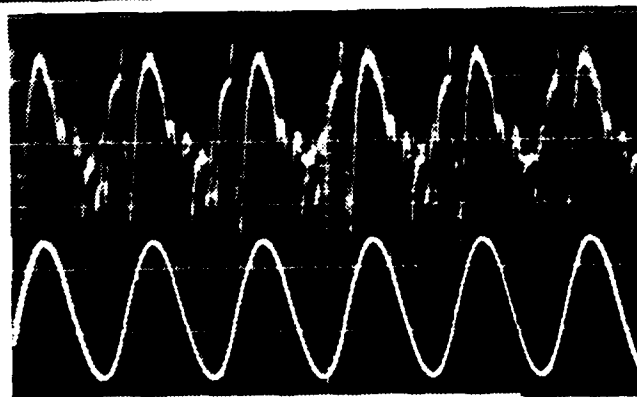
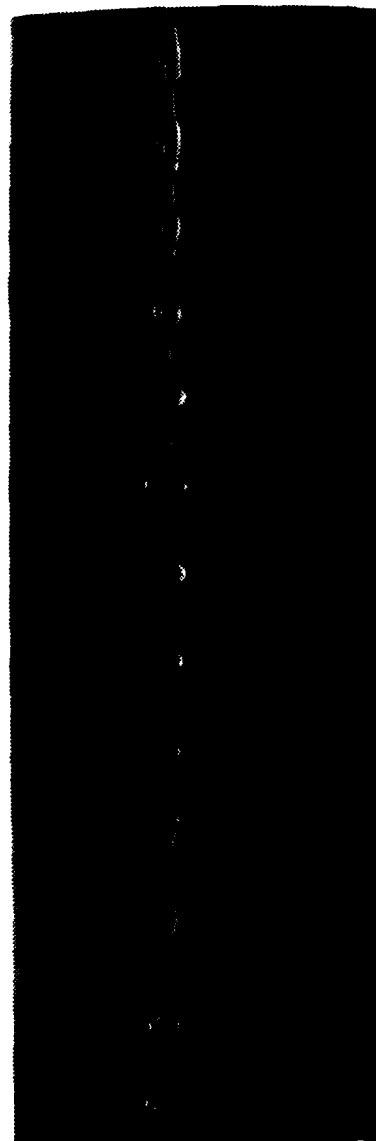
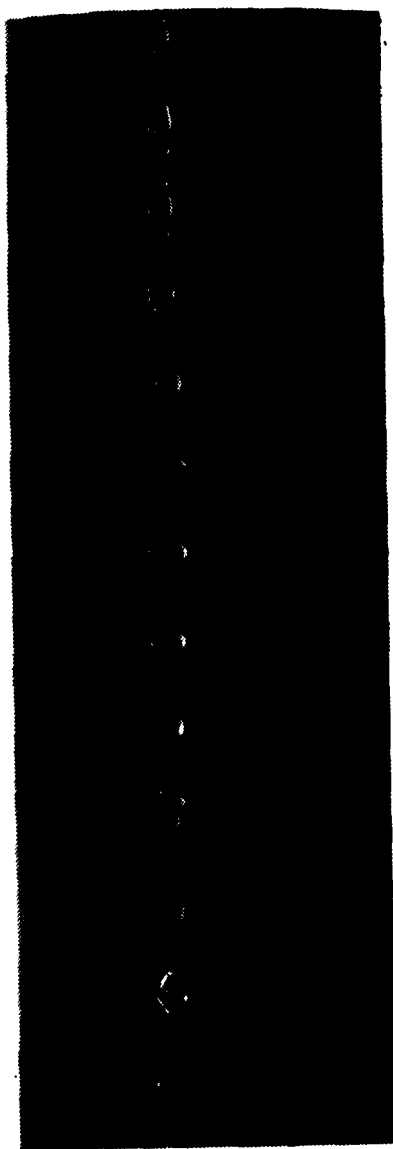


Figure 28. Photos Illustrating Jet Breakdown and Oscilloscope Trace of Pressure at $Re=2200$ and $f=300$ Hz

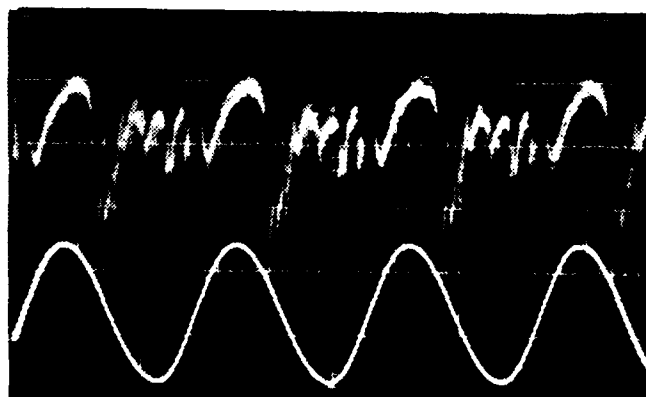
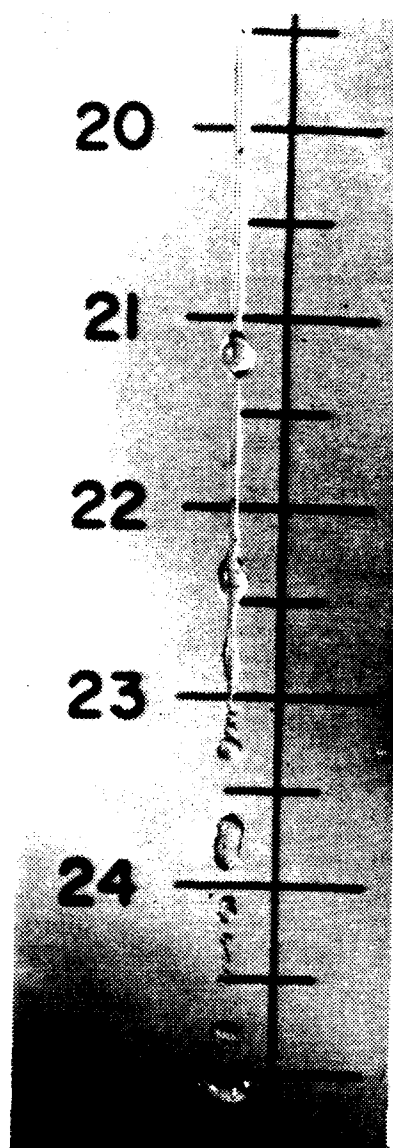
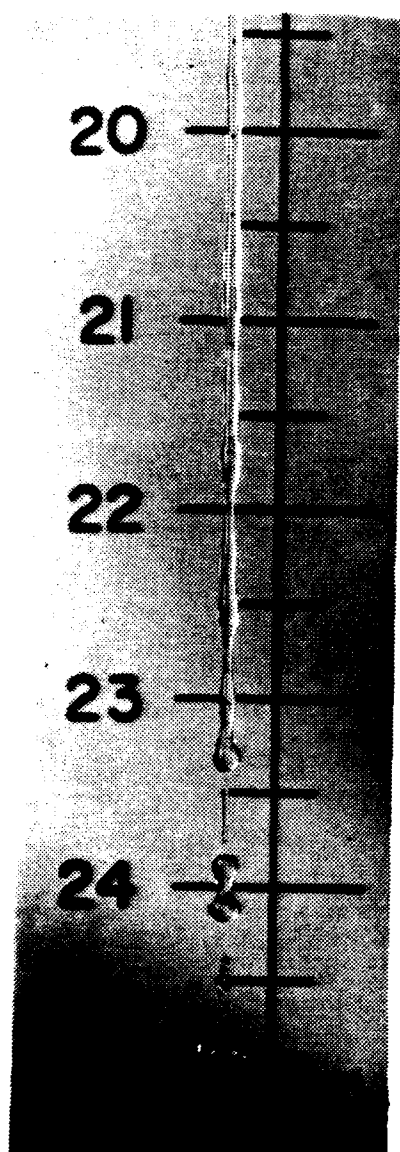


Figure 29. Photos Illustrating Jet Breakdown and Oscilloscope Trace of Pressure at $Re=2200$ and $f=380$ Hz

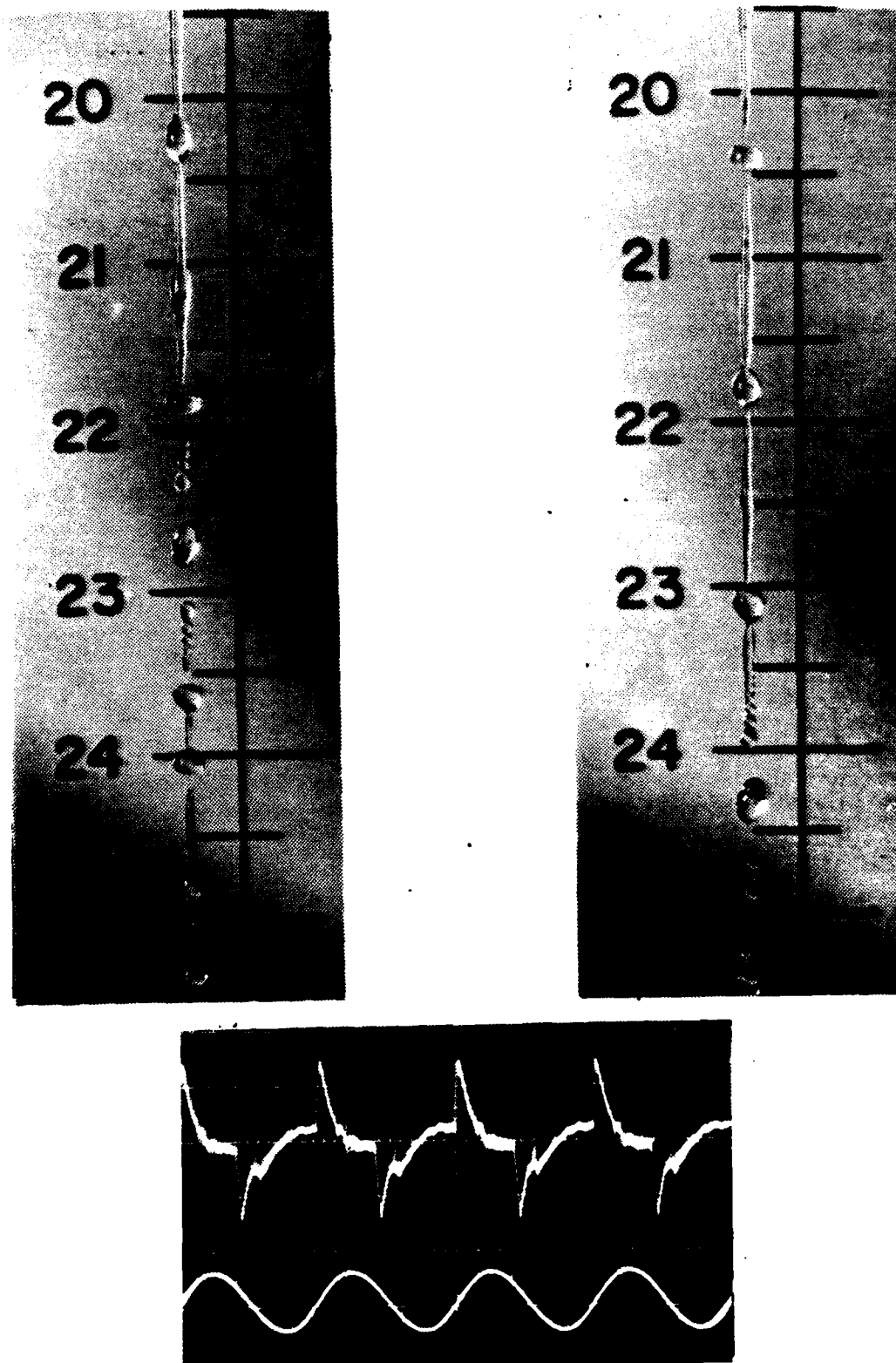


Figure 30. Photos Illustrating Jet Breakdown and Oscilloscope Trace of Pressure at $Re=2200$ and $f=787$ Hz

Referring to Fig. 12 , we may draw some conclusions concerning the average breakdown point. Up to 100 Hz a gradually movement of the breakdown point upstream is observed which is nevertheless more rapid than the laminar case as can be seen from comparison of the slope of the curves within this region . A nearly stable region then appears in the frequency range between 100 Hz and 266 Hz where the breakdown point is nearly fixed at 100 diameters. This region may be characterized as a **stabilized region** and was not observed at any other Reynolds number. A **singular point** was also observed at **300 Hz** as discussed previously. This frequency may be characterized as a **critical frequency** for the specific Reynolds number . Finally , we can see from Fig. 12 that the relaminarization rate was also greater for transitional flow, producing a steeper slope of the curve in the frequency range from 300 Hz to 400 Hz.

3. Turbulent Flow at Reynolds Number 2640

At this Reynolds number it was observed that the unexcited flow began to breakdown at an average distance of 30 diameters and no significant effect on the jet was observed up to a frequency of 100 Hz. Increasing the frequency a gradual movement of the average breakdown point downstream observed, which reached a maximum of 50 diameters at 250 Hz.

Further increase of the frequency produced a very slow movement of the average breakdown point upstream to about 42 diameters at a frequency of 366 Hz. The breakdown point then remained almost unchanged up to 2000 Hz. The only further change observed in the high frequency range, from 366 Hz to 2000 Hz, was the appearance of a corkscrew-like motion of the jet which became more pronounced with increasing frequency, making more readily observable the helical mode, which dominates the breakdown mechanism. These results are shown in Figs. 31 through 36.

B. CONCLUSIONS.

From the results, discussed above, we may draw the following conclusions concerning the effect of small perturbations on jet breakdown:

- a. In the case of laminar flow, ($Re=1640$), the breakdown point moves upstream as the frequency is increased up to 266 Hz. Downstream of the breakdown point the jet flow becomes turbulent and breaks into discrete droplets. Above 266 Hz this effect is observed to reverse itself and the jet returns to its laminar nature.
- b. In the case of transitional flow, ($Re=2200$), the breakdown point moves initially upstream as frequency is increased to 100 Hz. In the range of 100 Hz to 266 Hz an almost stable behavior of the breakdown point is observed. Singular behavior with very interesting results including a sudden shift of breakdown point is observed at 300 Hz. Finally a more effective relaminarization than observed at lower Reynolds number occurs above 300 Hz leading to a completely stabilized laminar flow at frequencies above 380 Hz.
- c. In the case of turbulent flow, ($Re=2640$), no noticeable effect is observed up to a frequency of 100 Hz. Above this frequency the breakdown point begins to move gradually downstream up to 250 Hz, returns back

upstream to a frequency of 333 Hz , and becomes almost completely unaffected by the pressure perturbations at higher frequencies.

- d. Changing the waveform of the disturbance produced only a slight deviation in the average breakdown point, however a markedly different pattern of droplet formation was observed.
- e. Although it was not possible to record the phenomena photographically for inclusion here , it was possible using the phase angle control incorporated in the stroboscope to observe the entire development of the droplet formation visually. This process was found to be a complex sequence of breakup and re-agglomeration.

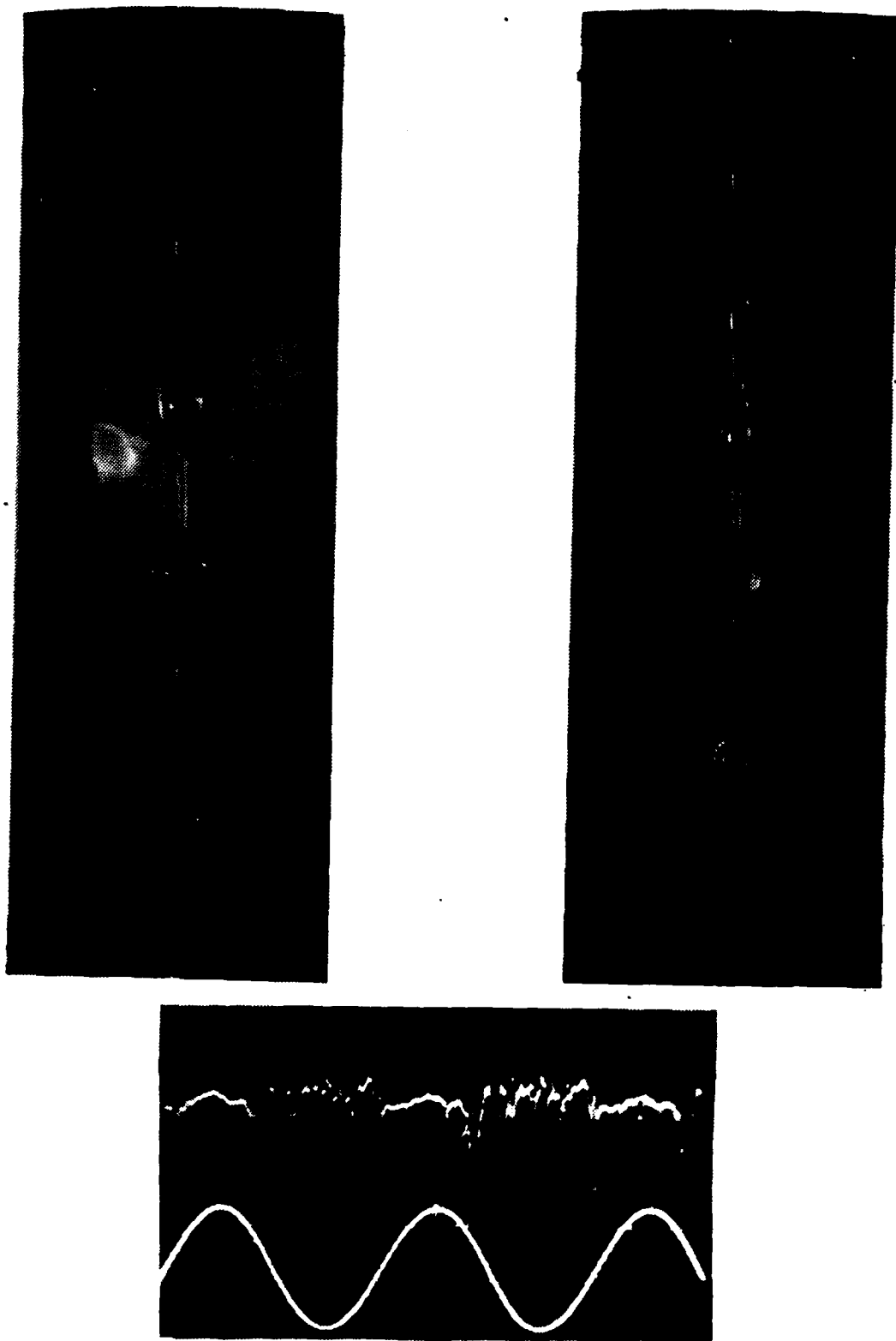


Figure 31. Photos Illustrating Jet Breakdown and Oscilloscope Trace of Pressure at $Re=2640$ and $f=50$ Hz

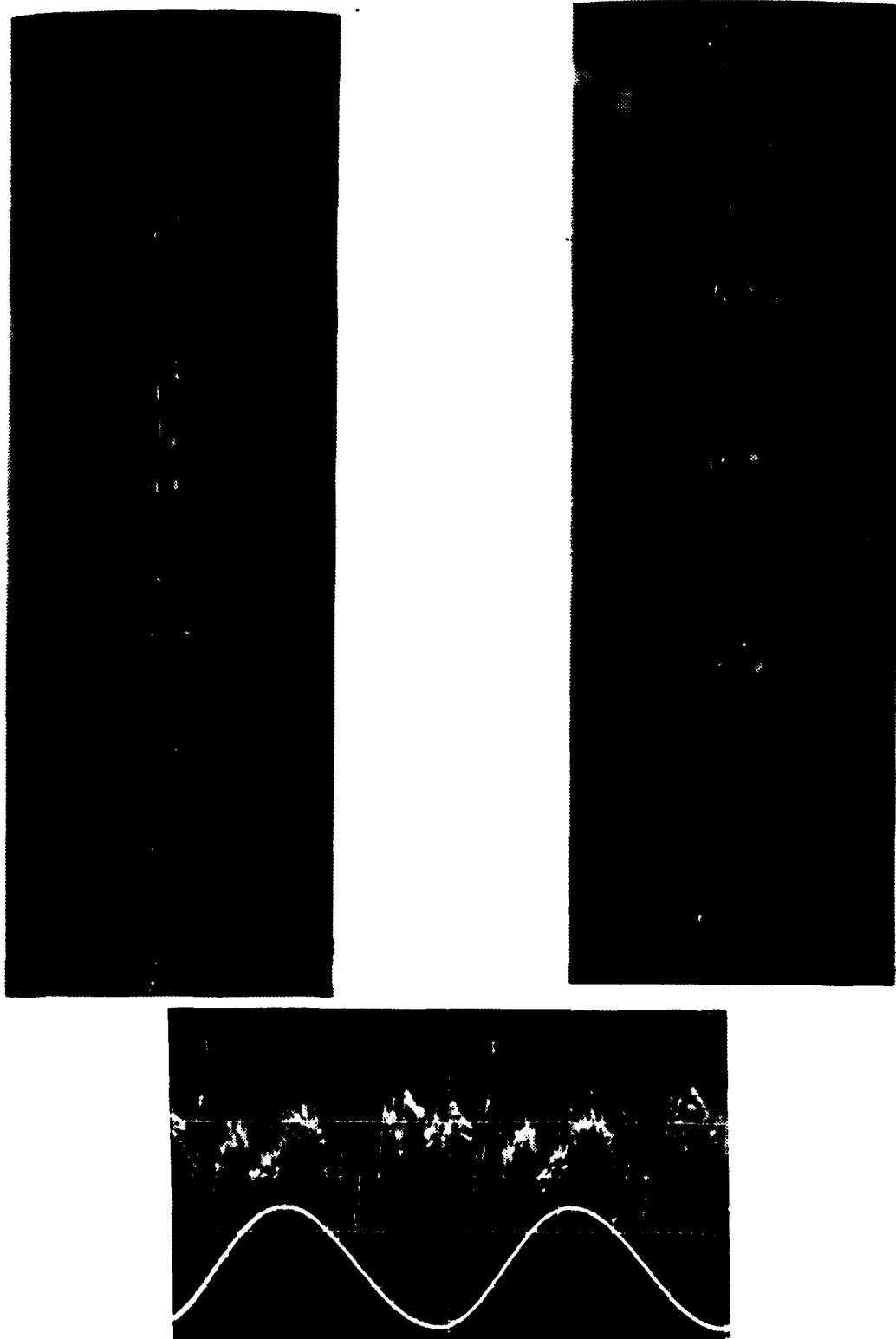


Figure 32. Photos Illustrating Jet Breakdown and Oscilloscope Trace of Pressure at $Re=2640$ and $f=100$ Hz

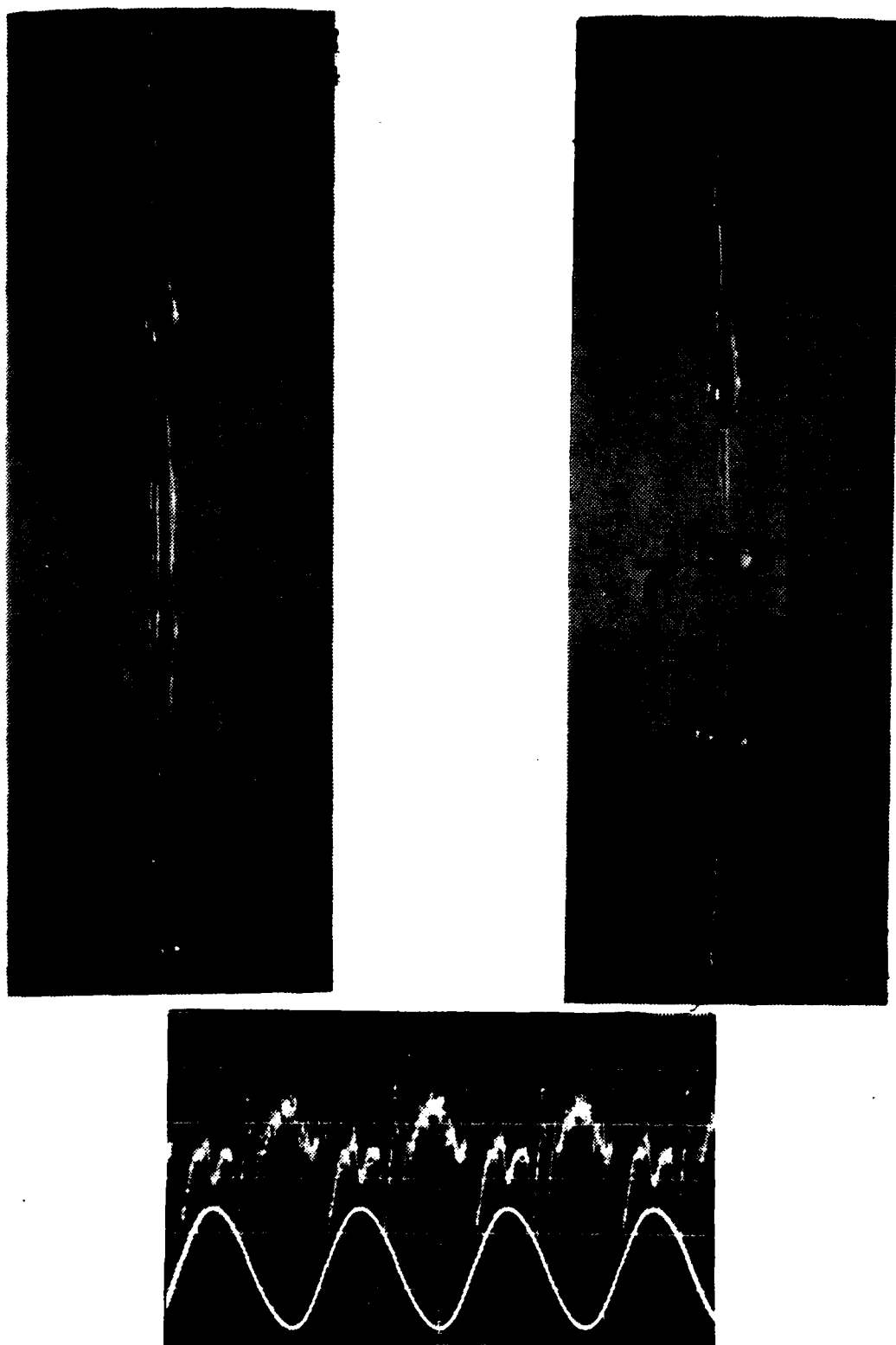


Figure 33. Photos Illustrating Jet Breakdown and Oscilloscope Trace of Pressure at $Re=2640$ and $f=200$ Hz

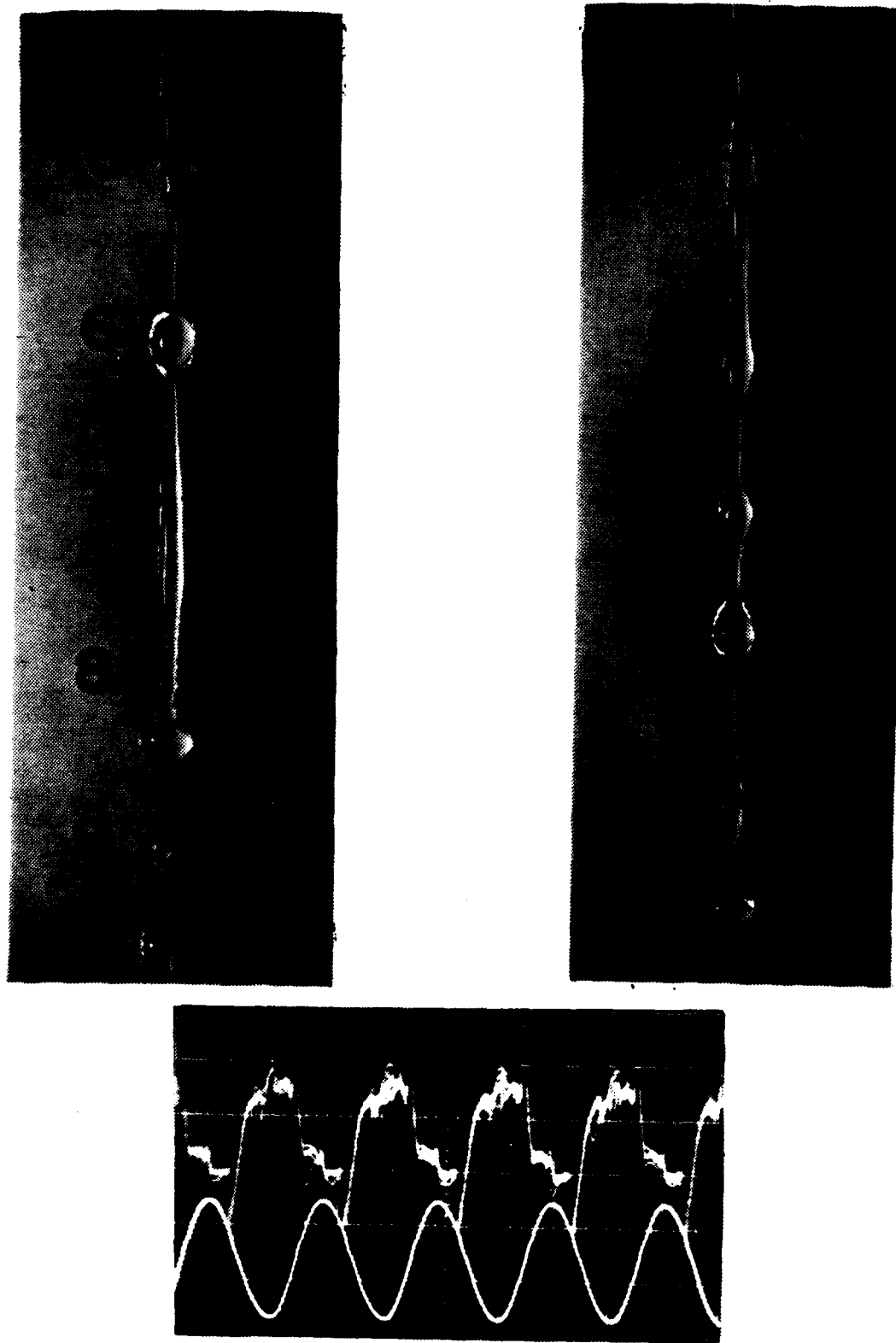


Figure 34. Photos Illustrating Jet Breakdown and Oscilloscope Trace of Pressure at $Re=2640$ and $f=250$ Hz

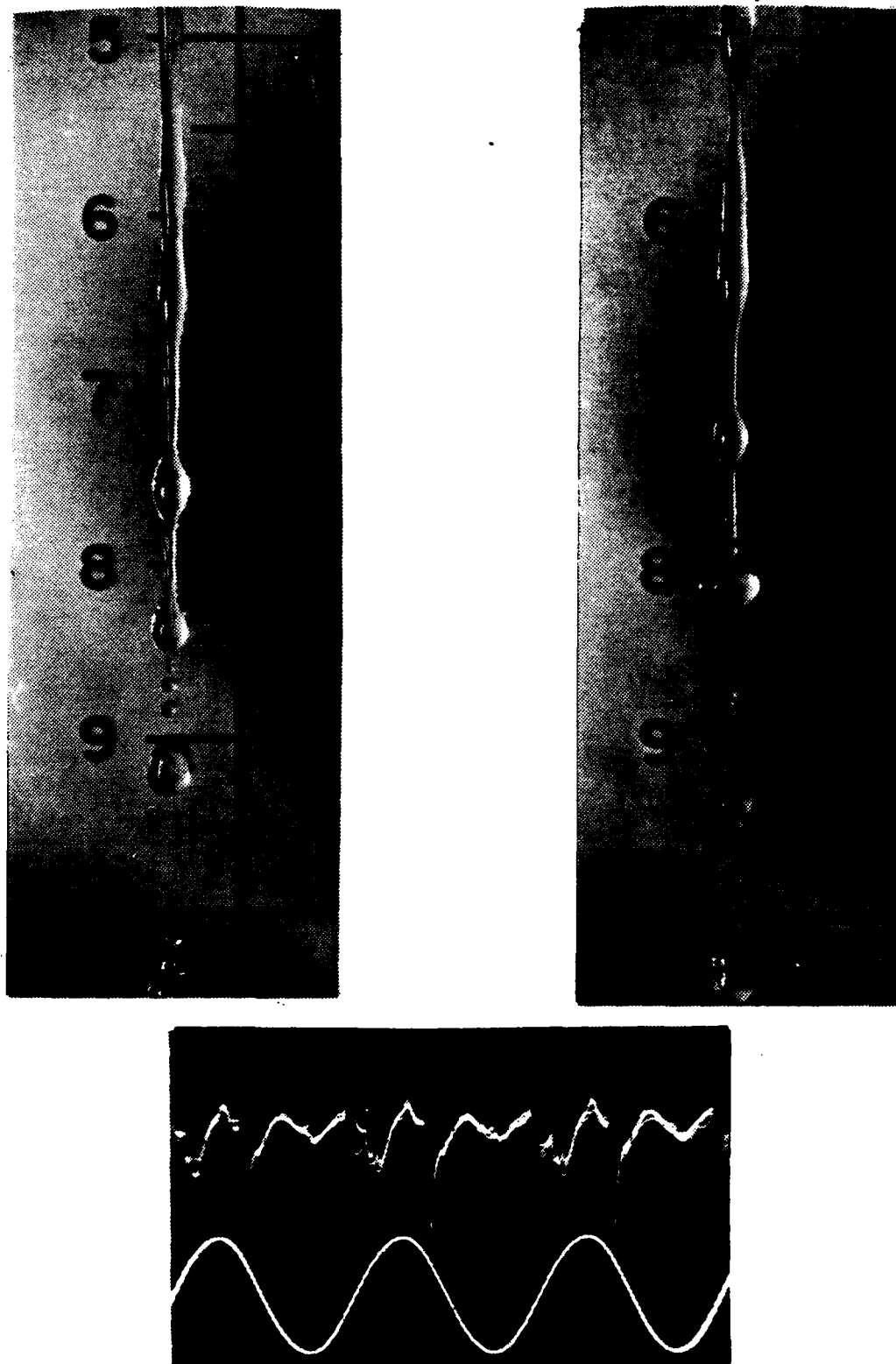


Figure 35. Photos Illustrating Jet Breakdown and Oscilloscope Trace of Pressure at $Re=2640$ and $f=300$ Hz

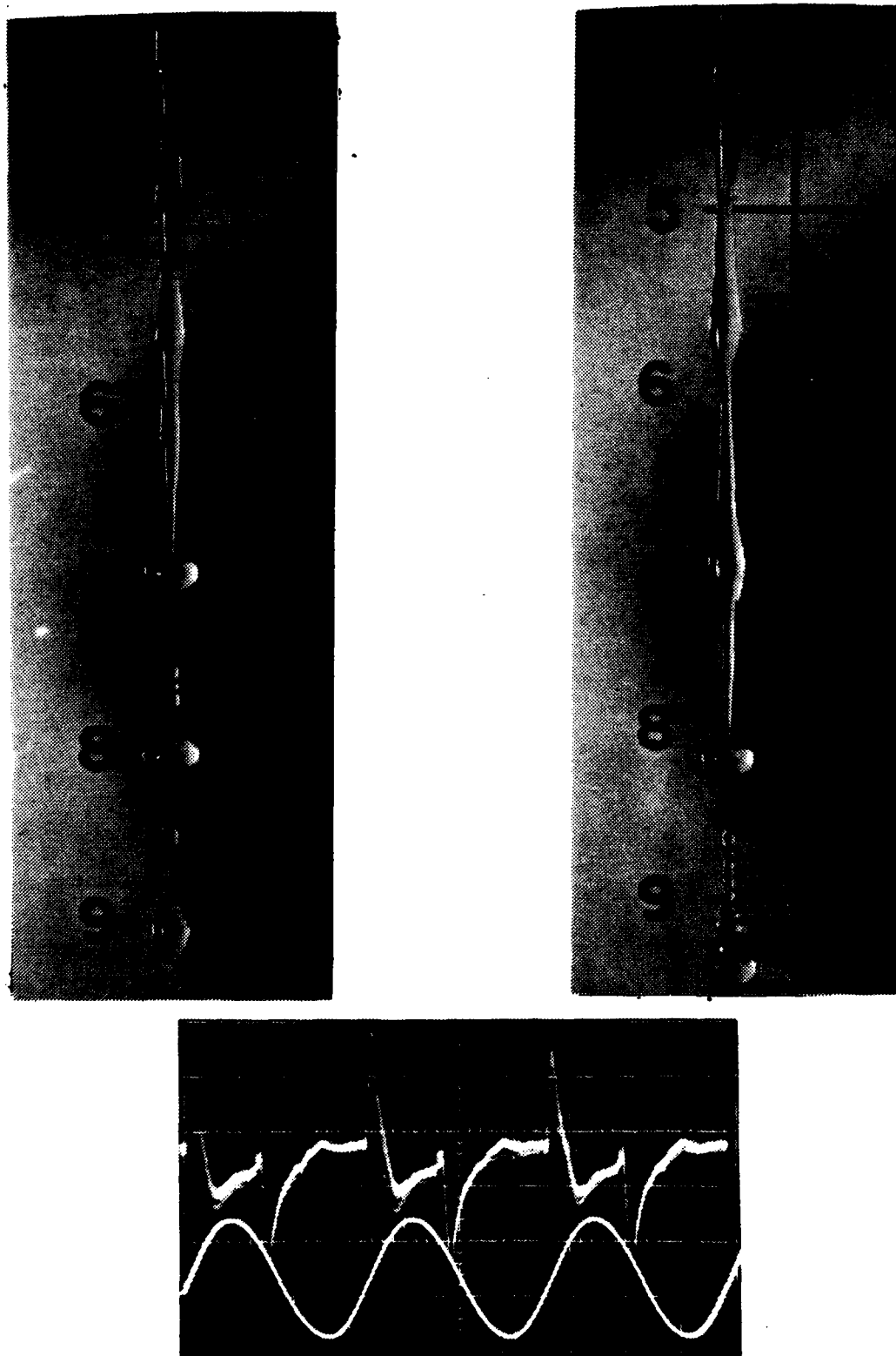


Figure 36. Photos Illustrating Jet Breakdown and Oscilloscope Trace of Pressure at $Re=2640$ and $f=600$ Hz

APPENDIX. CALCULATIONS AND DATA REDUCTION

A. CALCULATION OF CRITICAL REYNOLDS NUMBER

A visual observation of the flow was used in order to determine the critical Reynolds number. Adjusting the flow by the means of the needle valve, installed at the entrance of the plenum chamber, a laminar jet was observed up to the flow meter indication $\dot{m}_i = 25$. Above this value a turbulent flow resulted.

Using the equation of continuity :

$$\dot{m} = \rho AU \quad \text{or} \quad U = \dot{m} / \rho A \quad (\text{Eq. A-1})$$

where:

\dot{m} = the fluid mass rate.

U = the mean flow velocity.

$\rho = 62.34 \text{ lbm / ft}^3$, the water density (at 60° F).

A = the cross section area of the pipe.

Also:

$$A = \pi d^2 / 4 = (\pi / 4) [(3 / 16)(1 / 12)]^2 (\text{ft}^2)$$

$$\text{or: } A = 1.9175 \cdot 10^{-4} (\text{ft}^2)$$

and:

$$\dot{m} = [.6(25/100)](\text{gal/min}) \quad \text{or} \quad \dot{m} = .15 \text{ gal/min}$$

$$\text{or: } \dot{m} = (.15)(500.8)(1/3600) (\text{lbm/sec})$$

$$\text{or: } \dot{m} = .020867 (\text{lbm/sec})$$

Substituting the above values into Eq. A-1 we get:

$$U = \frac{.020867}{(62.34)(1.9175 \cdot 10^{-4})} (\text{ft/sec})$$

or: $U = 1.74562 \text{ (ft/sec)}$

The Reynolds number is given by:

$$Re = (\rho U d) / (\mu g_c) \quad (\text{Eq. A-2})$$

where:

$$\mu = 2.4 \cdot 10^{-5} \text{ (lbf-sec/ft}^2\text{)}$$

and:

$$g_c = 32.2 \text{ (lbm-ft)/(lbf-sec}^2\text{)}$$

Substituting the above values into (Eq. A-2) we get:

$$(Re)_{cr} = \frac{(62.34)(1.74562)(1/64)}{(2.4 \cdot 10^{-5})(32.2)}$$

or: $(Re)_{cr} = 2200$

The value obtained may be considered reasonable taking into account that is the most common value found in the Hydrodynamics Bibliography. The numerical values used in the above calculations were obtained from Ref. 25 .

B. CALCULATION OF INDICATED PRESSURE IN LAMINAR FLOW

Referring to Fig. B-1, where the exact dimensions used are indicated, we apply the **Energy Equation**:

$$\frac{P_1}{\rho} + b_1 \frac{U_1^2}{2g_c} + \frac{g}{g_c} z_1 = \frac{P_2}{\rho} + b_2 \frac{U_2^2}{2g_c} + \frac{g}{g_c} z_2 + h_l \quad (\text{Eq. B-1})$$

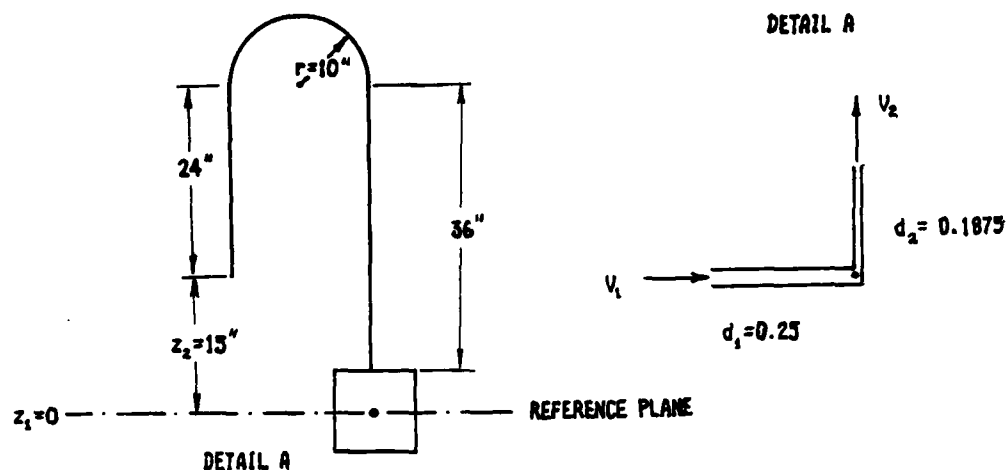


Figure B-1. Sketch of the Apparatus.

where:

P_1 : the pressure at point 1.

P_2 : the pressure at point 2 ($P_2 = P_{atm} = 14.7$ psia)

U_1 : the mean velocity of the fluid at point 1.

U_2 : the mean velocity of the fluid at point 2.

$b_1 = b_2 = 2$: the energy correction factor for laminar flow at points 1 and 2 respectively.

z_1, z_2 : the height difference from the reference plane

h_1 : the flow losses given by the relation:

$$h_1 = f \frac{1}{d} \frac{U^2}{2g_c} \quad (\text{Eq. B-2})$$

where:

$f = 64/Re$: friction factor for laminar flow.

l : the total pipe length.

Inserting the numerical values and the appropriate dimensions from Fig. B-1 into Eq. B-2 we get:

$$h_1 = (64/2200)(94.416/.1875)[(1.74562)^2/2(32.2)]$$

or: $h_1 = .69335 \text{ (lbf-ft/lbm)}$

Using the Continuity Equation referring to Detail A of Fig. B-1 and neglecting the minor turning losses we get:

$$\dot{m} = \rho AU_1 = \rho AU_2 \quad (\text{Eq. B-3})$$

or: $U_2/U_1 = A_1/A_2 = d_1^2/d_2^2 = (.25)^2/ (.1875)^2 = 1.7777$

Therefore:

$$U_1 = U_2/1.7777 = 1.74562/1.7777 \text{ (ft/sec)}$$

or: $U_1 = .982 \text{ (ft/sec)}$

From the Energy Equation, (Eq. B-1) we may write:

$$\frac{g_c}{\rho} (P_1 - P_2) = \frac{b}{2} (U_2^2 - U_1^2) + g(z_2 - z_1) + g_ch_1$$

Solving for $\Delta P = P_1 - P_2$ we get:

$$\Delta P = \frac{\rho}{g_c} \left[\frac{b}{2} (U_2^2 - U_1^2) + g(z_2 - z_1) + g_ch_1 \right] \quad (\text{Eq. B-4})$$

Substituting numerical values into Eq. B-4 we get:

$$\Delta P = \frac{62.34}{32.20} \left\{ \frac{2}{2} [(1.74562)^2 - (.982)^2] + 32.2 \frac{15}{12} + 32.2(.69335) \right\}$$

or: $\Delta P = 125.18 \text{ (lbf/ft}^2\text{)}$

or: $\Delta P = .8693$ (psig)

or: $\Delta P = 1.775$ (in.Hg) at 60° F

The latter is a reasonable result compared with the mercury manometer which indicated pressure $P_{ind} = 1.8$ in.Hg suggesting an error of 1.39 % .

The curvature of the pipe does not create a large effect in friction factor for this Reynolds number which is in good agreement with the experimental work of White [Ref.26].

C. DYNAMIC RESPONSE OF INDICATED PRESSURE

Since the pressure perturbations were introduced in the upstream plenum chamber and measured with a pressure transducer through a pressure tap, we may reasonably inquire into the accuracy of the pressure traces measured. In order to answer this question, we consider the dynamic response of the system under the assumption that the fluid pressure is applied uniformly at the transducer front surface .

The transient response of a pressure measuring instrument is dependent on two factors:

a. The response of the transducer element that senses the applied pressure.

b. The response of the pressure transmitting fluid contained in the connecting tubing.

This latter factor is frequently the one which determines the overall frequency response of a pressure measurement system, and eventually calibration must be relied upon for determining this response.

An estimate of this behavior may be obtained from the following analysis [Ref. 27].

Consider the system shown in Fig. C-1. The fluctuating pressure has a frequency, ω , and an amplitude, P_0 , and is impressed on a tube of length L , and radius r . At the end of this tube is a chamber of volume V , where connection with the pressure transducer is made. We seek an expression for the pressure indicated by the transducer, P_0 .

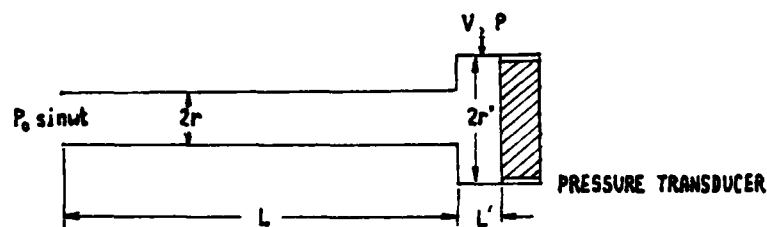


Figure C-1. Schematic Diagram of Pressure Transducer Connection.

The mass of the fluid oscillates under the influence of fluid friction in the tube which tends to dampen the motion. If the conventional formula for laminar friction resistance in tube flow is used to represent this friction, the resulting expression for the pressure amplitude ratio is:

$$\left[\frac{P}{P_0} \right] = \left\{ \left[1 - \left(\frac{\omega}{\omega_n} \right) \right]^2 + 4h^2 \left(\frac{\omega}{\omega_n} \right)^2 \right\}^{-1/2} \quad (\text{Eq. C-1})$$

where:

ω_n is the natural frequency given by the expression:

$$\omega_n = \sqrt{\frac{3\pi r^2 c^2}{4LV}} \quad (\text{Eq. C-2})$$

and h is the damping ratio given by the expression:

$$h = \frac{2\mu g_c}{\rho c r^3} \sqrt{\frac{3LV}{\pi}} \quad (\text{Eq. C-3})$$

In the above relations, Eqs. C-2 and C-3 :

c = the velocity of sound in the fluid.

μ = the dynamic viscosity of the fluid.

ρ = the fluid density.

The phase angle for the pressure signal is given by:

$$\phi = \tan^{-1} \frac{2h \left(\frac{\omega}{\omega_n} \right)}{1 - \left(\frac{\omega}{\omega_n} \right)^2} \quad (\text{Eq. C-4})$$

Introducing the physical dimensions of the present apparatus, referring to Fig. C-1 we have:

$$L = 3.5 \text{ in} \quad L' = 0.5 \text{ in}$$

$$r = 0.25 \text{ in} \quad r' = 0.25 \text{ in}$$

$$V = \pi r^2 L = \pi (.25/12)^2 (3.5/12) = 6.8177 \cdot 10^{-5} \text{ (ft}^3\text{)}$$

$$c = (K/\rho)^{1/2}$$

$$\text{or: } c = [144 (311 \cdot 10^3) / 1.938]^{1/2} = 4800 \text{ (ft/sec)}$$

$$\rho = 62.34 \text{ lbm/ft}^3$$

$$\mu = 2.4 \cdot 10^{-5} \text{ lbf-sec/ft}^2 \quad (\text{at } 60^\circ\text{F})$$

Substituting the above values into Eq. C-2 we get:

$$\omega_n = \frac{3\pi(.25/12)^2(4800)^2}{4(3.5/12)(6.8177 \cdot 10^{-4})}$$

or: $\omega_n = 10885 \text{ sec}^{-1}$

Substituting into Eq. C-3 we get:

$$h = \frac{2(2.4 \cdot 10^{-5})(32.2)}{(62.34)(4800)(.25/12)} \sqrt{\frac{3(3.5/12)(6.8177 \cdot 10^{-4})}{\pi}}$$

or: $h = 7.87 \cdot 10^{-6}$

From these results we see that the difference between pressure transducer indication and actual plenum chamber pressure is negligible for the working frequency range.

For example at $\omega = 1000 \text{ Hz}$, from Eq. C-1 we get:

$$\frac{P}{P_o} = \left\{ \left[1 - \left[\frac{1000}{10885} \right]^2 \right]^2 + 4(7.87 \cdot 10^{-6})^2 \left[\frac{1000}{10885} \right]^2 \right\}^{-1/2}$$

or: $P/P_o = 1.0085$

Therefore the pressure indication error due to dynamic response is 0.85 %

We can get for the phase angle of the pressure signal, from Eq. C-4 :

$$\phi = \tan^{-1} -[2(7.87 \cdot 10^{-6})(.09187) / (1 - .09187)]$$

or: $\phi = -8.355 \cdot 10^{-5} \text{ rad}$

D. CALIBRATION DIAGRAMS

In order to compare theoretical and experimental results concerning the indicated pressure from the mercury manometer, as well as the pressure variations from the digital multimeter, it was necessary to calibrate both of them. A pressure calibration diagram is plotted in Fig. D-1 where it is shown to be linear.

Since the Reynolds number is a function of flow rate, it was easier to adjust the flow more accurately with the aid of a pressure indicating digital multimeter than the rotameter. Therefore two diagrams were created, shown in Figs. D-2 and D-3 where are plotted the indicated flow rate versus the indicated pressure, expressed in inches Hg and D.C Volts respectively.

P(IN.HG) VS P(D.C VOLT)

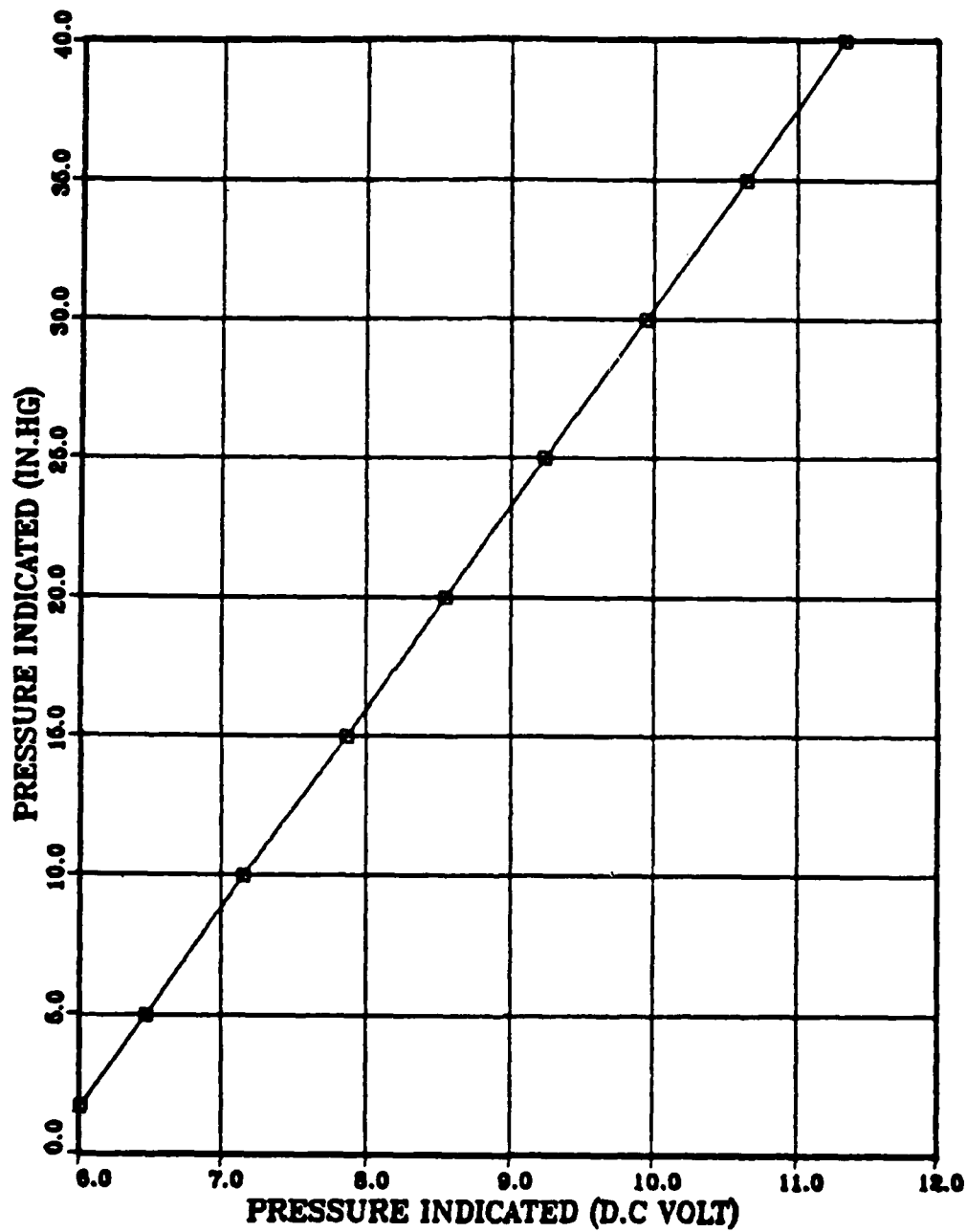


Figure D-1. Pressure Calibration Diagram

FLOW RATE VS P(IN.HG)

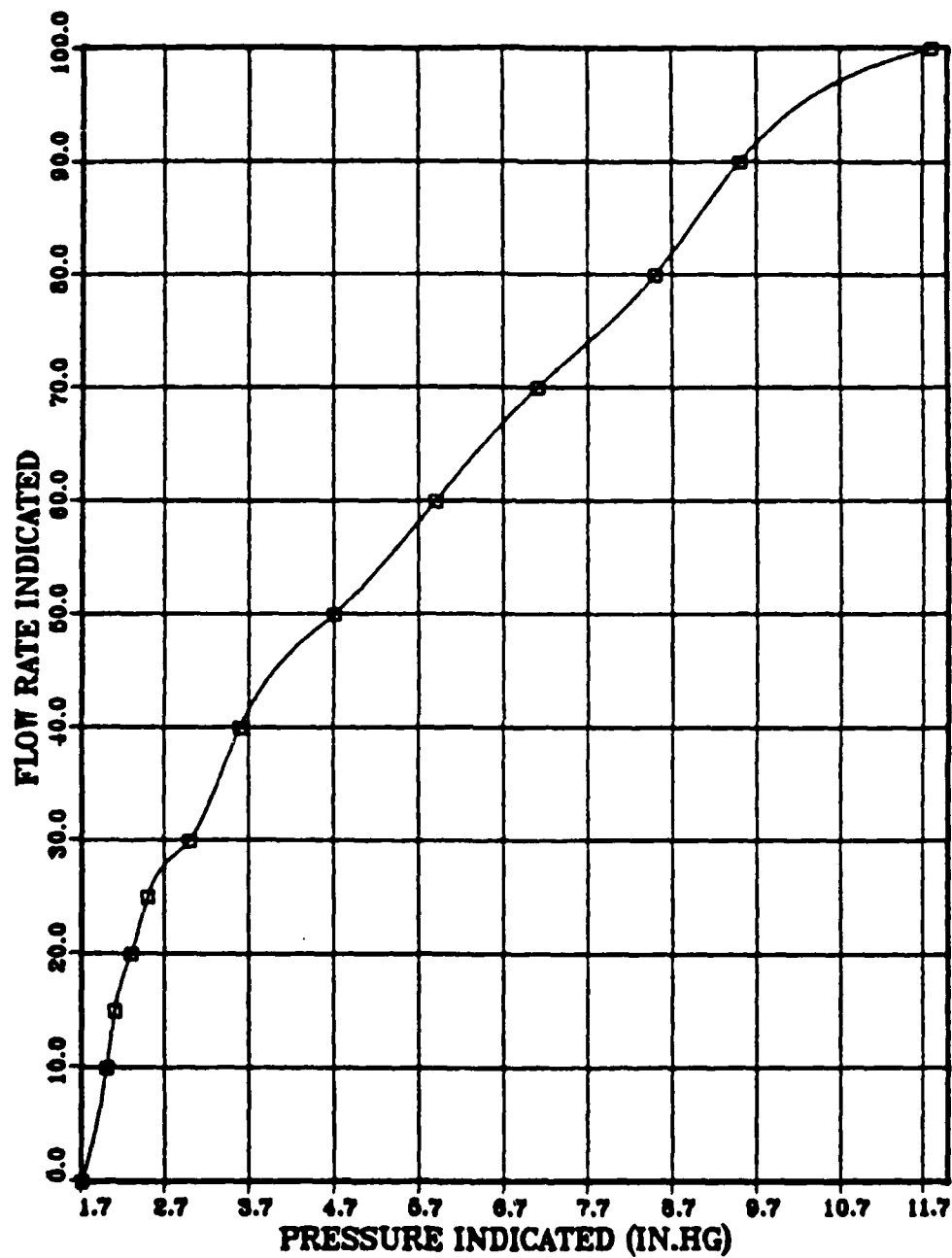


Figure D-2. Flow Rate vs. Pressure Indicated (in.Hg) Diagram

FLOW RATE VS P(D.C VOLT)

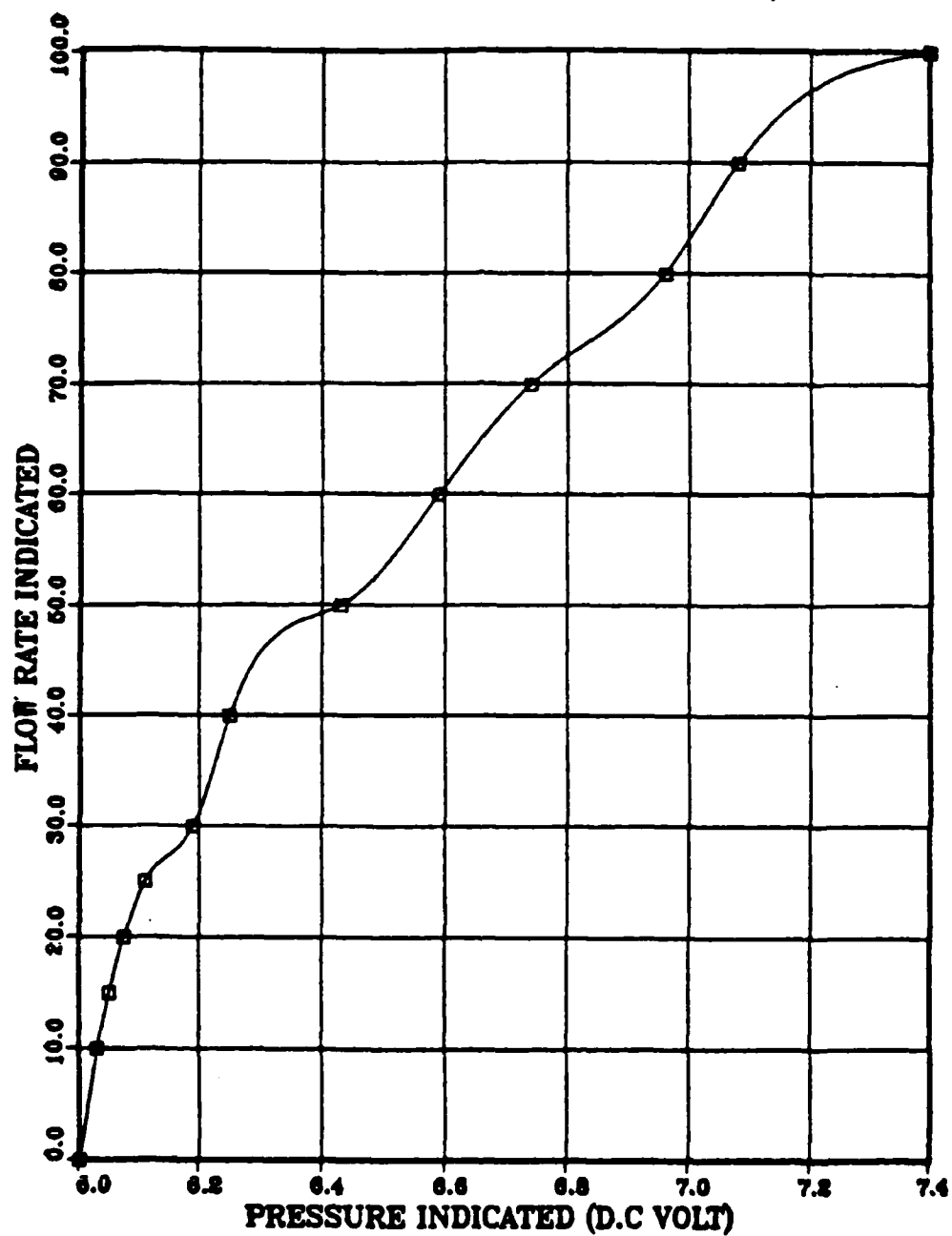


Figure D-3. Flow rate vs. Pressure Indicated (V.DC) Diagram

LIST OF REFERENCES

1. Rayleigh, J. W. S., Philosophical Magazine, v. 34, pp. 59, 1892.
2. Tatsumi, T., " Stability of the Laminar Inlet-flow Prior to the Formation of Poiseuille Regime,I,II ," Journal of the Physical Society of Japan, v. 7, pp. 489-502, 1952.
3. Batchelor, G. K., " Analysis of the Stability of Axisymmetric Jets ," Journal of Fluid Mechanics, v. 14, pp. 529-551, 1962.
4. Crow, S. C., Champagne, F. H., " Orderly Structure in Jet Turbulence ," Journal of Fluid Mechanics, v. 48, pp. 547-591, 1971.
5. Salwen, H., Grosch, C. E., " The Stability of Poiseuille Flow in a Pipe of Circular Cross-section ," Journal of Fluid Mechanics, v. 54, pp. 93-112, 1972.
6. Anderson, R., Bejan, A., " The Instability on a Round Jet Surrounded by an Annular Shear Layer ," Journal of Fluid Engineering , v. 107, pp.258-263, 1985.
7. Sarpkaya, T., " A Note on the Stability of Developing Laminar Pipe Flow Subjected to Axisymmetric and non Axisymmetric Disturbances ," Journal of Fluid Mechanics, v. 68, pp. 345-351, 1975.
8. Garg, V. K., Rouleau, W. T., " Linear Spatial Stability of Pipe Poiseuille Flow ," Journal of Fluid Mechanics, v. 54, pp. 113-127, 1972.
9. Leite, R. J., " An Experimental Investigation of the Stability of Poiseuille Flow ," Journal of Fluid Mechanics, v. 5, pp. 113-127, 1959.

AD-A161 149

EFFECT OF SMALL PRESSURE DISTURBANCES ON THE BREAKDOWN
OF ROUND LAMINAR AND TURBULENT JETS(U) NAVAL
POSTGRADUATE SCHOOL MONTEREY CA 2 2 GIKAS SEP 85

2/2

UNCLASSIFIED

F/G 20/4

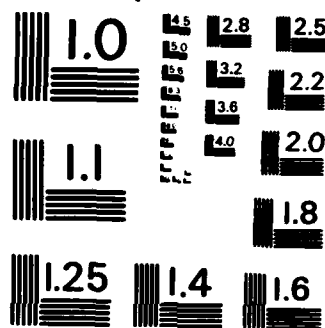
NL



END

FILED

DTIC



MICROCOPY RESOLUTION TEST CHART
NATIONAL BUREAU OF STANDARDS-1963-A

10. Darling, G. B., " Heat Transfer to Liquid in Intermittent Flow ," Petroleum , v. 22 , pp. 177-180, 1959.
11. Sarpkaya, T., " Experimental Determination of the Critical Reynolds Number for Pulsating Poiseuille Flow ," Journal of Basic Engineering, (ASME), v. 88, pp. 589-598, 1966.
12. Gilbrech, D. A., Combs, G. D., " Critical Reynolds Numbers for Incompressible Pulsating Flow in a Tube ," Developments in Theoretical and Applied Mechanics, Phenum Press, v. 1, pp. 292-304, 1963.
13. Gilbrech D. A., Combs G. D., " Pulsating Flow Research," University of Arkansas Engineering Experiment Station Research Paper No 4 , 1964.
14. Stuart, J. T., " On the Non-linear Mechanics of Wave Disturbances in Stable and Unstable Parallel Flows ," Journal of Fluid Mechanics, v. 9, pp. 353-370, 1960.
15. Spielberg, K., Timan, H., " On Three and Two Dimensional Disturbances of Pipe Flow ," Journal of Applied Mechanics , v. 9, pp. 381-389, 1960.
16. Sparrow, E. M., Lin, S. H., " Flow Development in the Hydrodynamic Entrance Region of Tubes and Ducts ," The Physics of Fluids, v. 7, pp. 338-347, 1964.
17. Klebanoff, P. S., Tidstrom, K. D., Sargent, L. M. " The Three Dimensional Nature of Boundary-layer Instability ," Journal of Fluid Mechanics, v. 12, pp. 1-34, 1962
18. Miller, J. A., Fejer, A. A., " Transition Phenomena in Oscillating Boundary-layer Flows ," Journal of Fluid Mechanics, v. 18, pp. 438-448, 1964.
19. Obremski, H. J., Fejer, A. A., " Transition in Oscillating Boundary-layer Flows ," Journal of Fluid Mechanics, v. 29, pp. 93-111, 1967.

20. Landahl, M. T., " Wave Mechanics of Breakdown," Journal of Fluid Mechanics, v. 56, pp. 775-802, 1972.
21. Shen, S. F., " Some Considerations on the Laminar Stability of Time-dependant Basic Flows ," Journal of Aerospace Science, v. 28, pp. 397-417, 1961.
22. Grenspan, H. P., " On Shear-Layer instability Breakdown and Transition, " Journal of Fluid Mechanics, v. 15, pp. 135-153, 1963.
23. Uchida, S., " The Pulsating Viscous Flow Superposed on the Steady Laminar Motion of Incompressible Fluid in a Circular Pipe , " Zeitschrift fur Angewandte Mathematik and Mechanik , v. 7, pp. 403-422, 1956.
24. Hoyt, J. W., Taylor, J. J., " Turbulence Structure in a Water Jet Discharging in Air ," Physics of Fluids , v. 20, pp. 253-257, 1977.
25. Zucker, R. D., Fundamentals of Gas Dynamics, pp. 3A-1 - 3D-6, Matrix Publishers, 1977.
26. White, C. M., " Streamline Flow Through Curved Pipes, " Royal Society Proceedings Series A, v. 123, pp. 645-663, 1929.
27. Holman, J. P., Experimental Methods for Engineers pp. 208-210, Mc Grow Hill, 1984.

INITIAL DISTRIBUTION LIST

		No. of Copies
1.	Defence Technical Information Center Cameron Station Alexandria, Virginia 22304-6145	2
2.	Library, Code 0142 Naval Postgraduate School Monterey, California 93943	2
3.	Department Chairman, Code 67 Department of Aeronautics Naval Postgraduate School Monterey, California 93943	1
4.	Professor. J.A. Miller, Code 67Mo Department of Aeronautics Naval Postgraduate School Monterey, California 93943	2
5.	Hellenic Air Force General Staff ATTN: Chief of Staff HAF/GS, Deputy CS HAF/GS Technical Inspector HAF/GS Holargos, Athens, GREECE	3
6.	Hellenic Air Material Command ATTN: Com. AMC Chief of Staff AMC Elefsina, GREECE	1
7.	Air Training Command ATTN: Com. ATC Chief of Staff ATC Tatoi-Dekelia, GREECE	2
8.	Commander Hellenic Air Force Academy Tatoi-Dekelia, GREECE	5
9.	Commander Air War College Tatoi-Dekelia, GREECE	3
10.	Hellenic Air Force Research & Development Center ATTN: Com. KETA KETA, T.G.A 1010 Palaion Faliron, Athens, GREECE	4
11.	Capt. Z.Z. Gikas 4 Agorakritou St., T.K 10446 Athens, GREECE	3

- | | | |
|-----|--|---|
| 12. | Capt. D.M. Petridis
SMC 1351
Naval Postgraduate School
Monterey, California 93943 | 1 |
| 13. | Lt. E.S. Mitrou
SMC 2777
Naval Postgraduate School
Monterey, California 93943 | 1 |

END

FILMED

12-85

DTIC